TR-0181

AD

Reports Control Symbol
OSD - 1366

THE BEHAVIOR OF CLOUD DROPLETS IN AN ACOUSTIC FIELD: A NUMERICAL INVESTIGATION

August 1985

by

Michael Phillip Foster

Approved for public release; distribution unlimited.

US Army Electronics Research and Development Command
Atmospheric Sciences Laboratory
White Sands Missile Range, NM 88002-5501

NOTICES

Disclaimers

The findings in this report are not to be construed as an official Department of the Army position, unless so designated by other authorized documents.

The citation of trade names and names of manufacturers in this report is not to be construed as official Government indorsement or approval of commercial products or services referenced herein.

Destruction Notice

When this document is no longer needed, destroy it by any method that will prevent disclosure of its contents or reconstruction of the document.

SECURITY CLASSIFICATION OF THIS PAGE *(When Date Entered)*

REPORT DOCUMENTATION PAGE

READ INSTRUCTIONS BEFORE COMPLETING FORM

1. REPORT NUMBER: ASL-TR-0181	2. GOVT ACCESSION NO.
3. RECIPIENT'S CATALOG NUMBER	
4. TITLE *(and Subtitle)*: THE BEHAVIOR OF CLOUD DROPLETS IN AN ACOUSTIC FIELD: A NUMERICAL INVESTIGATION	5. TYPE OF REPORT & PERIOD COVERED: Technical Report
	6. PERFORMING ORG. REPORT NUMBER
7. AUTHOR(s): Michael Phillip Foster	8. CONTRACT OR GRANT NUMBER(s)
9. PERFORMING ORGANIZATION NAME AND ADDRESS: US Army Atmospheric Sciences Laboratory, White Sands Missile Range, NM 88002	10. PROGRAM ELEMENT, PROJECT, TASK AREA & WORK UNIT NUMBERS: Not Applicable
11. CONTROLLING OFFICE NAME AND ADDRESS: US Army Electronics Research and Development Command, Adelphi, MD 20783	12. REPORT DATE: August 1985
	13. NUMBER OF PAGES: 90
14. MONITORING AGENCY NAME & ADDRESS *(if different from Controlling Office)*	15. SECURITY CLASS. *(of this report)*: UNCLASSIFIED
	15a. DECLASSIFICATION/DOWNGRADING SCHEDULE

16. DISTRIBUTION STATEMENT *(of this Report)*

Approved for public release; distribution unlimited.

17. DISTRIBUTION STATEMENT *(of the abstract entered in Block 20, if different from Report)*

18. SUPPLEMENTARY NOTES

acoustic agglomeration
acoustic coagulation
cloud droplet spectra
cloud modification
fog dispersal

19 KEY WORDS *(Continue on reverse side if necessary and identify by block number)*

20. ABSTRACT *(Continue on reverse side if necessary and identify by block number)*

The theory and practice of acoustic agglomeration have been evolving steadily since the late 1920's. In recent years there have been large technological advances in fields such as pollution control using the principles of acoustic agglomeration. With respect to the field of meteorology, there have been attempts in the past to modify atmospheric fogs using intense acoustic energy. These efforts enjoyed only mixed success and were abandoned. However, the theory of acoustic agglomeration suggests that clouds with higher liquid water

DD FORM 1 JAN 73 1473 EDITION OF 1 NOV 65 IS OBSOLETE

20. ABSTRACT (cont)

contents and greater number concentrations than fogs may be more sensitive to acoustic waves and may undergo significant changes in their spectra when acoustic energy is propagated through them. Thus, the application of the principles of acoustic agglomeration to the study of atmospheric phenomena may provide insight to the effect of thunder on cloud and precipitation processes as well as providing the basis for a new technology in weather modification.

In this thesis the theory of acoustic agglomeration is described and a one droplet model is developed to study the effects of acoustic waves on cloud droplets. A stochastic model used to predict changes in cloud droplet spectra due to gravitational sedimentation is modified to simulate the application of acoustic energy to various cloud volumes. The results are discussed and suggestions are made for further study of the phenomenon.

ACKNOWLEDGEMENT

The work described in this report was accomplished during the period of May 1983 to December 1984 while I was enrolled at the University of Oklahoma in Norman, Oklahoma. I would like to acknowledge the support of the people and facilities of the School of Meteorology of the University of Oklahoma.

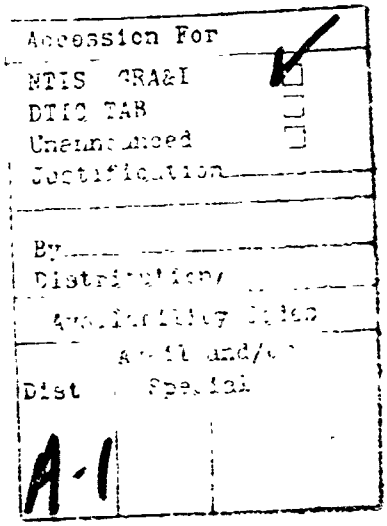

VARIABLES AND CONSTANTS

A_s	sound displacement amplitude	[L]
a	droplet or aerosol radius	[L]
a_o	mean aerosol radius of a spectrum	[L]
a'	particle vibrational displacement	[L]
c	speed of sound in air	$[LT^{-1}]$
E	energy density	$[ML^{-1}T^{-2}]$
E_g	gravitational collection efficiency	
E_{HY}	hydrodynamic collection efficiency	
E_{OK}	orthokinetic collection efficiency	
F	sound drift force	$[MLT^{-2}]$
f	sound frequency	$[T^{-1}]$
g	gravity	$[LT^{-2}]$
I	sound intensity	$[MT^{-3}]$
IL	sound intensity level (dB)	
K	collection kernel	$[L^3T^{-1}]$
k	sound wave number	$[L^{-1}]$
L	liquid water content	$[ML^{-3}]$
m_d	droplet mass	[M]
N	number concentration	$[L^{-3}]$
n	number concentration per volume interval	$[L^{-6}]$
P_a	sound pressure amplitude	$[ML^{-1}T^{-2}]$
p'	sound perturbation pressure	$[ML^{-1}T^{-2}]$

p	ambient air pressure	$[ML^{-1}T^{-2}]$
R	universal gas constant	$[L^2K^{-1}T^{-2}]$
s	droplet separation distance	$[L]$
T	temperature	$[K]$
t	time	$[T]$
v_a	air velocity amplitude	$[LT^{-1}]$
v_a	droplet velocity amplitude	$[LT^{-1}]$
v'	velocity of air	$[LT^{-1}]$
v_d	droplet velocity	$[LT^{-1}]$
v_t	droplet terminal velocity	$[LT^{-1}]$
x, x'	droplet volume	$[L^3]$
β	agglomeration refill coefficient	
γ	ratio of specific heats	
η	dynamic viscosity of air	$[ML^{-1}T^{-1}]$
μ_a	flow around factor	
μ_d	drop entrainment factor	
μ_{12}	relative entrainment factor	
ν	kinematic viscosity coefficient	$[L^2T^{-1}]$
ξ	phase angle	
ρ_a	air density	$[ML^{-3}]$
ρ_d	droplet density	$[ML^{-3}]$
τ	droplet relaxation time	$[S]$
ω	angular sound frequency	$[T^{-1}]$

CONTENTS

LIST OF TABLES

LIST OF FIGURES

Chapter I

INTRODUCTION

In the late 1920's a number of experiments were conducted to investigate the properties of high intensity, ultrasonic vibrations in liquids. The results led to similar experiments in gases where it was noted that particulates suspended in the gas tended to cluster and form aggregates. Thus began research in the field of acoustic (or sonic) agglomeration (or coagulation). As described by Mednikov (1965) perhaps the most notable of the early experiments in this field were those of Brandt, Freund, and Hiedeman using tobacco smoke suspended in air. Among other things they showed the strong frequency dependence of the phenomenon. In particular they discovered that agglomeration occurred more readily when sound frequencies were reduced to within the audible range.

Through the 1930's the interest in exploring the fundamental nature of the subject waned while the search for practical applications continued. According to Boucher (1960) it was in 1931 that interest in the meteorological application of the process first occured when A. Amy took out a U. S. patent for a device to clear fogs around airports by agglomeration of droplets to precipitable size. The device was to consist of a set of whistles arranged in a gimbaled frame which was to be attached to an aircraft. When the aircraft flew over or through the fog the device would emit a sonic beam which could be swept back and

forth like a searchlight and saturate the cloud with acoustic energy. It is not mentioned whether the device was actually ever assembled or tested.

Significant advances in the application of sonic agglomeration came during the World War II years when efficient, high energy output sound sources became available in the form of sirens manufactured by U.S. firms. Since then there has been continuous progress in the area of industrial application. Uses include the removal of particulate matter from the exhaust of industrial plants. It has been proposed (Shaw and Rajendran, 1979) that acoustic agglomeration could be used to control the radioactive sodium particles that would result from a fire in a Liquid Metal Fast Breeder Reactor plant.

There have also been some attempts at applications of acoustic agglomeration to the atmosphere. Most of the work was done from World War II through the mid 1950's and was directed toward clearing fog from the vicinity of airfields. In a series of field experiments (Boucher, 1960) it was shown that warm fogs could be acoustically treated to increase visibility by as much as 100 percent. This success seemed to be limited to quiescent conditions and no improvements in visibility were noted when wind speeds were greater than around 5 to 10 m.p.h. Nevertheless, the important point was the demonstration that cloud droplet spectra can be modified by the application of acoustic energy. This fact suggests the mechanism of acoustic agglomeration has possible ramifications for the field of meteorology in the effects of thunder on cloud processes and as a potential tool for use in weather modification efforts.

The purpose of this thesis is to briefly review pertinent acoustical theory and aerosol mechanics relating to acoustic agglomeration and to describe the results of two numerical models simulating acoustically stimulated cloud droplets.

Chapter II

THE SOUND FIELD AND THE SINGLE AEROSOL

The theory of acoustic agglomeration has been reviewed by Mednikov (1965), Shirokova (1970), and Shaw (1978). In this chapter the theory is outlined in some detail since it is a topic not frequently encountered in meteorology. The discussion closely follows Mednikov (1965). The theory discussed here is limited to the traveling wave phenomena since in the free atmosphere significant standing sound wave phenomena are not expected to occur. In the following pages the theory is developed by considering the structure of the sound field and then examining the forces a single aerosol in that field encounters. It should be noted that the word aerosol will be used generically to refer to any dispersed matter suspended in air and, in particular, is used synonymously with droplet throughout this thesis.

A discussion of the interactions between droplets in a sound field is deferred until the next chapter.

2.1 THE SOUND FIELD

The coagulation or agglomeration of aerosol particles is described by Shirokova (1970) as a series of basic subprocesses, namely, particle convergence, collision of the particles, coalescence of the particles, and precipitation of the agglomerates. Here we are concerned with the forcing of these subprocesses due to the application of sonic waves to the medium.

2.1.1 Plane progressive sound waves

In an ideal gas when the sound intensity level is less than about 110 db the sound field may be described in terms of variations in the pressure p', the velocity u', and the fluid displacement a' of the medium. These three periodic functions are expressed in the familiar forms

$$p' = P_a \cos\omega t \ , \tag{2.1}$$

$$u' = U_a \cos\omega t \ , \tag{2.2}$$

and

$$a' = A_a \sin\omega t \tag{2.3}$$

where P_a, U_a, and A_a are the pressure, velocity, and displacement amplitudes respectively, and the frequency in rad s^{-1} (ω) or in Hz (f) is related to the wave speed c and the wave number k by

$$\omega = 2\pi f = ck \ . \tag{2.4}$$

The speed of the sound wave propagation is given by

$$c = (\gamma RT)^{1/2} = (p\gamma/\rho_a)^{1/2} \ . \tag{2.5}$$

where γ is the ratio of the specific heats, R is the universal gas constant, T is the mean temperature of the fluid, p is the ambient pressure of the fluid, and ρ_a is the density of the fluid.

The velocity, pressure, and displacement amplitudes are related to the sound intensity by

$$U_a = \left(\frac{2I}{\rho_a c}\right)^{1/2} , \tag{2.6}$$

$$p_a = \rho_a c U_a , \tag{2.7}$$

and

$$A_a = \frac{U_a}{\omega} , \tag{2.8}$$

where the sound intensity I, which is a measure of acoustic energy flux, is given by the expression

$$I = \frac{p_a^2}{\rho_a c} . \tag{2.9}$$

The sound intensity is usually expressed as a sound intensity level in decibels (db) given by

$$IL = 10 \log_{10}(I/I_0) \tag{2.10}$$

where $I_0 = 10^{-12}$ W m^{-2} (10^{-16} W cm^{-2}).

This description of a sound wave assumes a plane wave front in an ideal medium and the relationships are derived by linearization of the equations governing fluid motion where second and higher order terms have been neglected. For situations in which the intensity of the sound is large there are higher order effects which must be considered. Some of these effects include inhomogeneities in the sound field, distortion

in the shape of the wave, increased absorption by the medium, radiation pressure, acoustic wind, and acoustic turbulence. In subsequent sections some higher order effects which relate to the behavior of aerosol particles in the sound field will be discussed.

2.2 THE MOTION OF AN AEROSOL IN A SOUND FIELD

In this section the forces acting on a single droplet are considered as an introduction to the effects of sound on aerosol mixtures. The forces acting on the isolated aerosol can be classified into two categories, namely, viscous forces and drift forces. The viscous effects of the fluid produce entrainment of the aerosols in the fluid motion while the drift forces, which arise due to second and higher order effects of sound in the fluid, produce a steady drift of the aerosols. Both of these categories are discussed in the following pages.

2.2.1 Entrainment

Entrainment refers to the degree to which aerosol particles participate in the vibrational motion of the fluid. When a sound field is set up in a volume of air the fluid particles will begin to oscillate in a periodic manner. Aerosols contained in the volume will also tend to oscillate but will not be fully entrained in the oscillatory motion. The amount of entrainment may be approximated from the Stokes equation for the motion of a particle given by

$$m_d \frac{du_d}{dt} = 6\pi\eta a(u' - v_d) \tag{2.11}$$

where v_d is the aerosol speed, m_d is the aerosol mass, η is the dynamic viscosity coefficient of the fluid, and a is the radius of the aerosol. The relaxation time for the droplet, i.e., the time required for the droplet and the air to come to equilibrium if either is impulsively pushed past the other, is defined by

$$\tau = \frac{2\rho_d a^2}{9\eta} . \tag{2.12}$$

Since

$$m_d = \frac{4}{3}\rho_d \pi a^3 ,$$

equation (2.11) may be rewritten using (2.2) and (2.12) to obtain

$$\tau \frac{du_d}{dt} + u_d = U_a \sin\omega t \tag{2.13}$$

which has a general solution

$$u_d = \frac{U_a \sin(\omega t - \xi)}{(1 + \omega^2\tau^2)^{1/2}} + \frac{U_a \omega\tau}{1 + \omega^2\tau^2} e^{-t/\tau} \tag{2.14}$$

where ξ is a phase shift such that

$$\tan\xi = \omega\tau . \tag{2.15}$$

This phase shift arises due to the inertia of the droplet which prevents it from moving exactly with the air motion. The second R.H.S. term of (2.14) approaches zero after a time $t = \tau$ so that the droplet motion may be described by

$$u_d = \frac{U_a \sin(\omega t - \xi)}{(1 + \omega^2\tau^2)^{1/2}} \cdot \tag{2.16}$$

The droplet and the air each reach maximum velocity when the cos term in (2.2) and sin term in (2.16) each equal one. The maximum speed of the drop is then

$$u_d = \frac{U_a}{(1 + \omega^2\tau^2)^{1/2}} \cdot$$

Equation (2.16) may be rewritten as

$$u_d = \mu_d U_a \sin(\omega t - \xi) \tag{2.17}$$

where

$$\mu_d = \frac{1}{(1 + \omega^2\tau^2)^{1/2}} \cdot \tag{2.18}$$

Equation (2.18) may be rewritten using equation (2.15) to get

$$\mu_d = \cos\xi \ . \tag{2.18a}$$

Substituting for ω and τ from (2.4) and (2.12) yields the two equations for entrainment

$$u_d = \frac{1}{\left[1 + \left(\frac{4\pi\rho_d a^2 f}{9\eta}\right)^2\right]^{1/2}} \tag{2.19}$$

and

$$\tan\xi = \frac{4\pi\rho_d a^2 f}{9\eta} . \tag{2.20}$$

Thus the degree of entrainment is determined by the size of the term $(4\pi\rho_d a^2 f/9\eta)^2$ and in particular by the product $a^2 f$.

Another useful parameter is the flow around factor, i.e., the flow of the medium relative to the entrained droplet. An expression may be derived by subtracting the drop speed (2.17) from the speed of the air (2.2)

$$u_{ad} = U_a \sin\omega t - \mu_d U_a \sin(\omega t - \xi) .$$

Now using trigonometric identities and equation (2.18a) the flow around speed is written

$$u_{ad} = (\sin\omega t - \sin\omega t \cos^2\xi + \cos\omega t \sin\xi\cos\xi) U_a$$

or

$$u_{ad} = \mu_a U_a \cos(\omega t - \xi) \tag{2.21}$$

where

$$\mu_a = \sin\xi = \frac{\omega\tau}{(1 + \omega^2\tau^2)^{1/2}} \tag{2.22}$$

Additionally, it can be seen from (2.18a) and (2.22) that

$$\mu_a = \sin\xi = \frac{\omega\tau}{(1 + \omega^2\tau^2)^{1/2}} \quad (2.22)$$

Additionally, it can be seen from (2.18a) and (2.22) that

$$\mu_d^2 + \mu_a^2 = 1 \quad . \quad (2.23)$$

Fig. 1 shows the plots of entrainment and flow around for various droplet sizes and sound frequencies. It can be seen from the figure that for small droplets at low sound frequencies entrainment is almost complete while for large droplets at high frequencies the amount of entrainment is minimal.

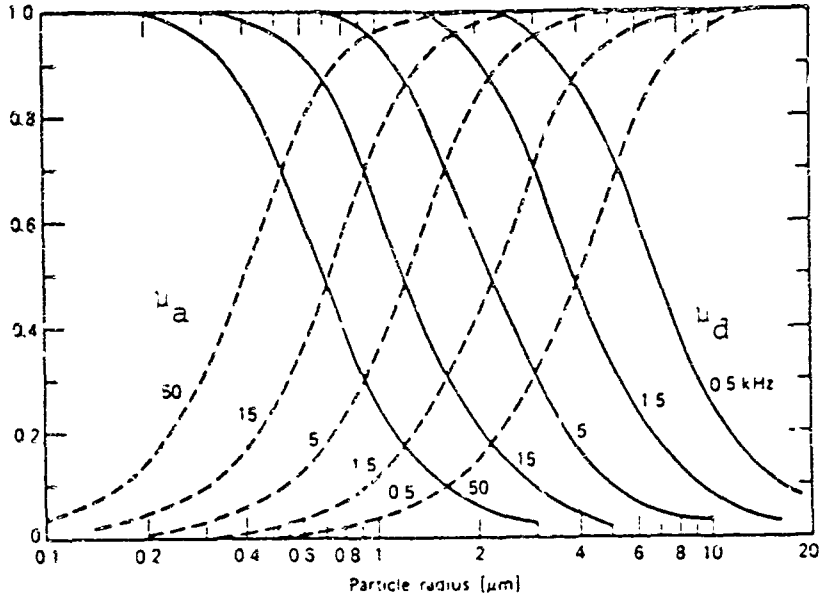

Figure 1: Entrainment and Flow-around Factors for Various Sound Frequencies. (Solid - entrainment, dashed - flow-around: after Shaw and Rajendran, 1979.)

2.2.2 Particle drift

Aerosol particle drift may play an important role in acoustic agglomeration by moving aerosols close to one another so that mechanisms discussed in Chapter III can cause collisions to occur. Among the factors contributing to particle drift in a traveling wave are radiation pressure, periodic viscosity changes, vibrational phase differences, and distortion of the sound wave. These will be described in turn.

When a sound wave encounters any obstacle in the fluid the wave energy is scattered. In the case of a drop some of the energy is scattered in the direction of propagation. There is a momentum transfer

associated with this process and since more momentum is transferred to the drop by the wave than is transferred by the drop in the direction of propagation, there remains a net force on the drop which is the momentum back-scattered toward the source. Expressions for the radiation pressure force on a drop have been derived by King (1934) and Landau and Lifshitz (1959). The radiation pressure force for spherical particles is given by

$$F_R = \frac{11}{9}\pi\left(\frac{\omega}{c}\right)^4 a^6 \mu_a^2 E \tag{2.24}$$

where $E = 2I/c$ is the sound energy density.

The next two drift forces were proposed by Westervelt (1950) in a paper dealing with the mean pressure and particle velocity in a sound wave. In that paper Westervelt treated the two forces as a single force which he termed a Stokes force. Mednikov (1965) separated the two forces attributing one to changes in viscosity and the other to phase differences in the vibration of the fluid particles.

First the drift force due to changes in viscosity is discussed. Because of the periodic adiabatic compressions and rarefactions of a sound wave there occur periodic temperature changes. Therefore, since it is a function of temperature, viscosity increases during compression and decreases during rarefaction. During compression a droplet is being moved in the direction of propagation and because the viscosity is greater the droplet is more fully entrained in the fluid motion. The exact opposite process occurs during a rarefaction. The result is a net force in the direction of propagation given by

$$F_n = 3\pi(\gamma-1)\frac{v}{c}a\mu_a^2 E \quad . \tag{2.25}$$

The drift force which arises due to phase differences in the vibration of adjacent fluid particles is very complex and difficult to explain in either a dynamic or kinematic sense. For a detailed discussion the reader is referred to Westervelt (1950), Westervelt (1951), and Mednikov (1965). An expression for the resulting force on aerosols suspended in the fluid is given by

$$F_p = -6\pi\frac{v}{c}a\mu_a^2 E \quad . \tag{2.26}$$

The last drift force discussed is the one due to distortion or wave asymmetry. High intensity sound waves can become distorted and assume a sawtooth structure. During a compression the fluid particles are moving in the direction of propagation and thus pick up some of the wave speed. During rarefaction the particles move opposite to propagation with the pressure induced velocity less some of the wave velocity. As a result the wave slope is usually steeper during the compression portion of the wave than during the rarefaction portion, and, therefore, the velocity usually increases rapidly in the direction of propagation while increasing more slowly in the opposite direction. Since an aerosol in the region of rapidly increasing speed will be less fully entrained than when it is in the region of slowly increasing speed there results a net force in the direction opposite to propagation. This force may be expressed as

$$F_h = -6h_2 \sin\lambda \; a^2 \mu_a^2 E \; . \qquad (2.27)$$

where h_2 is the relative velocity amplitude of the second harmonic and λ is the phase angle of the second harmonic.

The relative importance of the drift forces under various conditions can be seen by evaluating (2.21) through (2.25) using typical values for the variables and factoring the common term $a\mu_a^2 E$ from each expression. Table 1 shows relative values (cm) of the scaled forces for three droplet sizes. Here f = 1000 Hz, $c = 3 \times 10^4$ cm s^{-1}, $v = 10^{-1}$ cm^2 s^{-1}, and $\gamma = 1.4$. The values for h_2 and $\sin\lambda$ are taken to be unity in order to obtain the maximum value of the expression. It is clear that the largest force is that due to asymmetry of the sound wave when the sound wave is significantly distorted. When distortion is not a factor then the drift due to particle vibration phase differences is generally the largest. Also it is clear that for applications of interest in this study the radiation pressure force is negligble. However, being strongly dependent on particle radius, this force can become dominant for large particles and is responsible for the phenomenon of suspended objects in a sound field (St. Clair, 1949).

TABLE 1

Relative Values of Drift Forces

FORCE		a (μ) 1	10	100
Radiation	$\frac{11}{9}\pi(\frac{\omega}{c})^4 a^5$	7.0×10^{-23}	7.0×10^{-18}	7.0×10^{-13}
Viscosity	$3\pi(\gamma-1)\frac{v}{c}$	1.3×10^{-5}	1.3×10^{-5}	1.3×10^{-5}
Phase	$-6\pi\frac{v}{c}$	-6.3×10^{-5}	-6.3×10^{-5}	-6.3×10^{-5}
Asymmetry	$-6h_2 a \sin\lambda$	-3.0×10^{-5}	-5.4×10^{-3}	-6.0×10^{-2}

2.3 A SINGLE DROP MODEL

A single droplet numerical model is used to examine the motions of a drop within a sound field. As noted earlier this model simplifies the problem of droplet behavior in an acoustic field since it neglects the presence of other droplets or particles which certainly force motions upon the droplet under consideration. But, this deficiency aside, it is of interest to study the motions of different sized drops under the influence of sound.

2.3.1 The Model Equations

The sound intensity required for the agglomeration of aerosols is high enough that distortion of the sound wave is significant. Thus, for the purposes of this example, the radiation pressure, viscosity change,

and vibrational phase forces are neglected based on the results described in Table 1.

In the previous section it was shown that the motion of a droplet due to the vibration of the air is given by equation (2.16). To describe the motion due to the drift forces it is assumed the drop relaxation times are very small while changes in the drift forces are much longer. These assumptions approximate an equilibrium where the drift forces are in a continuous balance with the Stokes resistive force. Thus the velocity due to each force is obtained by equating the force to the Stokes drag force

$$F_{ST} = 6\pi\eta a u_d \ .$$

Then the approximate total velocity of the drop is given by

$$u_d = U_a \sin(kx-wt) - \frac{h_2 \sin\lambda}{\pi n} a\mu_a^2 E \qquad (2.28)$$

where it is assumed that the phase shift of the second harmonic is $\pi/2$.

In order to examine the validity of the Stokes flow assumption a Reynolds number for a drop in an acoustic field is defined by the expression

$$Re_{AC} = \frac{2aU_d}{v} \qquad (2.29)$$

where v is the kinematic viscosity coefficient and U_d is the maximum velocity of the droplet given by $U_d = \mu_d U_a$. The Reynolds numbers for drops at different sound intensity levels are plotted in Fig. 2. The

solid curve in the figure is a plot for drops falling at their terminal velocities. The dashed curves, by increasing slope, represent sound intensity levels of 100 db, 120 db, 140 db, and 160 db, respectively. As an example, the Reynolds number is less than one for drops up to 10 μ radius at a sound intensity level of 140 db. For situations in which the Reynolds number is greater than one, an Oseen correction (Mednikov, 1965) is applied to the Stokes velocity by use of the equation

$$u_{oc} = \frac{4v}{3a} + \left[\left(\frac{4v}{3a}\right)^2 + \frac{8v}{3a} u_d\right]^{1/2} . \qquad (2.30)$$

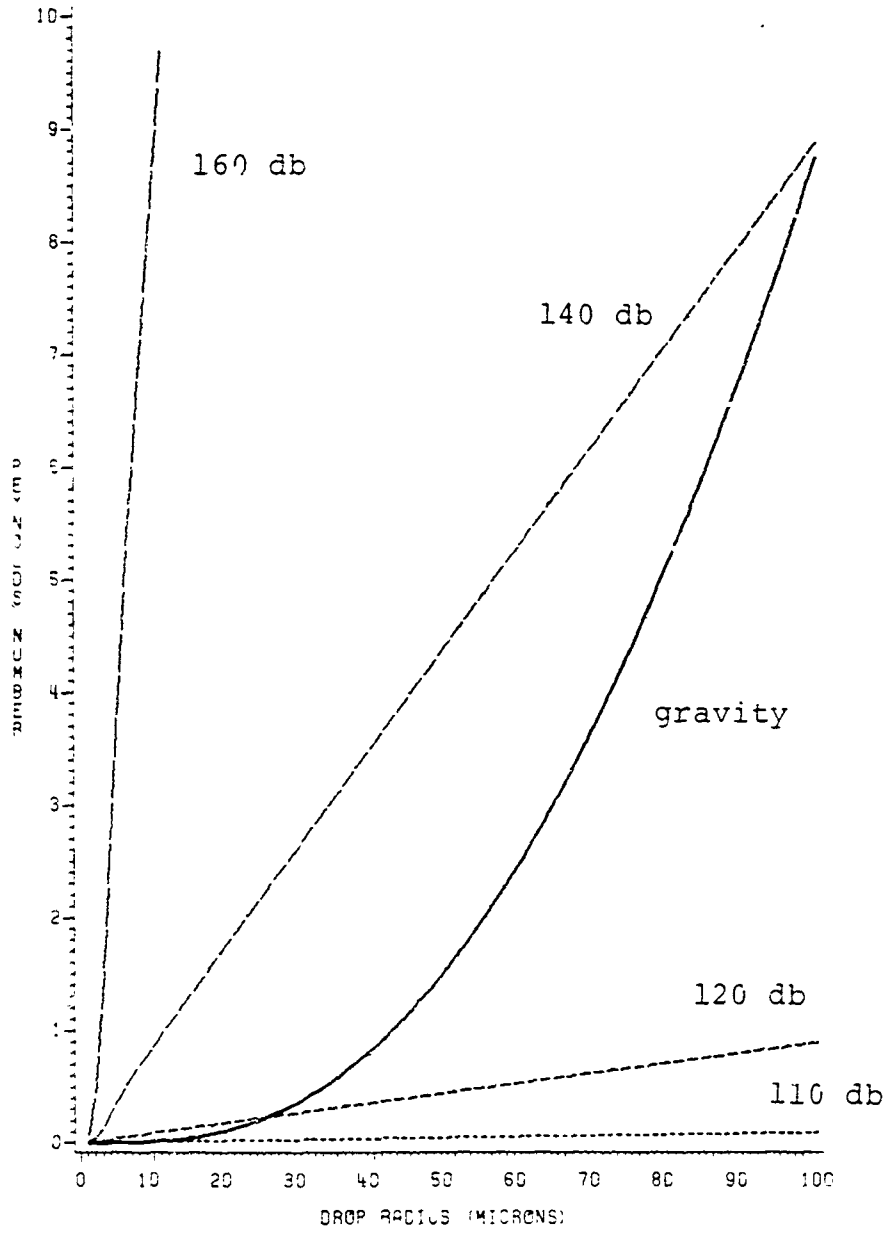

Figure 2: Acoustic Reynolds Numbers.(Solid curve is for drops at terminal velocity, dashed curves for drops at various acoustic intensities.)

2.3.2 Results

A model based on equation (2.28) has been used to examine the motions of various sized droplets. In the examples discussed here the values of the atmospheric and sound variables included p = 765 mb, T = 283 K, IL = 140db, and f = 1000 Hz.

In Fig. 3 through Fig. 5 plots of displacement vs. time are shown for drops of 1, 10, and 20 μ respectively. The scale of the plots is the same in each figure. It is evident that the greatest amplitude of vibration occurs in the case of the 1 μ droplet while there is no apparent drift for this same droplet. Further, it is clear from these figures that as drop size increases, vibrational amplitude decreases and drift velocity increases.

In this section the motions of isolated droplets were examined. In the next chapter the discussion focuses on the more important case where adjacent aerosols induce motions on one another.

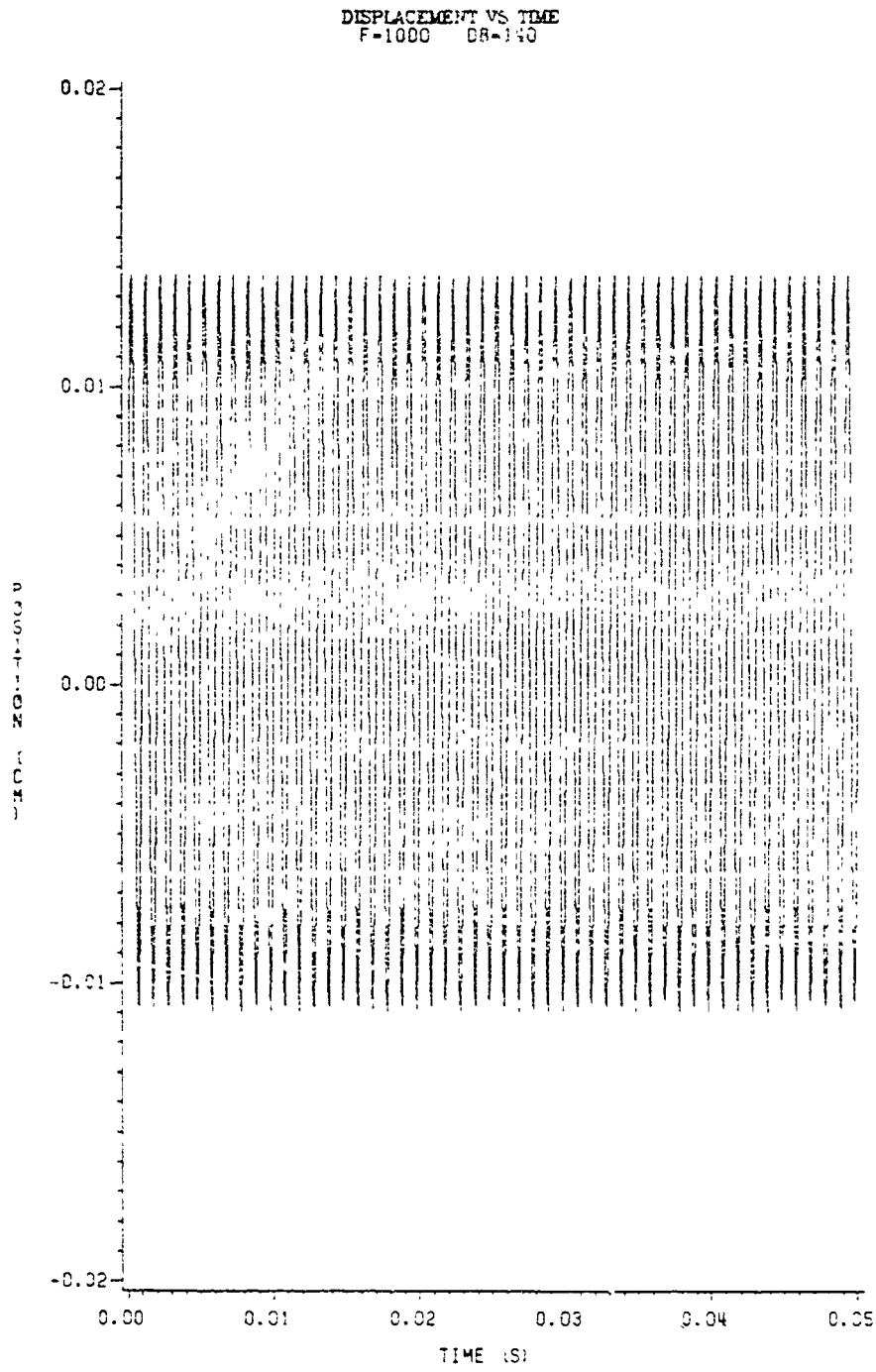

Figure 3: Motion of a 1 micron droplet.

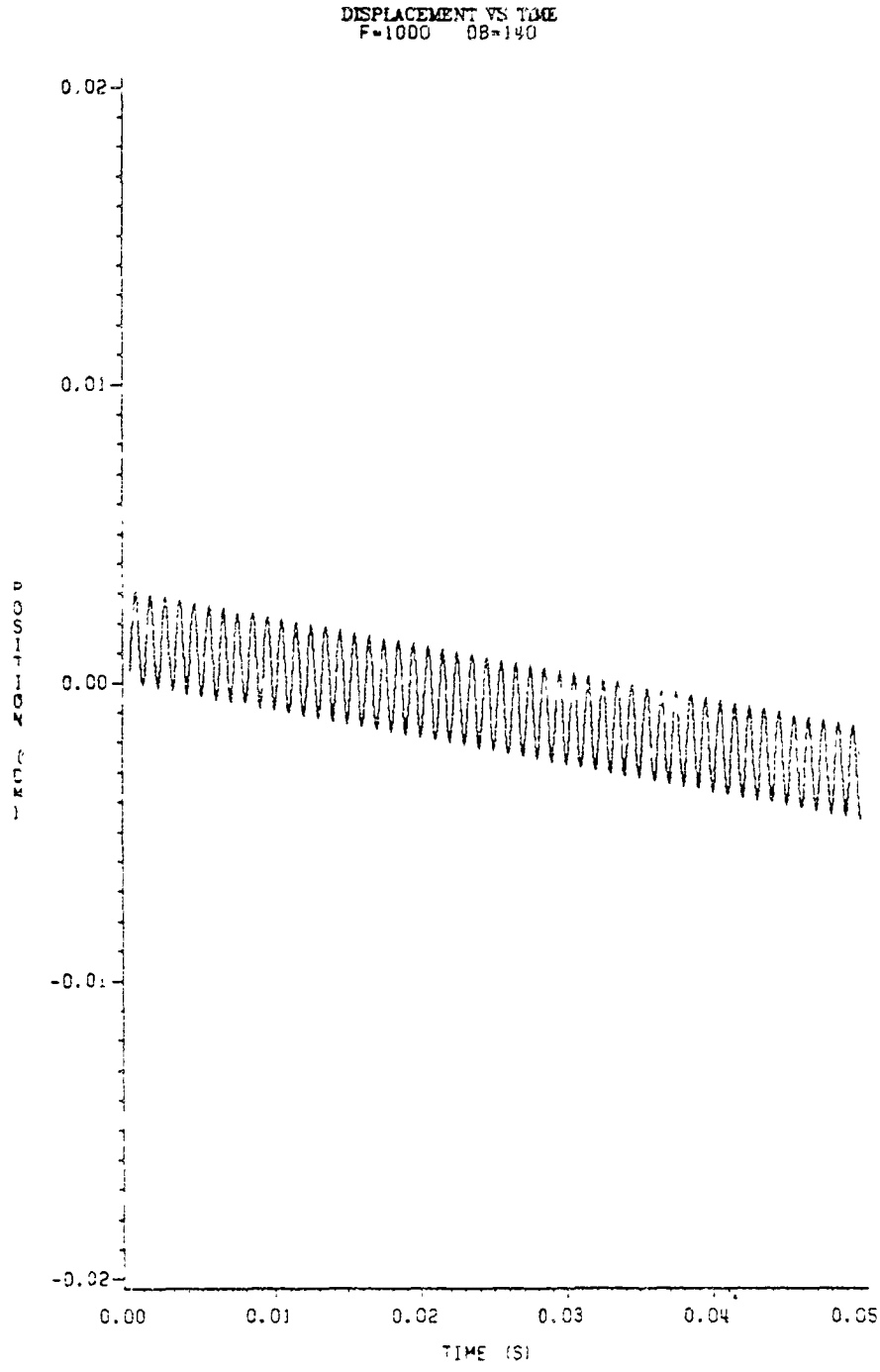

Figure 4: Motion of a 10 micron droplet.

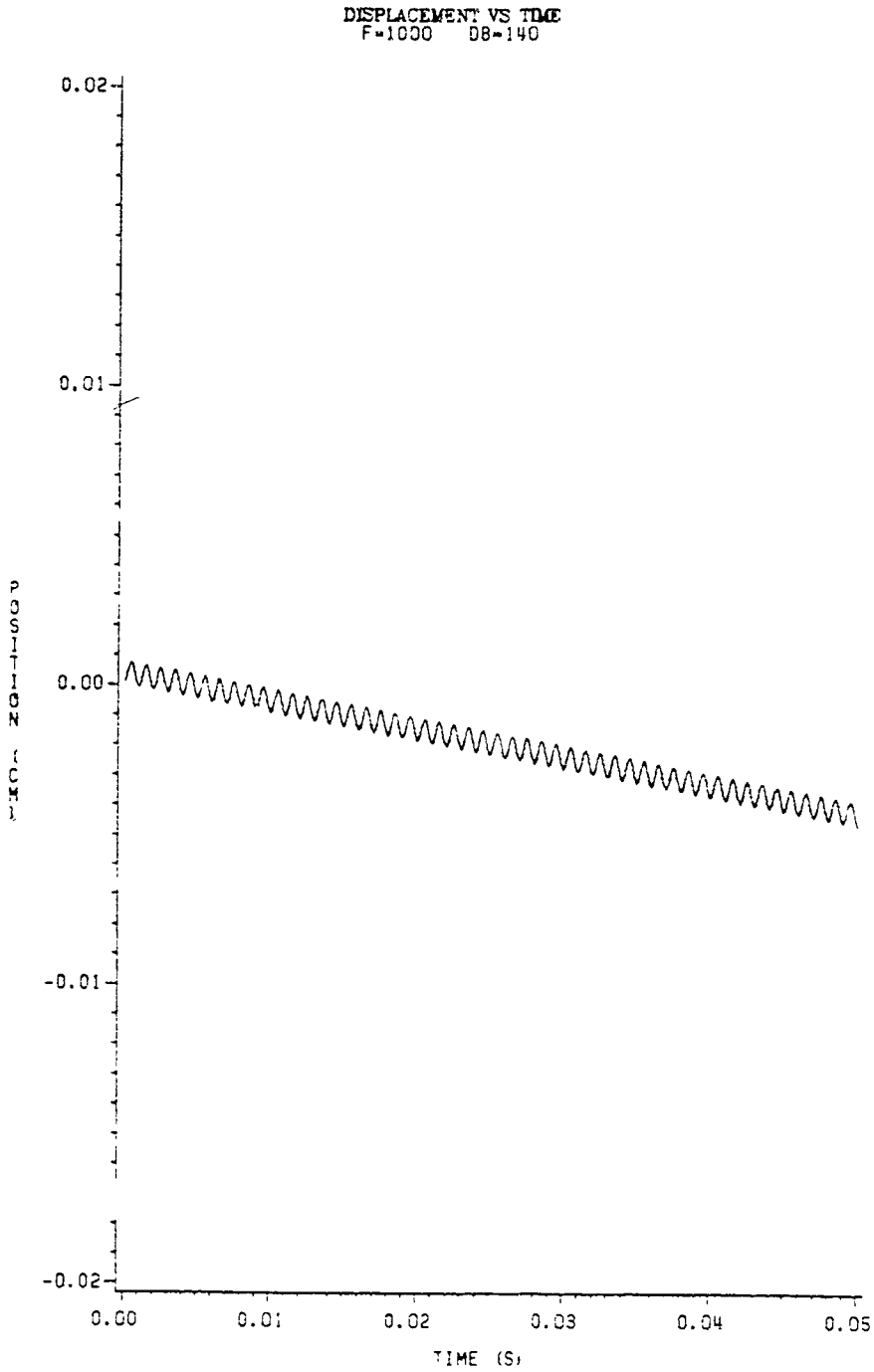

Figure 5: Motion of a 20 micron droplet.

Chapter III

INTERACTIONS OF AEROSOLS IN A SOUND FIELD

The motions discussed in the previous chapter do not take into account the presence of nearby aerosols which can have important and even dominating effects on aerosol motion. In this chapter some of the motions due to drop interactions in an acoustic field are discussed.

Mednikov (1965) classifies four types of motions due to interaction as orthokinetic, parakinetic, attractional, and pulsational. In the following description the interactions are more generally classified as orthokinetic, hydrodynamic, and turbulent where the parakinetic and attractional interactions are grouped under the hydrodynamic classification. The pulsational interaction will be called turbulent interaction in this thesis.

3.1 ORTHOKINETIC INTERACTION

The orthokinetic interaction is that which occurs between drops whose centers lie along a line which is parallel to the direction of motion. This motion may be the result of drift or some turbulent pulsation but the most significant contributor is the vibrational motion induced by the periodic sound wave. An expression for the relative velocity of two droplets may be found by subtracting the respective velocities given by (2.17) to get

$$u^* = \mu_{d1} U_a \sin(\omega t - \xi_1) - \mu_{d2} U_a \sin(\omega t - \xi_2).$$

To find the maximum difference in speed the above equation is differentiated with respect to time and set equal to zero to get an expression for the frequency. Using equations (2.18a) and (2.22) the result is written

$$\tan\omega t_0 = \frac{\mu_{d2}^2 - \mu_{d1}^2}{\mu_{d1}\mu_{a1} - \mu_{d2}\mu_{a2}}$$

where t_0 is the time at which the maximum difference occurs. Now the maximum relative velocity is termed U^* and is given by

$$U^* = \mu_{d1} U_a \sin(\omega t_0 - \xi_1) - \mu_{d2} U_a \sin(\omega t_0 - \xi_2)$$

or

$$U^* = [\mu_{d1}(\sin\omega t_0 \cos\xi_1 - \cos\omega t_0 \sin\xi_1) - \mu_{d2}(\sin\omega t_0 \cos\xi_2 - \cos\omega t_0 \sin\xi_2)]\, U_a .$$

Using (2.18a) and (2.22) gives

$$U^* = [\sin\omega t_0 (\mu_{d1}^2 - \mu_{d2}^2) - \cos\omega t_0 (\mu_{d1}\mu_{a1} - \mu_{d2}\mu_{a2})]\, U_a .$$

Thus,

$$U^* = \mu_{12} U_a$$

where

$$\mu_{12} = \omega(\tau_1-\tau_2)(1 + \omega^2\tau_1^2)^{-1/2}(1 + \omega^2\tau_2^2)^{-1/2} . \qquad (3.1)$$

Equations (2.18) and (2.22) have been used to rewrite μ_{12} in terms of ω and τ. By taking the derivative of (3.1) with respect to ω and setting it equal to zero, an optimium frequency for agglomerating two droplets by the orthokinetic mechanism is found to be

$$\omega_{OPT} = \frac{1}{\tau_1 a_2/a_1}$$

or, with (2.12),

$$f_{OPT} = \frac{9\eta}{4\pi\rho_d a_1 a_2} . \qquad (3.2)$$

While giving useful information about the frequency to use on an initial spectrum, this expression is of limited practical applicability because the droplet sizes begin changing as soon as coagulation begins.

3.2 HYDRODYNAMIC INTERACTIONS

The physical basis for the hydrodynamic (attractional and parakinetic) interactions is well known and has been described theoretically by several authors (e.g. Lamb, 1932). It consists of the motions introduced as a result of the superposition of the flow fields around each droplet. In the simplest case there are two spheres of the same dimensions located in a fluid and separated by some distance. If the fluid flows past the spheres such that the streamlines are parallel to the line joining the centers of the spheres, the spheres will move

toward one another. Thus the attractional interaction in a sound field pertains to the approach and collision of droplets whose centers are essentially aligned with the streamlines of the acoustically induced fluid flow.

The parakinetic interaction, on the other hand, pertains to motion that occurs between two droplets whose centers are along a line not parallel to the streamlines. The idealized motion as described by Mednikov (1965) is a zig-zagging of the smaller droplets in the vicinity of a larger drop. The zig-zagging motion is such that droplets to the front or back of the collector tend to become centered along the collector's line of motion. Those droplets which are initially along a flank of the collector tend to be moved transversly away from the collector until they are caught up in streaming of the fluid past the collector and are carried forward or aft of the collector where they may begin the centering motions described previously.

Since the hydrodynamic interactions are important to the modeling of the agglomeration process, an expression for the speed of approach of two droplets in an acoustic field is needed. The agglomeration model that will be discussed in Chapter IV is based on the work of Chou, et. al., (1981) who used an expression derived from theory by Dianov, et. al., (1968). This is a general expression for the relative velocity of two spheres, not necessarily of the same size, under the conditions of Oseen flow in an acoustic field. The relative velocity is given by

$$u_{rel} = \frac{3U_a}{2\pi s}\{a_1 l_1 + a_2 l_2 + [(a_1 l_1)^2 + (a_2 l_2)^2]\frac{U_a}{\pi v}\}$$

$$- \frac{6v}{\pi^2 s^2}(a_1 + a_2)$$

$$- \frac{9U_a}{16\eta s^2}(a_1^2 l_1 + a_2^2 l_2)$$

$$+ \frac{3U_a^2}{8s^2\omega}\{a_1 l_1[q_2\cos(\xi_2-\xi_1)-q_1]$$

$$+ a_2 l_2[q_1\cos(\xi_1-\xi_2)-q_2]\} \qquad (3.3)$$

where s is the separation distance of the droplets. Other terms in (3.3) are defined by

$$l = \frac{\mu_a}{(1 + h\mu_a^2)} ,$$

$$q = \frac{\mu_d + h\mu_a^2}{(1 + h\mu_a^2)} ,$$

$$h = \frac{9\rho_a U_a}{2\pi\rho_d \omega a} ,$$

and

$$\xi = \tan^{-1}\left(\frac{\mu_a}{\mu_d + h\mu_a^2} \right)$$

where μ_a and μ_d are given by equations (2.18) and (2.22) respectively. The first three terms of (3.3) represent the velocity due to the mutual distortion of the flow fields around the two droplets. The fourth term represents the velocity due to the vibrational phase difference of the droplets.

Figure 6 shows plots of the relative velocities of various droplet pairs due to gravitational sedimentation and the acoustic hydrodynamic interaction. The relative velocities due to gravity were computed by subtracting the terminal velocities of the droplets. The hydrodynamic relative velocities were computed from equation (3.3). For this acoustic relative velocity calculation the droplet separation is 100 μ, the sound intensity level is 140 db, and the frequency is 1000 Hz. The top pair of solid and dashed curves is for a droplet with a radius of 22 μ. The other sets are for 16 and 10 μ, respectively. The relative velocity of two droplets falling at their terminal velocities approaches zero the closer the droplets are to the same size. However, in an acoustic field the relative velocity increases as the ratio of the drop sizes approaches unity. As can be seen in the figure, larger droplets may be expected to approach one another in an acoustic field at a rate significantly greater than experienced under the force of gravity alone.

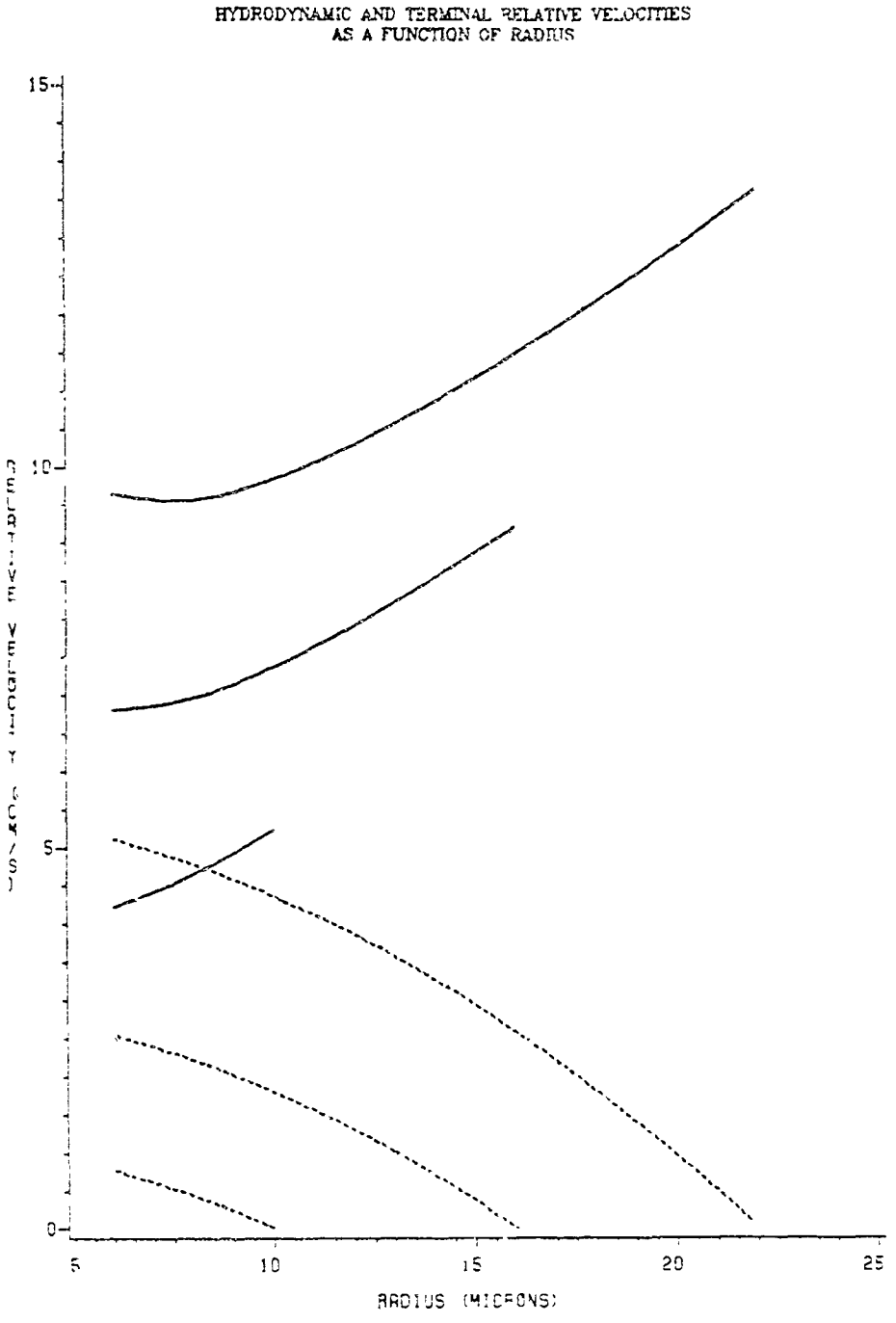

Figure 6: Relative Velocities Due to Gravity and Acoustics. (Solid curve is for drops in an acoustic field, dashed curves for drops falling at terminal velocity.)

3.3 TURBULENT INTERACTIONS

The onset of significant acoustic turbulence does not occur until sound intensities reach a relatively high level. With respect to the agglomeration process the onset of the turbulence effect does not occur until the sound intensity reaches levels around 160 db (Chou, et.al., 1981). Since sound intensities that high are generally not expected to be present over large cloud volumes, the models discussed in this thesis do not incorporate any turbulent processes. However, a short discussion of the turbulent effects is provided for general background in the subject of acoustic agglomeration.

The turbulent or pulsational interactions are due to motions arising from the acoustically induced turbulence in the flow field. There are essentially two interactions. The first is described as inertial and is characterized by a turbulence length scale small compared to the aerosols. Thus, the droplets are not fully entrained in the fluid motion and, since the motion field itself is inhomogenecus, the droplets simply cannot follow the rapid fluctuations in the fluid motion and collisions occur in a stochastic manner.

The second turbulent interaction is a diffusion process in which the length scale of the turbulence is large compared to the aerosols. Here droplets become fully entrained in the fluid motion, but, adjacent droplets have collisions because they have differing relative velocities due to the spatial inhomogeneities of the turbulent motion.

3.4 SUMMARY

Though all the motions and interactions described to this point certainly play some part in the process of acoustic agglomeration a complete theory of the process has not been fully developed. It was first believed (Brandt and Hiedemann, 1936) that the orthokinetic effect was the cause of agglomeration but since that effect requires size differences among the particles and agglomeration occurs in monodisperse populations as well as polydisperse, the theory required extension. Mednikov (1965) proposed that the most significant cause of agglomeration was the orthokinetic interaction while all the other motions acted to refill the collision volume. Shirokova (1970) argued that the orthokinetic mechanism is not as important as the hydrodynamic interaction of the particles. However, Cheng, et. al., (1982) demonstrated that the orthokinetic effect was dominant for the agglomeration of submicron particles when there was no acoustic turbulence present. In his review article Shaw (1978) states that the hydrodynamic interaction may be the most important cause of agglomeration particularly for relatively large sized particles. Shaw and Tu (1979) demonstrated experimentally that the hydrodynamic mechanism is important for aerosols greater than about 0.5 μ in radius.

In the next chapter a model of the agglomeration process is described and the results of numerical experiments for atmospheric conditions are discussed.

Chapter IV

MODELING CHANGES IN CLOUD DROPLET CONCENTRATIONS

Recent work on acoustic agglomeration in the United States has been done by Shaw and his associates at the Laboratory for Power and Environmental Studies at the State University of New York at Buffalo. They have developed numerical models which predict changes in aerosol spectra in good agreement with their experimental observations. The work to be described in this chapter is based on the work of Chou, Lee, and Shaw (1981) in which the results of a numerical model designed to simulate the acoustic agglomeration process in an aerosol mixture are compared to the results of laboratory experiments. Their numerical model was based on the theory of acoustic agglomeration and its results were in good agreement with the experimental results. In the research described here a similar numerical model has been used to examine the effects of acoustic agglomeration in an environment more characteristic of clouds.

4.1 THE MODEL EQUATIONS

4.1.1 The Stochastic Collection Equation (SCE)

The model used here is based on the stochastic collection equation given by

$$\frac{\partial n(x,t)}{\partial t} = \int_0^{x/2} K(x',x-x')n(x-x',t)n(x',t)\,dx' - n(x,t)\int_0^{\infty} K(x',x)n(x',t)\,dx' \qquad (4.1)$$

where K is a collection kernel, x and x' are droplet volumes, and n is the number concentration per drop volume at time t. The first R.H.S. term represents the gain in number of droplets of volume x due to collisions between droplets with volumes less than that of x. The second R.H.S. term represents a loss of droplets of volume x due to collisions with drops of all other volumes resulting in drops of volume greater than x. The physics of the collection kernel will be discussed in the next section.

4.1.2 The Collection Kernel

Previous work on acoustic agglomeration has been mainly concerned with highly concentrated aerosols contained within small volumes over which it is feasible to maintain high sound intensities. In the Chou study, which was concerned with conditions such as those just listed, four collection kernels were used. There was one kernel defined for each of the following acoustic aerosol interactions: orthokinetic, hydrodynamic, diffusional turbulent, and inertial turbulent. However, practical limitations suggest that it is not feasible to maintain high intensity level (>150 db) sound over the volumes encountered in working with atmospheric clouds. For this reason the model used in this work

neglects the effects of turbulent processes which become important at sound intensity levels of around 160 db. Thus, the acoustic agglomeration kernels used in this work are for the hydrodynamic and orthokinetic processes. In addition, a kernel for gravitational sedimentation is added to simulate the coalescence process that continues after the simulated sound is terminated.

The concept of a collection kernel is based on the volume swept out per unit time by a colliding droplet pair. The volume is called a collision volume and its cross section is the geometric cross section multiplied by a collection efficiency. The length or height of the volume is the distance traveled by the approaching drops per unit time. The most generally recognized collection kernel is that for gravitational sedimentation or geometric sweep out given by

$$K_g = E_g \pi (a_1+a_2)^2 (v_{t1}-v_{t2}) \tag{4.2}$$

where E_g is the collection efficiency due to gravity and v_t is the terminal velocity of the droplet.

The two acoustic collection kernels used here are the same as those used in Chou, et. al. (1981). The orthokinetic collection kernel was derived by Mednikov (1965). In this case the cross sectional area of the collision volume is the same as described above. But the length of the volume is twice the relative displacment amplitude of the drops multiplied by the frequency or number of oscillations per unit time. The collection kernel may be written

$$K' = 2\pi E_{OK} (a_1+a_2)^2 A_{12} t$$

where A_{12} is the relative amplitude of vibration of the two droplets. After one complete vibration the large drop is assumed to have collected all the little drops within the agglomeration volume. However, additional small drops may move into the volume due to any of the drift or interaction motions discussed in earlier chapters. Therefore, an additional coefficient, called a refill factor, is necessary to account for small droplets moving back into the volume after each oscillation. Thus,

$$K = 2\beta\pi E_{OK}(a_1+a_2)^2 A_{12} f$$

where β is the refill factor. Now, using $A_{12} = \mu_{12} A_a$ and equations (2.4) and (2.8) the orthokinetic kernel is written

$$K_{OK} = E_{OK}\frac{N_1}{N_t}(a_1+a_2)^2 \mu_{12} U_a \tag{4.3}$$

where N_1 is the number concentration of large droplets, N_t is the total concentration, and μ_{12} is the relative entrainment coefficient given by equation (3.1). In this final form Chou has used $\beta = N_1/N_t$ to define the refill factor. The validity of this choice is assumed to be empirically based since no analytical expression for the refill factor has yet been found. However, as mentioned before, the results of Chou's model agree well with experimental results.

The second acoustic kernel is the hydrodynamic kernel which is given by

$$K_{HY} = E_{HY}\pi(a_1+a_2)^2 u_{rel} \tag{4.4}$$

where u_{rel} is the relative velocity given by (3.3). The physical basis of this kernel is directly analogous to that of the gravitational kernel. Here the relative motion of the two droplets is due to acoustic forces rather than gravity.

It is appropriate to make a few comments about the collision efficiencies in the collection kernel equations. As noted above each of the collision efficiencies is different for each process. For the gravitational kernel the collision efficiency is that used in the Leighton and Rogers (1974) version of the Berry and Reinhardt (1974a) SCE model. That is the Shafrir and Neiburger (1963) scheme for pairs with $a_1 > 30$ μ and Hocking and Jonas (1970) for pairs with $a_1, a_2 \leq 30$ μ.

In order to find values for the collision efficiencies of aerosols in an acoustic field Shaw (Shaw, 1978μ Shaw and Rajendran, 1979μ Shaw and Tu, 1979μ and Chou, et. al., 1981) examined the dynamical similarity of aerosols in close proximity in a gravitational field versus aerosols in an acoustic field. He reasoned that, because of differences in acoustic entrainment, aerosols in an acoustic field approach one another with some relative velocity in much the same manner as aerosols falling at their terminal velocities. By non-dimensional analysis of the equations of motion of aerosols in the two different fields, he showed that the collision process is similar as long as the actual radius of the larger aerosol is replaced by an acoustically equivalent radius given by

$$a_e = a_1 \left(\frac{\mu_a}{g\tau_1}\right)^{1/3} \left(\frac{2I}{\rho_a c}\right)^{1/6} . \qquad (4.5)$$

This formulation accounts for the fact that aerosols of a given size have greater relative velocities in an intense acoustic field than due to gravity alone. Thus, by using the value of a_e for the large drop in an expression for the collision efficiency due to gravitional sedimentation, the collision efficiency due to acoustically driven motion can be found. In particular, Chou (1981) uses the formula of Langmuir (1948) for the orthokinetic collision efficiency and the formulation of Scott and Chen (1970) for the hydrodynamic collision efficiencies. The same formulas are used in the model described in this thesis.

It is of some value to examine the sensitivity of the acoustic collection kernels to variations in the environment. It should be kept in mind that the discussion does not describe the extremely complex agglomeration process. The intent of the following is to construct some framework for understanding the complete process by examining very limited interactions. The relative effects of environmental variables on each kernel are illustrated in Fig. 7 through Fig. 13. These curves were calculated for the following environmental and sound field values: p = 765 mb, T = 283 K, a_o = 12 μ, var = 1.0, IL = 140 db, f = 1000 Hz, and L = 1.0 g m^{-3}. Each of these parameters was varied in turn to obtain the kernel values depicted in the figures. The radii of the droplet pair for each kernel were selected arbitrarily and the results depicted would change only in magnitude for different droplet pairs. In the gravitational and orthokinetic kernels a_1 = 4 μ and a_2 = 20 μ for all cases. In the calculation of the hydrodynamic kernels $a_1 = a_o$ and $a_2 = 0.7a_o$. In all of the diagrams the solid line represents the

orthokinetic kernel and the dashed line represents the hydrodynamic kernel. For reference purposes the value of the gravitational kernel for $a_1 = 4\ \mu$ and $a_2 = 20\ \mu$ is $K_g = 6.14 \times 10^{-6}\ cm^3\ s^{-1}$ and is relatively insensitive to the environmental variations studied here.

Fig. 7 shows that both the orthokinetic and hydrodynamic kernels increase with increasing sound intensity. Both of these effects can be attributed to the increase in the amplitude and velocity of the medium's oscillations as shown in equations (2.8) and (2.10). In the orthokinetic interaction the displacement of each aerosol increases thereby increasing the size of the collision volume. Also, the relative velocities of the collision pairs are greater. For the hydrodynamic interaction the relative velocity of the pair increases due to the increased speed of the fluid past the aerosols.

The sensitivity to sound frequency changes is shown in Fig 8. For the orthokinetic effect the kernel increases to a peak around 200 Hz and falls off asymptotically from there. The response of the orthokinetic kernel to changes in frequency is explained in terms of the entrainment of the drops which is governed by equation (2.19). For example, the decrease in magnitude of the kernel with increasing frequency arises because both droplets are less fully entrained in the air motion. The increasing followed by decreasing behavior of the curve occurs since there are also relative entrainment effects. The maximum value for a droplet pair occurs at the frequency given by equation (2.27). Dianov, et. al., (1968) show how the hydrodynamic relative velocity increases asymptotically with increasing frequency. Since the hydrodynamic kernel is proportional to the relative velocity it increases in the same manner.

In Fig. 9 it can be seen that both acoustic kernels decrease with increasing pressure and in Fig. 10 both kernels are seen to increase slightly with increasing temperature. The effects of temperature and pressure changes on both the hydrodynamic and orthokinetic processes are a complex combination of viscosity and sound wave properties. For the range of atmospheric values these effects are not very significant.

In addition to the sound and environmental variables discussed so far, the acoustic collection kernels are also sensitive variations in the aerosol spectrum. In the orthokinetic case the kernel is a function of a concentration term as can be seen in equation (4.3). Recall this term parameterizes the refilling of the agglomeration volume with small droplets. The hydrodynamic kernel given by equation (4.4) is a function of the relative velocity which is a function of droplet separation as shown in equation (3.3). Average droplet seperation is a function of droplet concentration. Thus, both acoustic kernels are dependent on the aerosol concentration.

The aerosol concentration is dependent upon the specification of the intial aerosol spectrum. In this research work the spectra used are all of a gamma or Pearson Type III distribution and are specified by liquid water content L, initial mean radius a_o, and shape factor or variance σ^2. In Fig. 11 through Fig. 13 the effects of changes in the parameters that specify the initial aerosol spectrum are illustrated. In Fig. 11 it is shown that when the initial mean radius is increased the orthokinetic effect increases and reaches a maximum around 15 μ and then falls off toward larger sizes. In terms of equation (4.3) this behavior results from the relative concentration term reaching a maximum

at a_c = 15 μ. Here the hydrodynamic kernel behavior is an artifact of the method of calculation, i.e., the radius a_1 in equation (4.4) is equal to a_o. In general, for a given droplet pair, the hydrodynamic kernel will decrease with increasing initial mean radius because the droplet concentration will decrease thereby increasing the mean separation of the droplets.

When the initial spectrum variance is increased the orthokinetic effect increases as seen in Fig 12. Physically, increasing the variance increases the relative numbers of large collectors and small collectible droplets. For the orthokinetic interaction there are more droplets with different relative entrainment in the fluid motion resulting in more collisions. Again, in terms of equation (4.3), the relative concentration term is increased. The hydrodynamic effect shows no significant change. In terms of equation (4.4) any changes are due to variations in the relative velocity which is inversely dependent on the separation of the droplets.

The effect of increasing the liquid water content is demonstrated in Fig 13. This effect is a droplet concentration effect since increasing the liquid water proportionately increases the number of droplets. The orthokinetic kernel varies directly with the relative concentration. Once again the concentration effect on average separation changes the relative velocity and thus the hydrodynamic kernel.

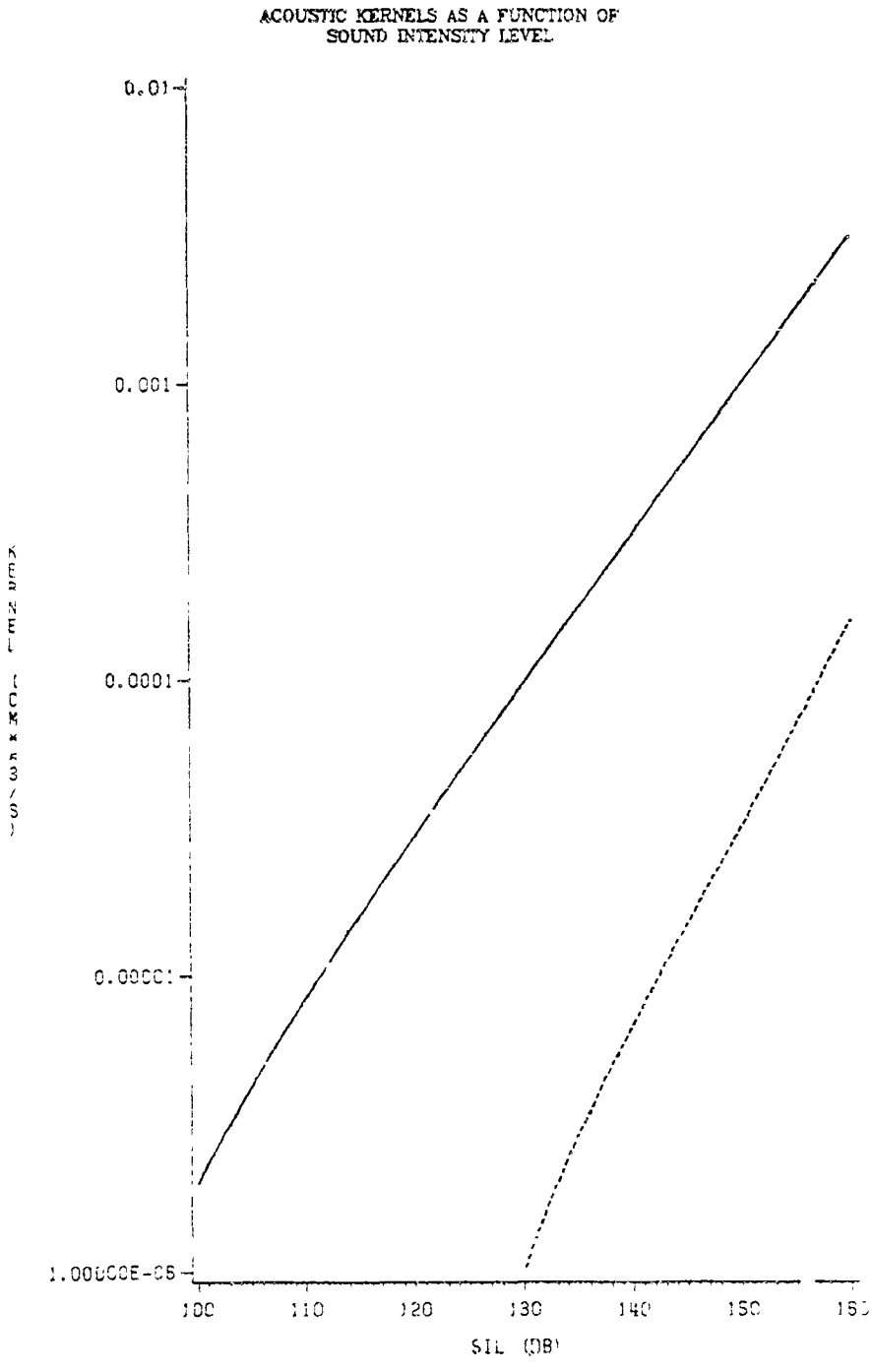

Figure 7: Kernels as a Function of Sound Intensity Level. (Solid curve is for orthokinetic, dashed for hydrodynamic.)

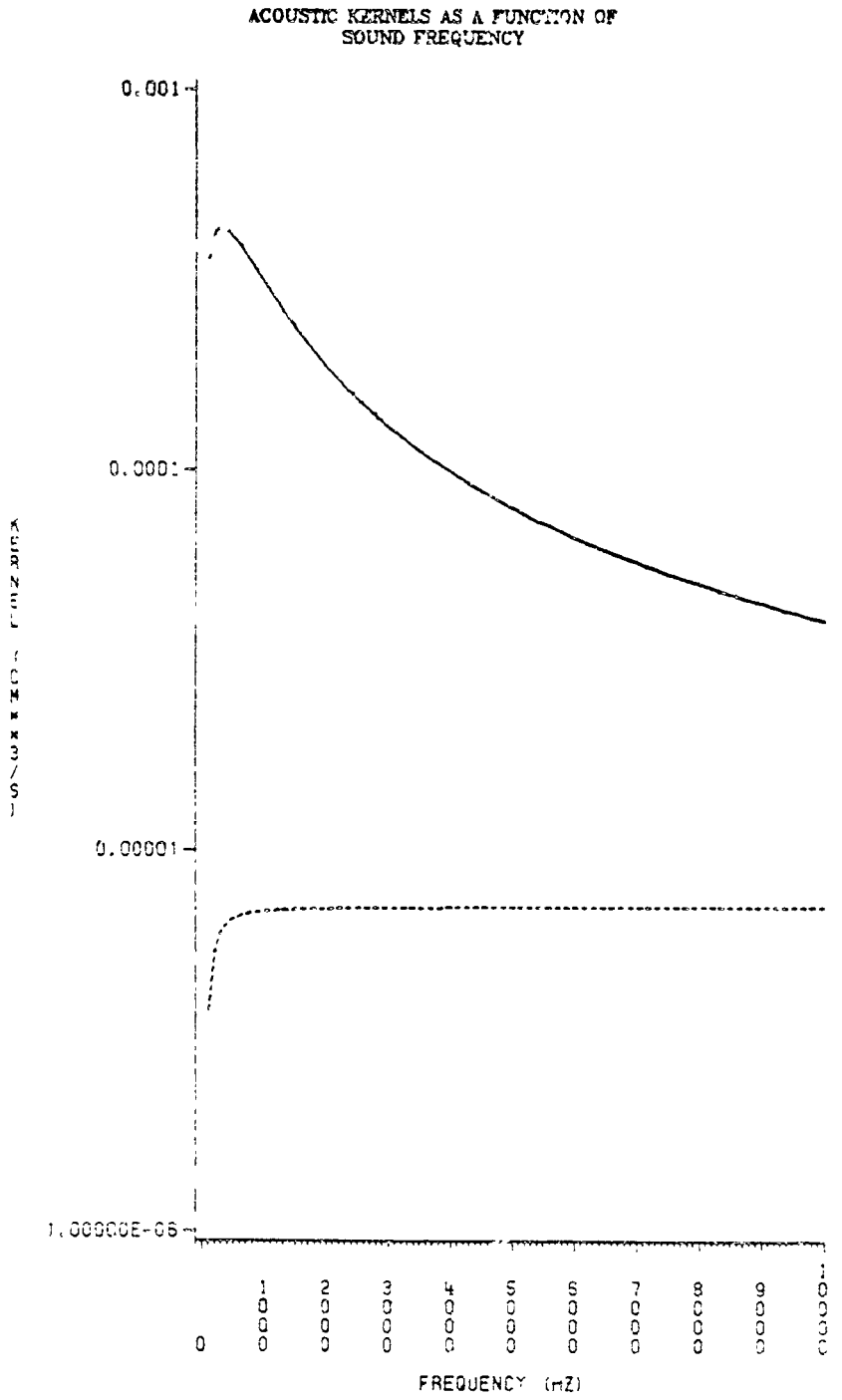

Figure 8: Kernels as a Function of Sound Frequency. (Solid curve is for orthokinetic, dashed for hydrodynamic.)

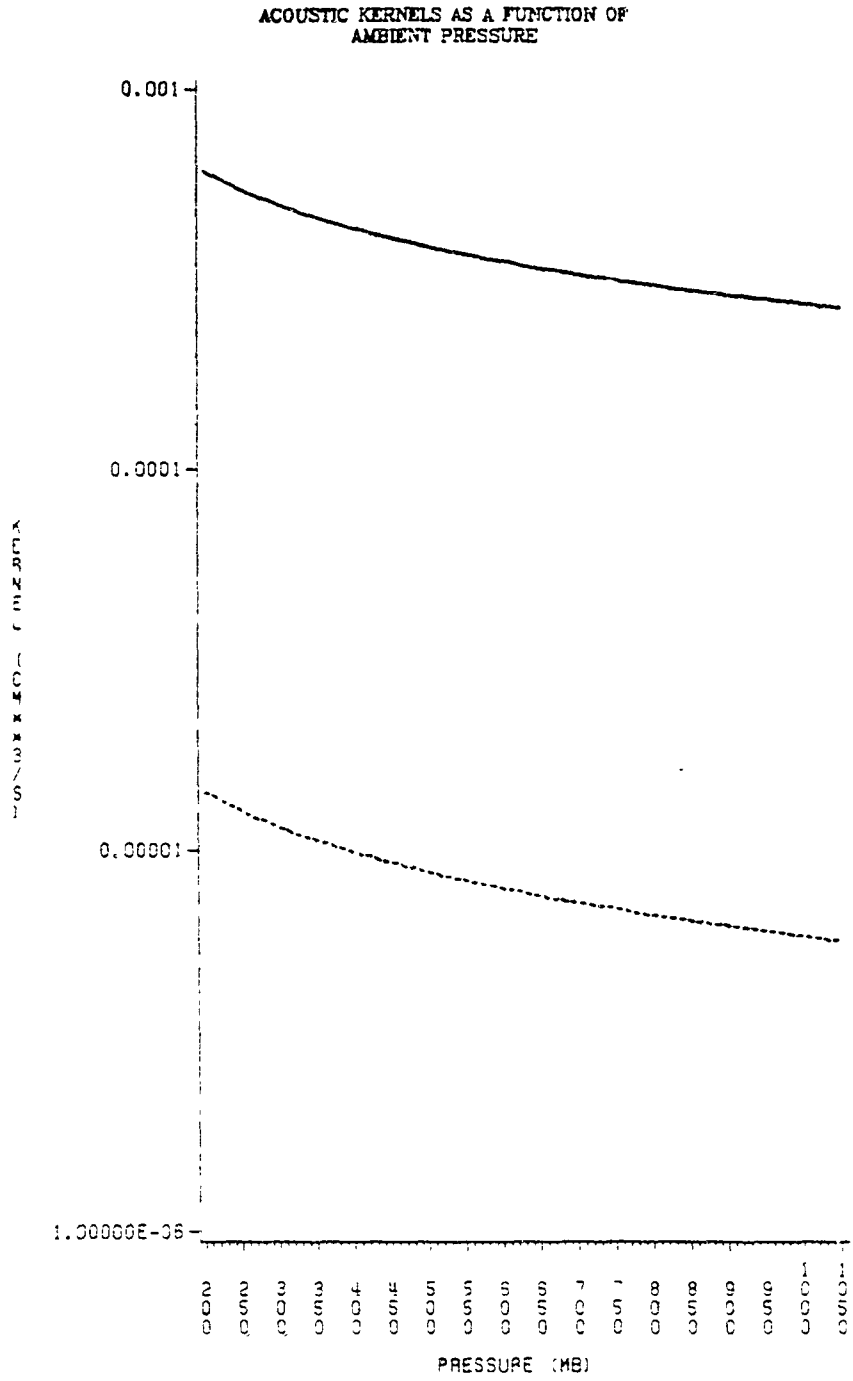

Figure 9: Kernels as a Function of Ambient Pressure. (Solid curve is for orthokinetic, dashed for hydrodynamic.)

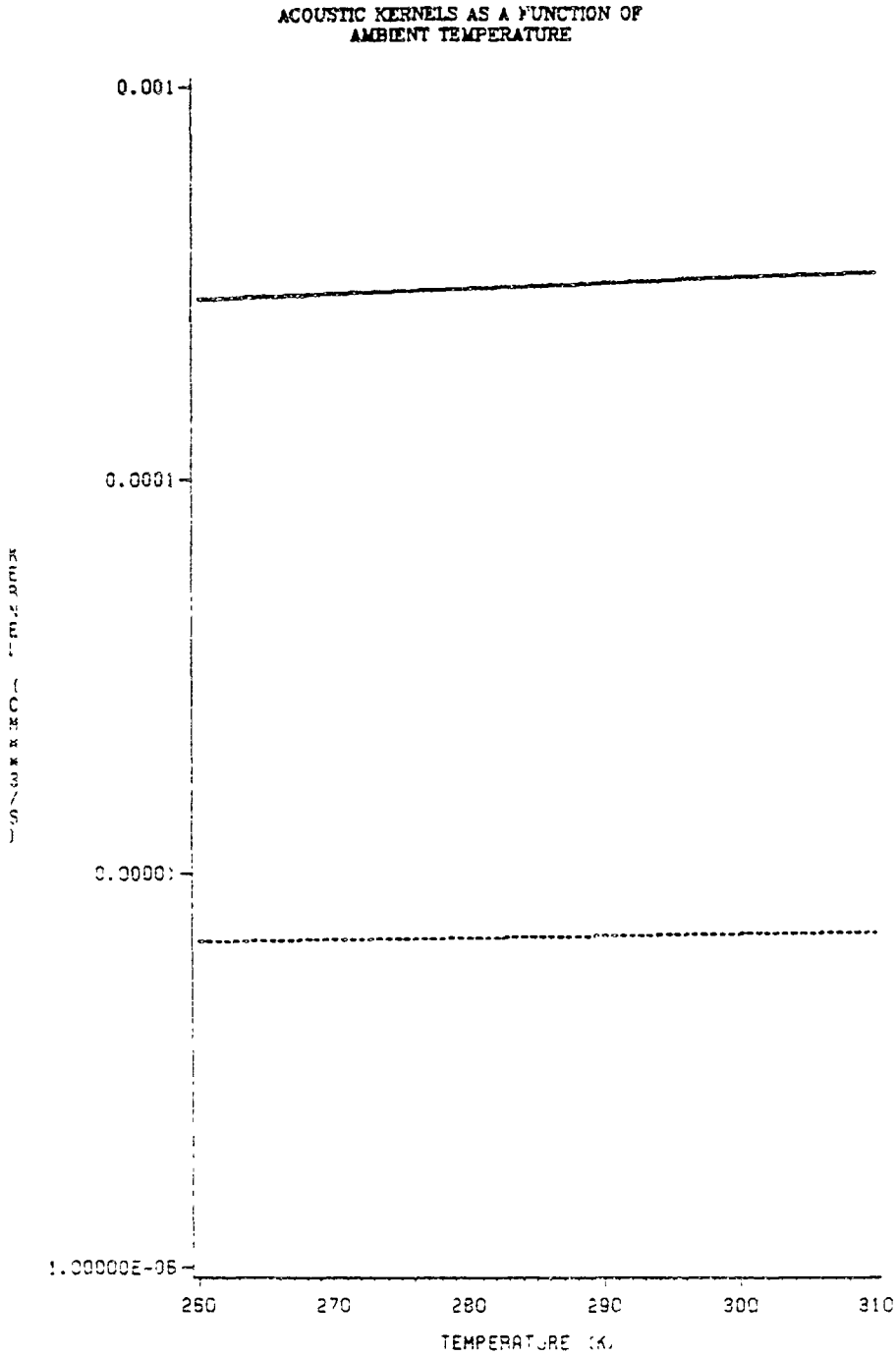

Figure 10: Kernels as a Function of Ambient Temperature. (Solid curve is for orthokinetic, dashed for hydrodynamic.)

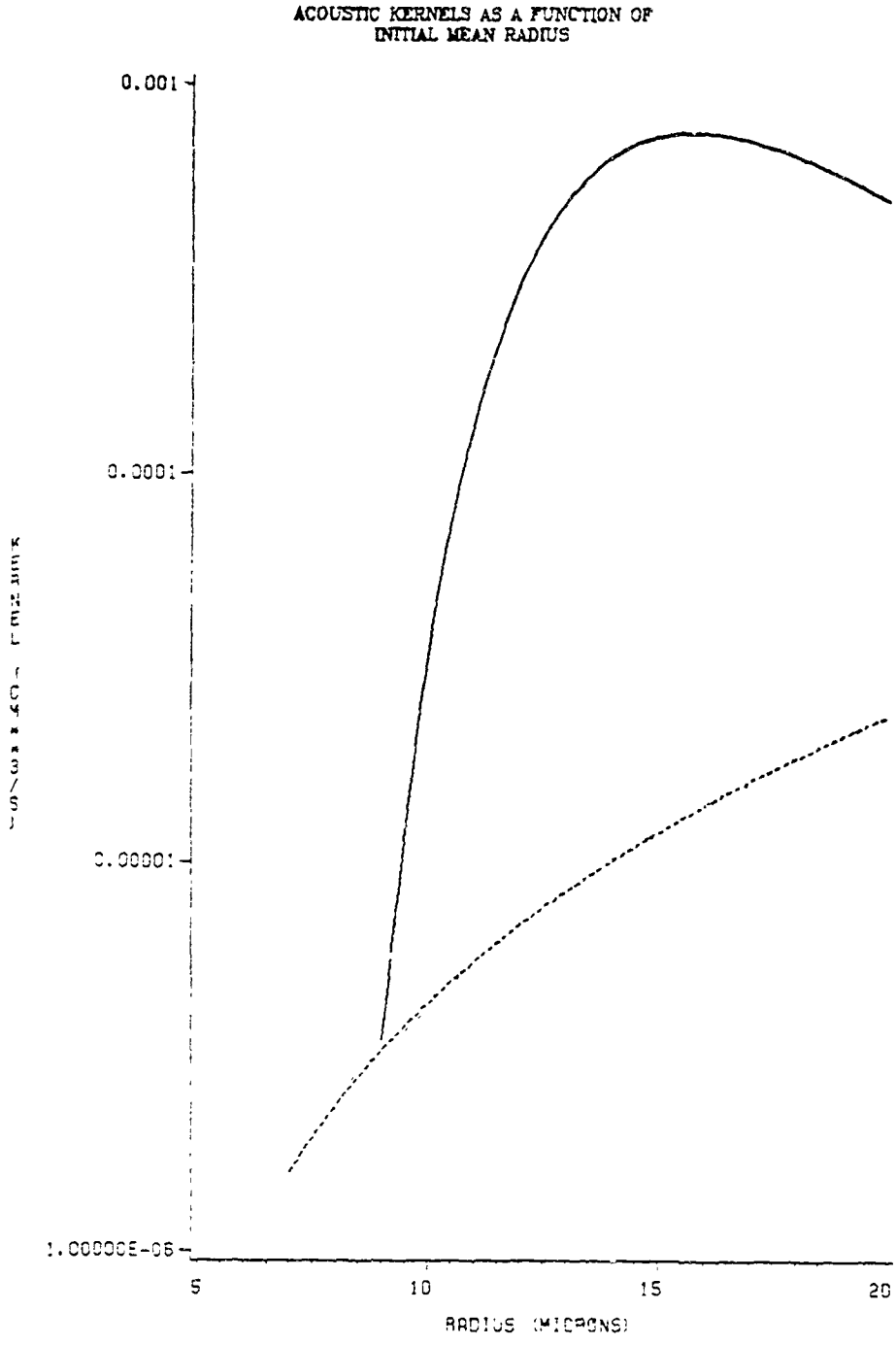

Figure 11: Kernels as a Function of Initial Mean Radius. (Solid curve is for orthokinetic, dashed for hydrodynamic.)

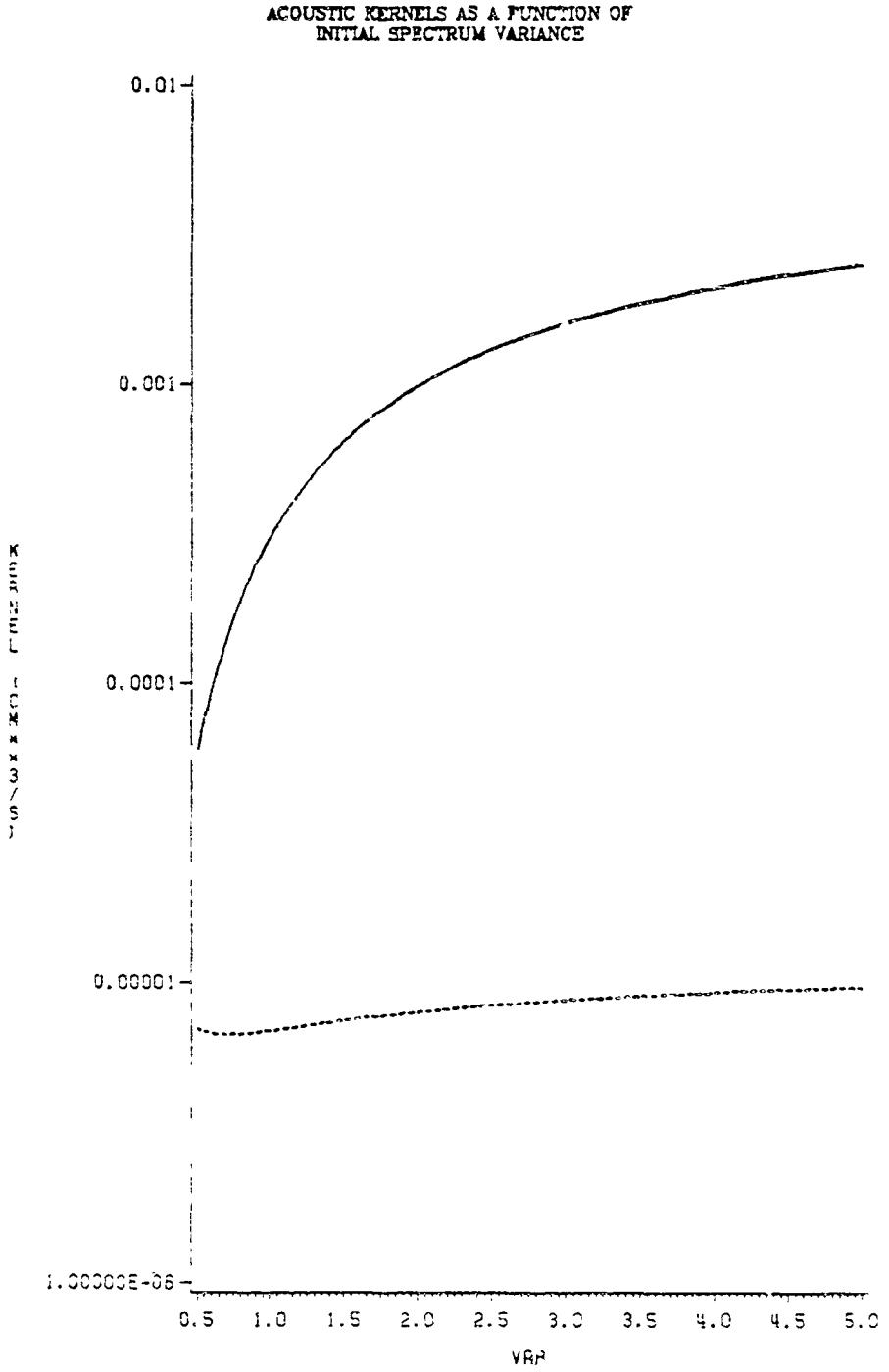

Figure 12: Kernels as a Function of Initial Spectrum Variance. (Solid curve is for orthokinetic, dashed for hydrodynamic.)

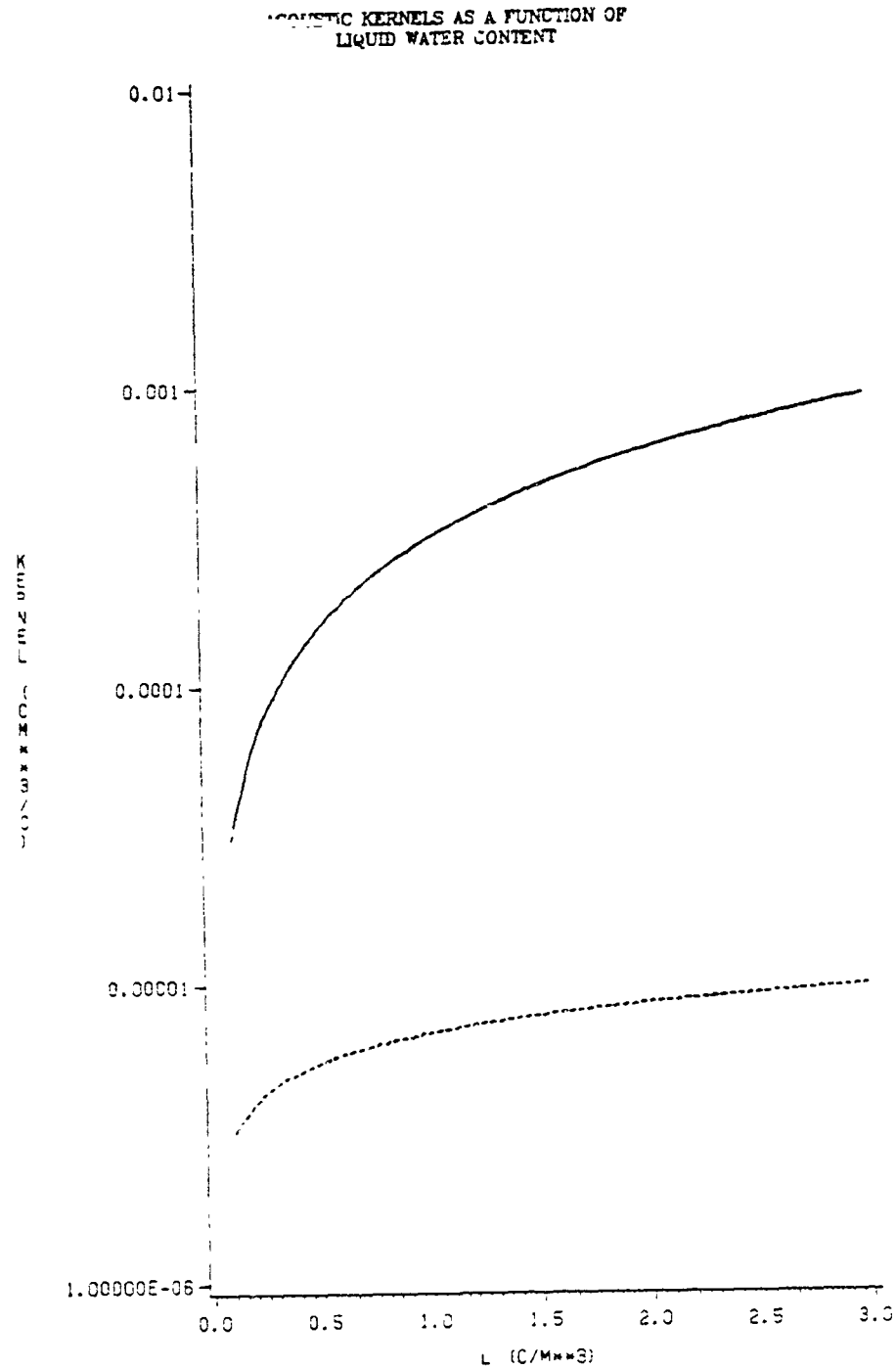

Figure 13: Kernels as a Function of Liquid Water Content. (Solid curve is for orthokinetic, dashed for hydrodynamic.)

4.2 RESULTS

Methods for evaluating the SCE are discussed in Pruppacher and Klett (1980) including the method of Berry and Reinhardt (Berry (1967), Berry and Reinhardt (1974), and Leighton and Rogers (1974)). The range of sizes from cloud droplet to precipitation is approximately 10^{-4} cm to 10^{-1} cm. In order to keep the number of size classes of the discrete spectrum to a reasonable number Berry devised an exponential subdivision so that the j^{th} drop radius is given by

$$a(j) = a_0 \exp[(j-1)/J] \ . \tag{4.6}$$

In the present work the model code used is that of Leighton and Rogers in which $J = 12/\ln 2$. There are 130 size classes ranging from 3.94×10^{-4} cm to 6.79×10^{-1} cm. For each simulated cloud there is an initial droplet density function as a function of droplet mass which is specified by a mean radius and variance in a gamma or Pearson Type III distribution. The values selected for the atmospheric variables for the tests described in this work were $\bar{p}$ = 765 mb, T = 283 K, and ρ = 1.0–2.0 g m^{-3}.

The model code was modified to include the two collection kernels defined by equations (4.3) and (4.4). At each time step the collection kernel used in integrating the SCE is the sum of equations (4.2) through (4.4). During the time that a simulated sound is being applied to the cloud the time step is one second. After the sound is turned off the acoustic collection kernels are set equal to zero and the time step remains one second. For the rest of the run the only process being modeled is coalescence due to gravitational effects. The tests

discussed here are limited to 14 to 15 minutes of simulated time because numerical instabilities set in after that. However, there is a high degree of confidence in the results because the graphical results using only the gravitational collection process have been compared to the results of Berry and Reinhardt (1974b) and were found to be in excellent agreement. Also, the process modeled is one of constant mass and mass checks show gains or losses of less than two percent throughout the runs.

The remainder of this chapter will be devoted to discussion of the model runs. All of the results are presented graphically in plots that show the mass density functions of the droplet spectra. The advantage of this method is that it shows how the water mass is distributed over droplets of various radii and the area under the curve between two radii represents the water mass contained in drops of those diameters. Also, in this type of plot equal areas represent equal amounts of water mass. It should be noted that the mean radius of the spectrum is the radius of the droplet with mass equal to the liquid water content divided by the droplet number concentration. The predominant radius is that of the droplet category containing the most mass. The predominant radii of all the cases discussed occur at the peaks of the spectra. The characteristics of the cases discussed in the following pages are outlined in Table 2.

The results for cases 1 and 2 are shown in Fig. 14 through Fig. 23. The droplet concentration for the original spectrum is 166 cm^{-3}. This spectrum exhibits little change due to the effects of gravity and by 15 minutes shows no indication of the development of precipitation sized

TABLE 2

Cloud Spectra Cases

Case	Spectrum Mean (μ)	Spectrum Var.	Sound Freq. (Hz)	Sound Intensity (db)	Time (s)
		LWC = 1.0 g m^{-3}			
1	10	0.25	300	140	5
2	10	0.25	300	140	10
3	10	1.00	300	140	5
4	10	1.00	300	140	10
5	10	1.00	300	150	5
		LWC = 2.0 g m^{-3}			
6	10	1.00	300	140	5

drops. In case 1 the application of sound of 140 db and 300 Hz for 5 seconds at the start of the run causes a shift in the predominant radius and an increase in the mass dispersion of the spectrum. However, even with some larger sized droplets and greater dispersion the new spectrum does not produce precipitable drops in 15 minutes. Case 2 is similar to case 1 except the sound is applied for 10 seconds. The result is an even larger predominant radius but the acoustically altered spectrum still does not produce precipitation sized drops within 15 minutes.

The results for case 3 are shown in Fig. 24 through Fig. 28. This spectrum is initially more disperse than in cases 1 and 2 but the sound frequency and intensity are the same. The droplet concentration for this case and cases 4 and 5 is 225 cm^{-3}. Again, the effect of gravity alone is not sufficient to develop large drops during the fifteen minute run. When sound is applied there is a shift of mass up the scale to

larger radii. In Fig. 28 it is evident that some larger drops have developed but a secondary maximum has yet to appear. It is not clear from this case if precipitable drops would develop if more time was allowed for continued gravitational sedimentation.

In case 4 the conditions are similar to case 3 except the sound is applied for 10 seconds. At the end of the sound application the new spectrum has a larger predominant radius than was seen in case 3. Now at the end of the 15 minute run it can be seen that a definite tail has formed for droplets of precipitation size. Berry and Reinhardt (1974b) showed in their numerical cases that once a large drop signature began to develop, mass rapidly moved up the scale to the precipitation regime.

The results for case 5 are shown in Fig.34 through Fig.38. Here the effects of gravity are the same as in case 3. The effect of the higher intensity sound is to shift mass even further up the scale with an even smaller mass variance after the sound is turned off. However, it becomes clear by ten minutes that a secondary maximum is forming for drops of precipitable size. The process is well under way by fifteen minutes.

Case 6 is illustrated in Fig. 39 through Fig. 43. Here the liquid water content has been increased to 2.0 g m^{-3} and the sound parameters set to 140 db and 300 Hz applied for 5 seconds. The droplet concentration is 450 cm^{-3} which is around the lower limit for continental cumulus clouds. The beginning of a precipitation tail is seen after 5 minutes and by 14 minutes a well formed precipitation hump is evident. It can also be seen that a precipitation tail begins to form by 14 minutes due to gravity alone. However, the acoustic

agglomeration has produced significant enhancement of the precipitation process.

The model has been run with some other initial spectra which will be discussed only qualitatively here. When the initial spectrum has a larger mean radius with the same liquid water content, precipitation sized drops form in about the same time with or without the simulated application of sound energy. In cases where the initial mean radius is smaller than 10 μ the current model does not initialize correctly so it has not yet been possible to study some potentially interesting cloud spectra. The important point is that the results shown in this section strongly suggest that modification may take place for spectra with concentrations and liquid water contents less than those found in clouds over the continents. Since theory and experiment show that acoustic agglomeration is strongly concentration dependent, then the process may be expected to be even more efficient for continental type spectra.

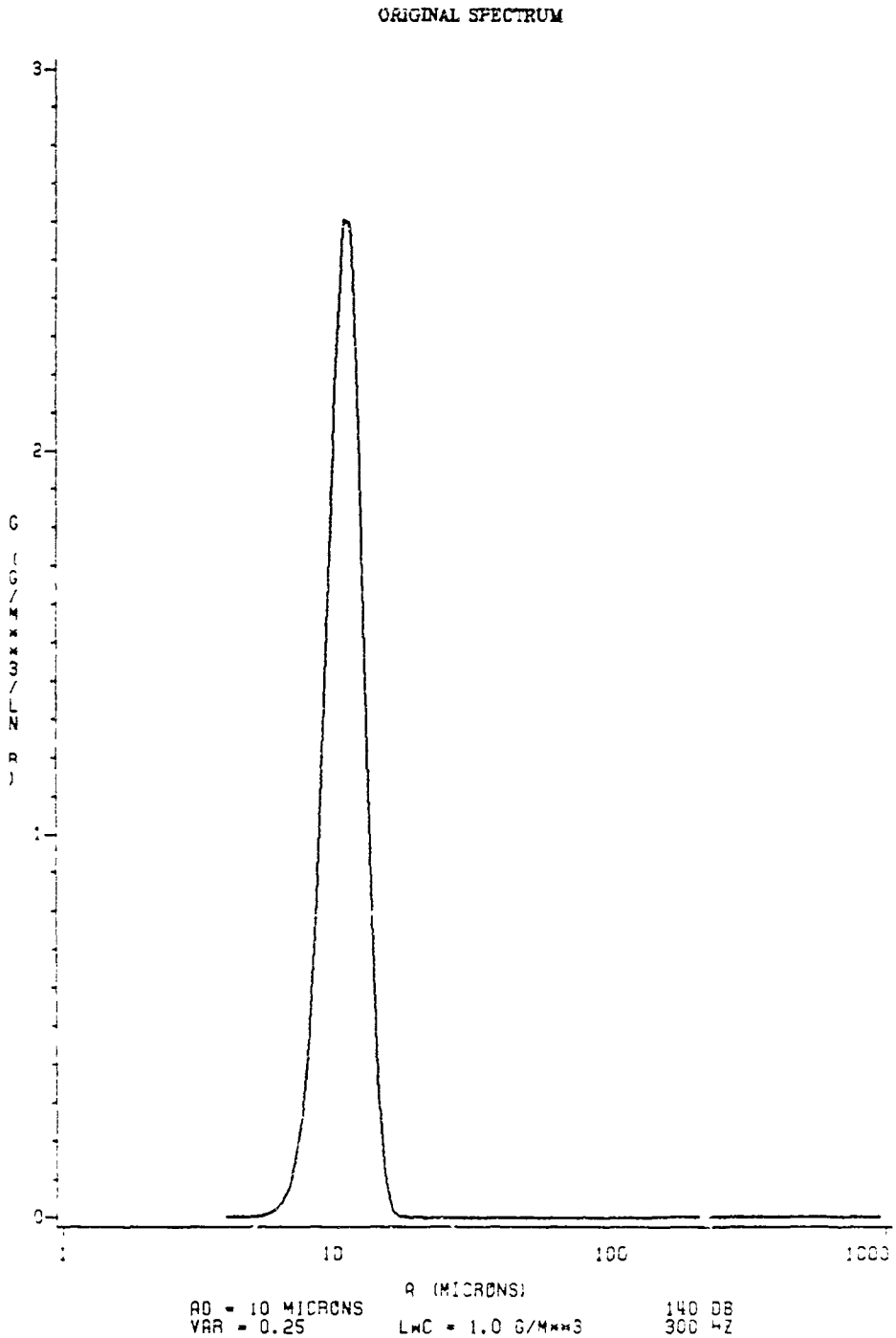

Figure 14: Case 1 - Initial Spectrum.

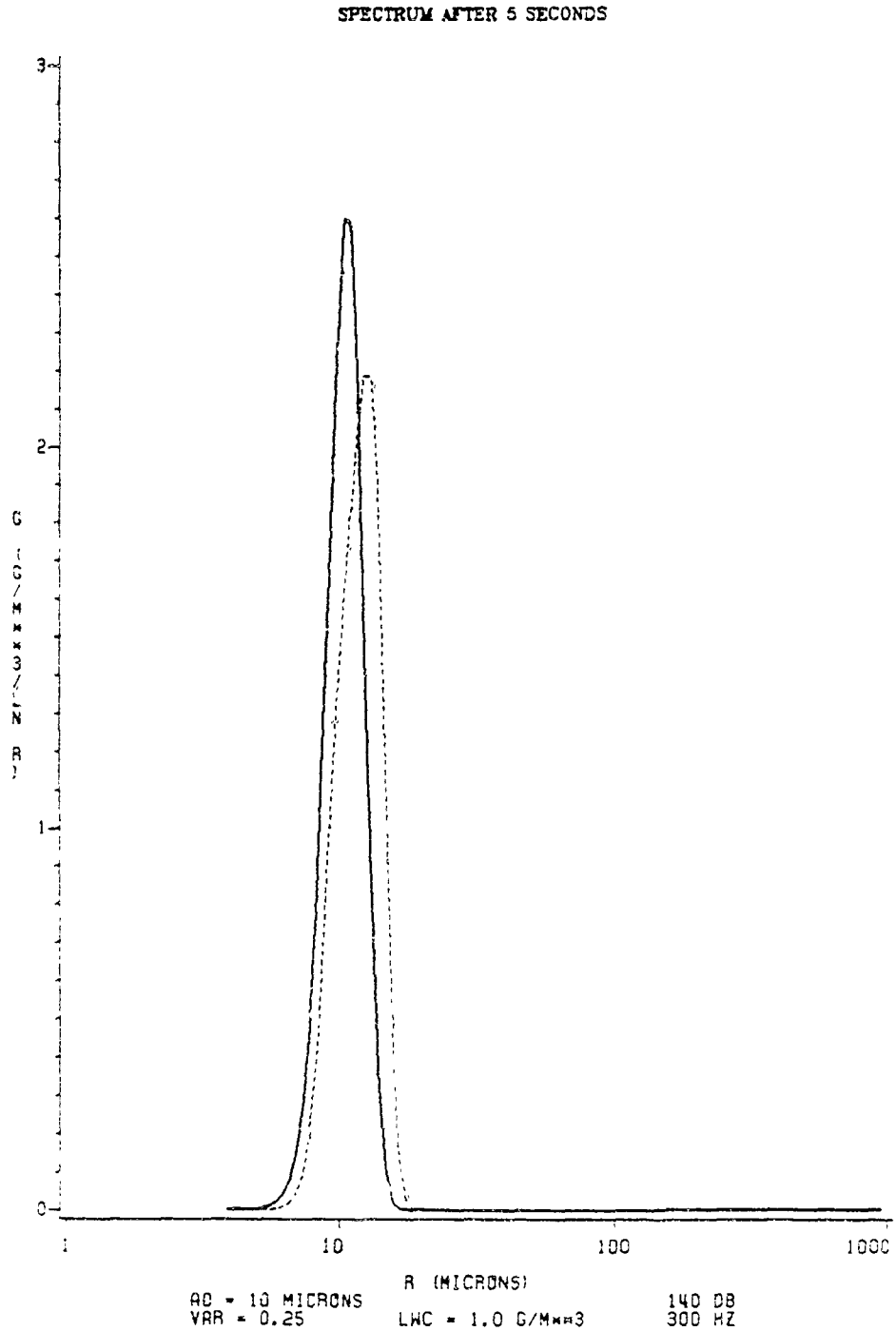

Figure 15: Case 1 - Spectrum After 5 Seconds. (Solid curve for gravitational effect alone, dashed curve for acoustic and gravitational effects.)

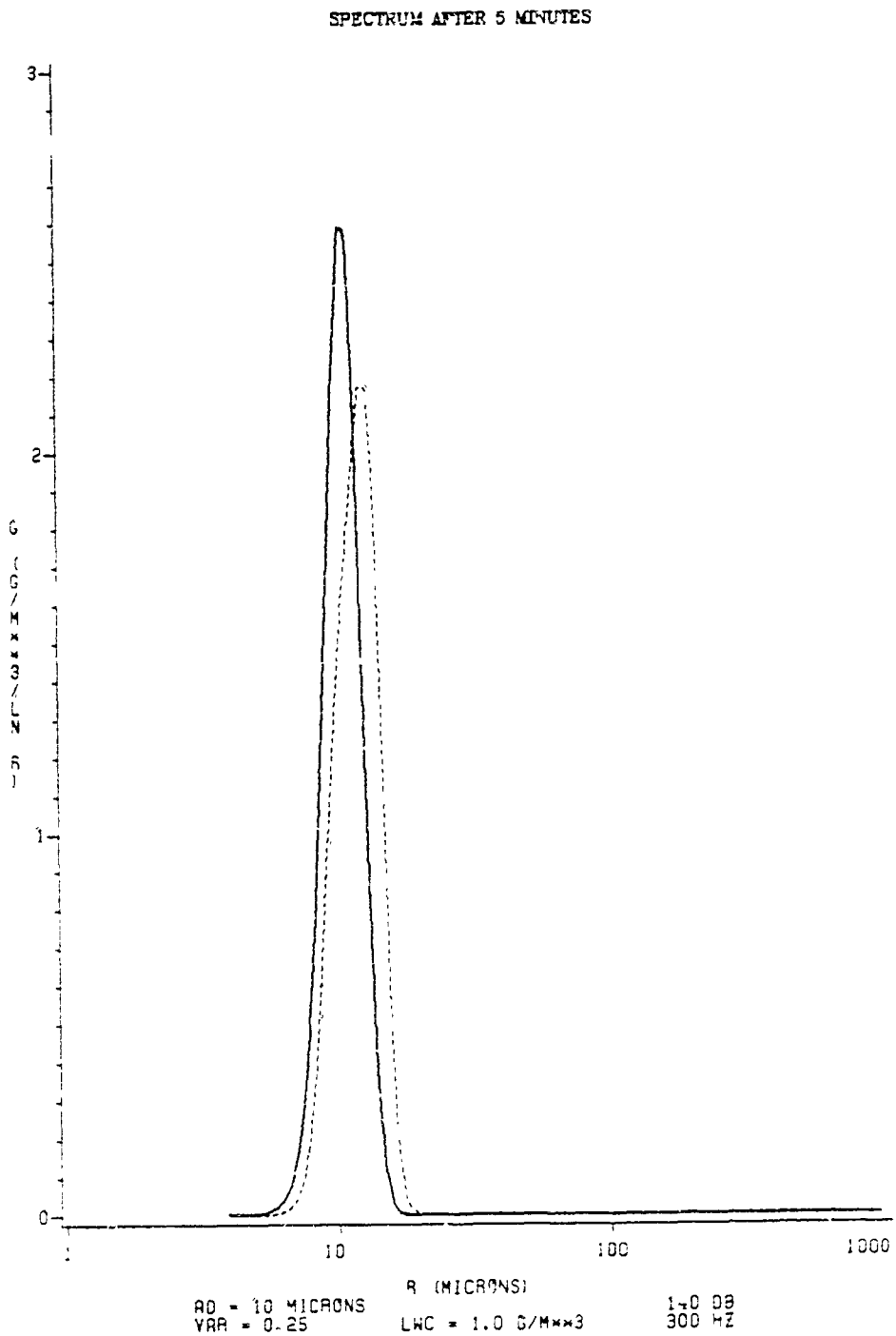

Figure 16: Case 1 - Spectrum After 5 Minutes. (Solid curve for gravitational effect alone, dashed curve for acoustic and gravitational effects.)

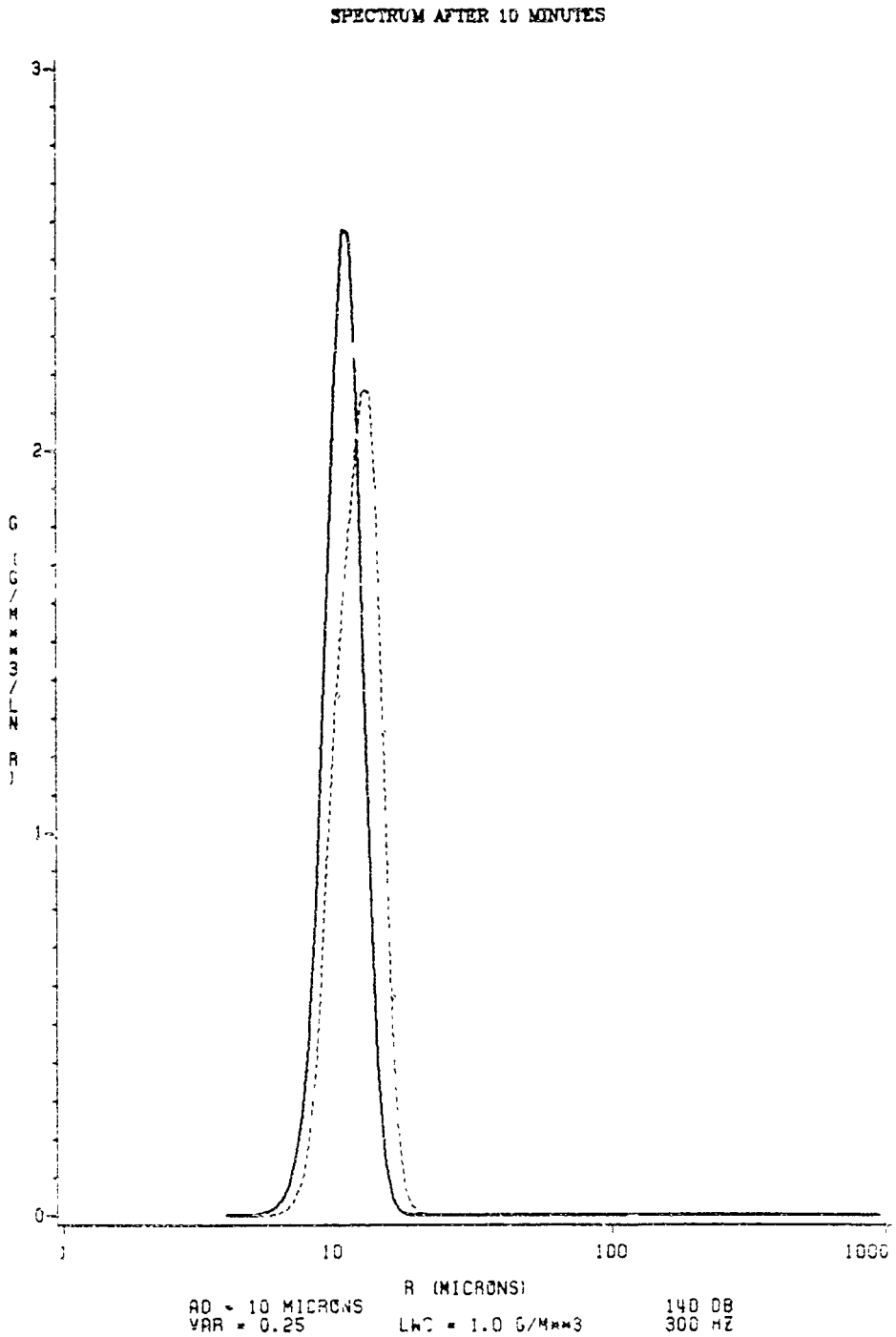

Figure 17: Case 1 - Spectrum After 10 Minutes. (Solid curve for gravitational effect alone, dashed curve for acoustic and gravitational effects.)

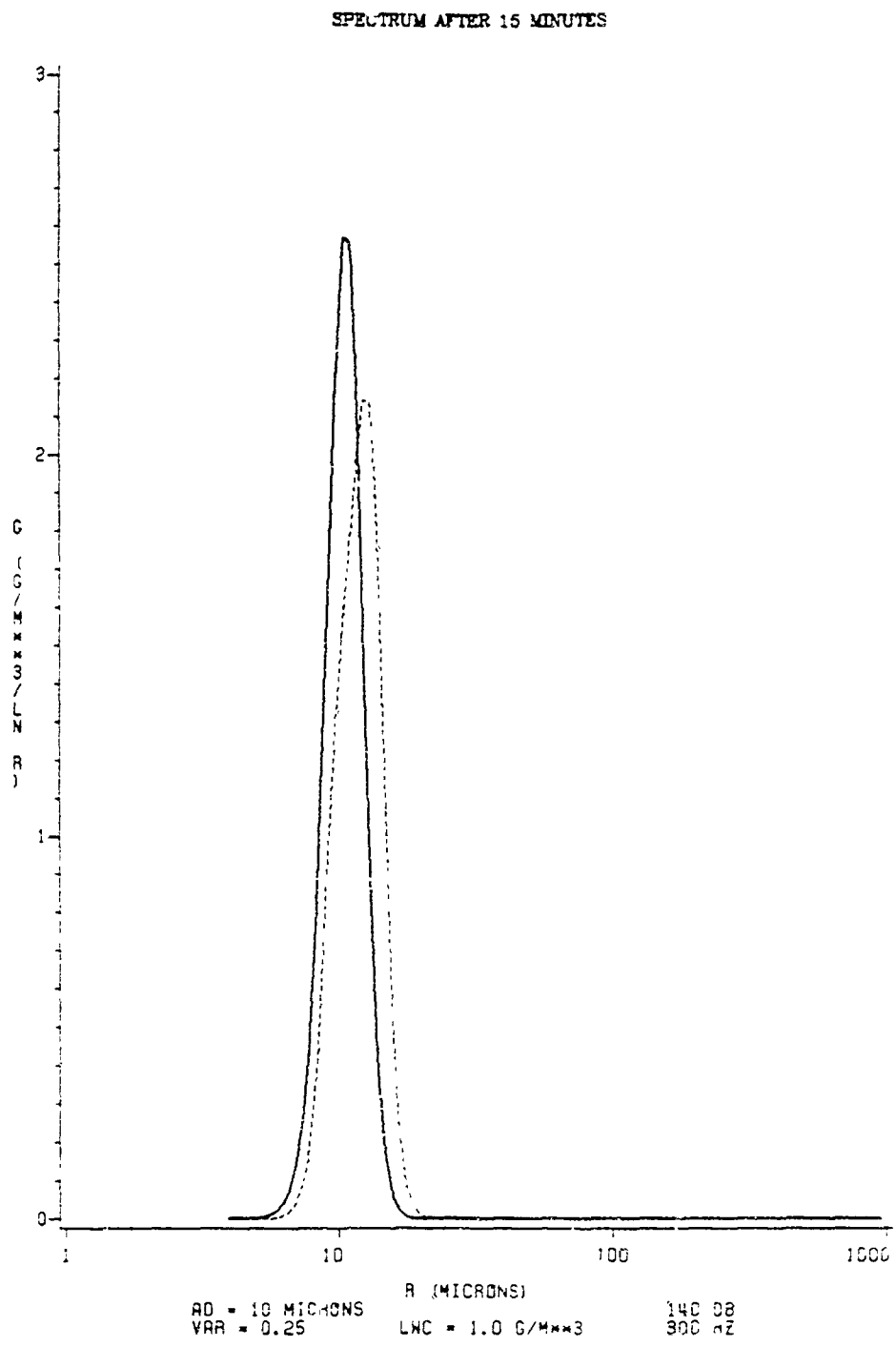

Figure 18: Case 1 - Spectrum After 15 Minutes. (Solid curve for gravitational effect alone, dashed curve for acoustic and gravitational effects.)

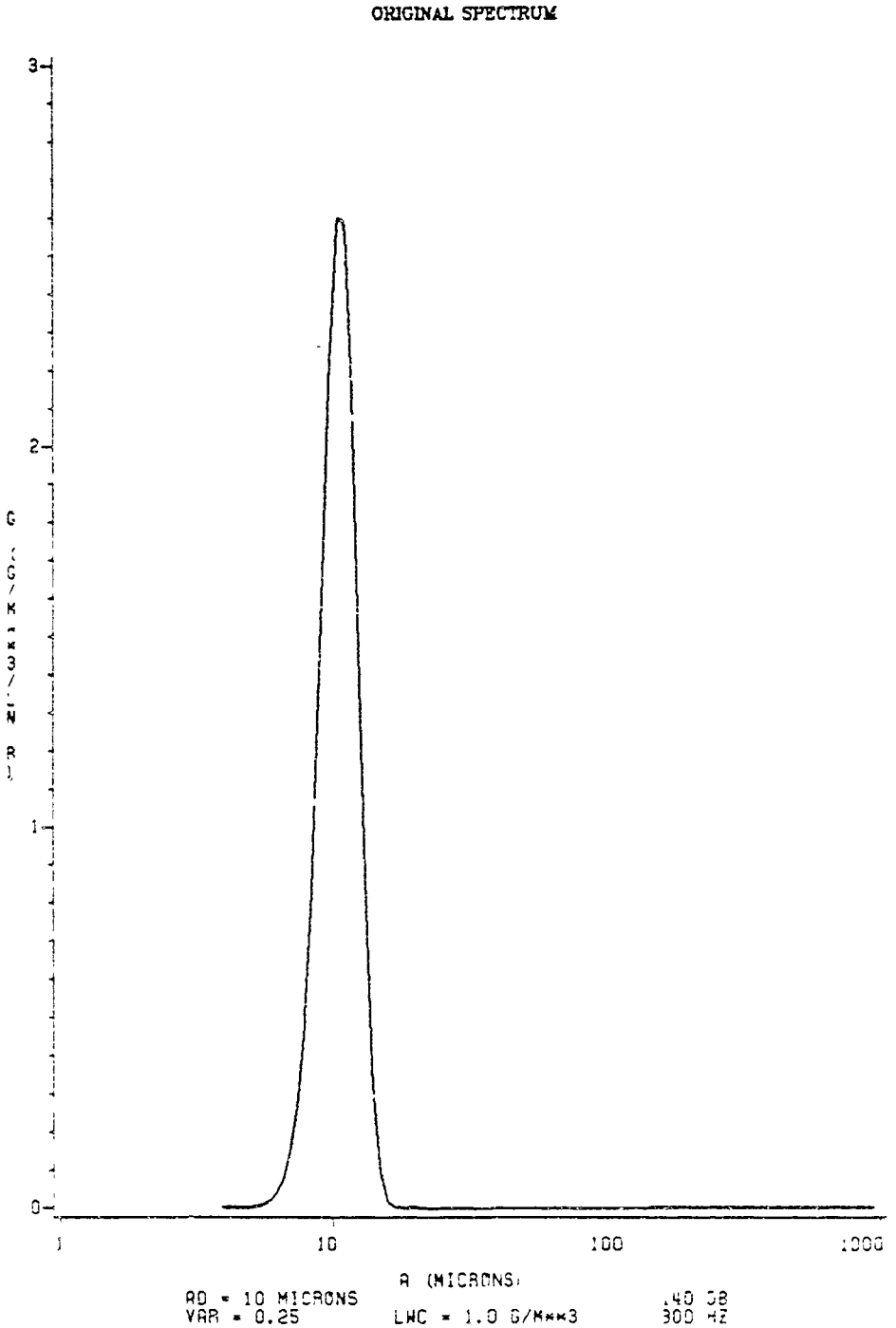

Figure 19: Case 2 - Initial Spectrum.

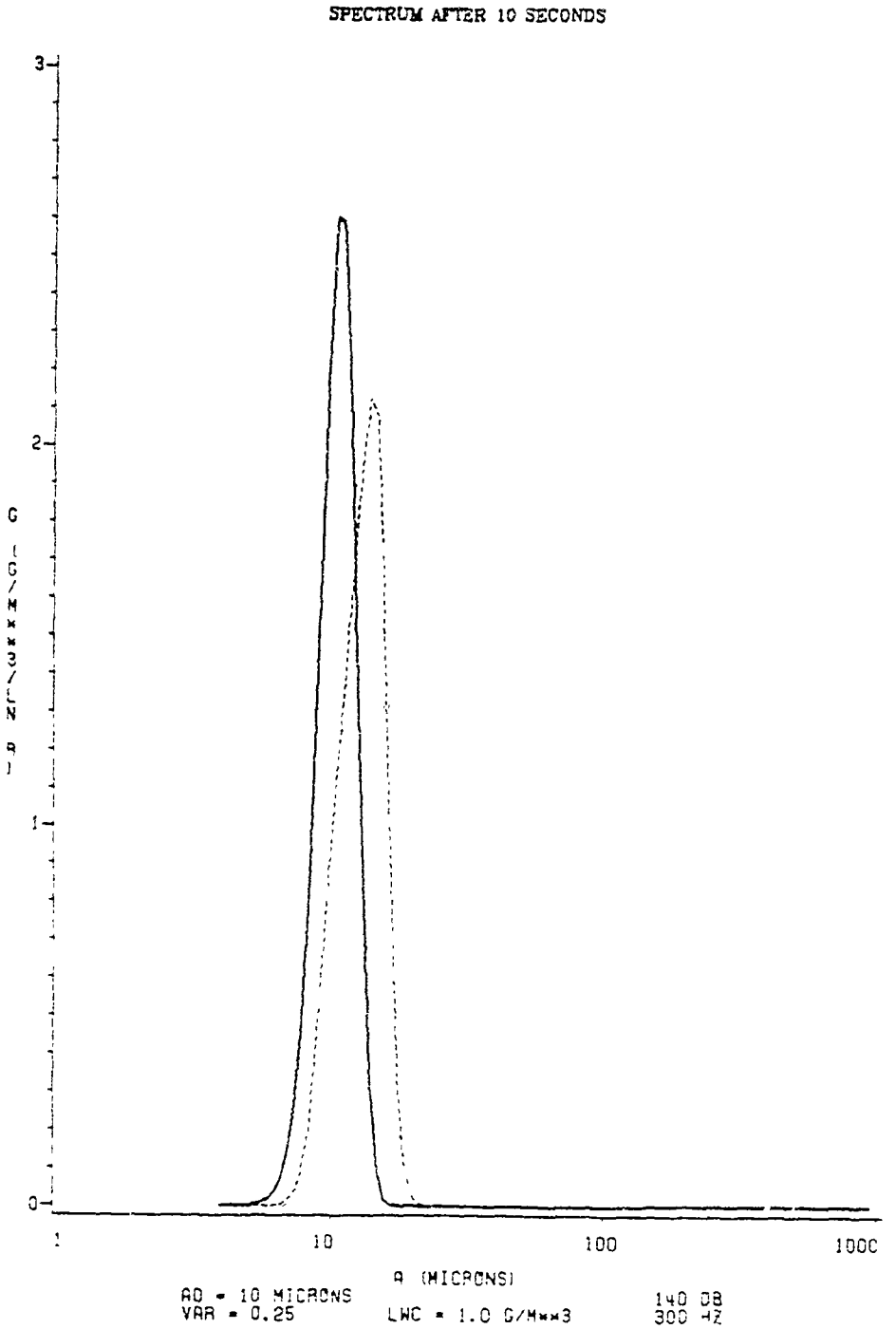

Figure 20: Case 2 - Spectrum After 10 Seconds. (Solid curve for gravitational effect alone, dashed curve for acoustic and gravitational effects.)

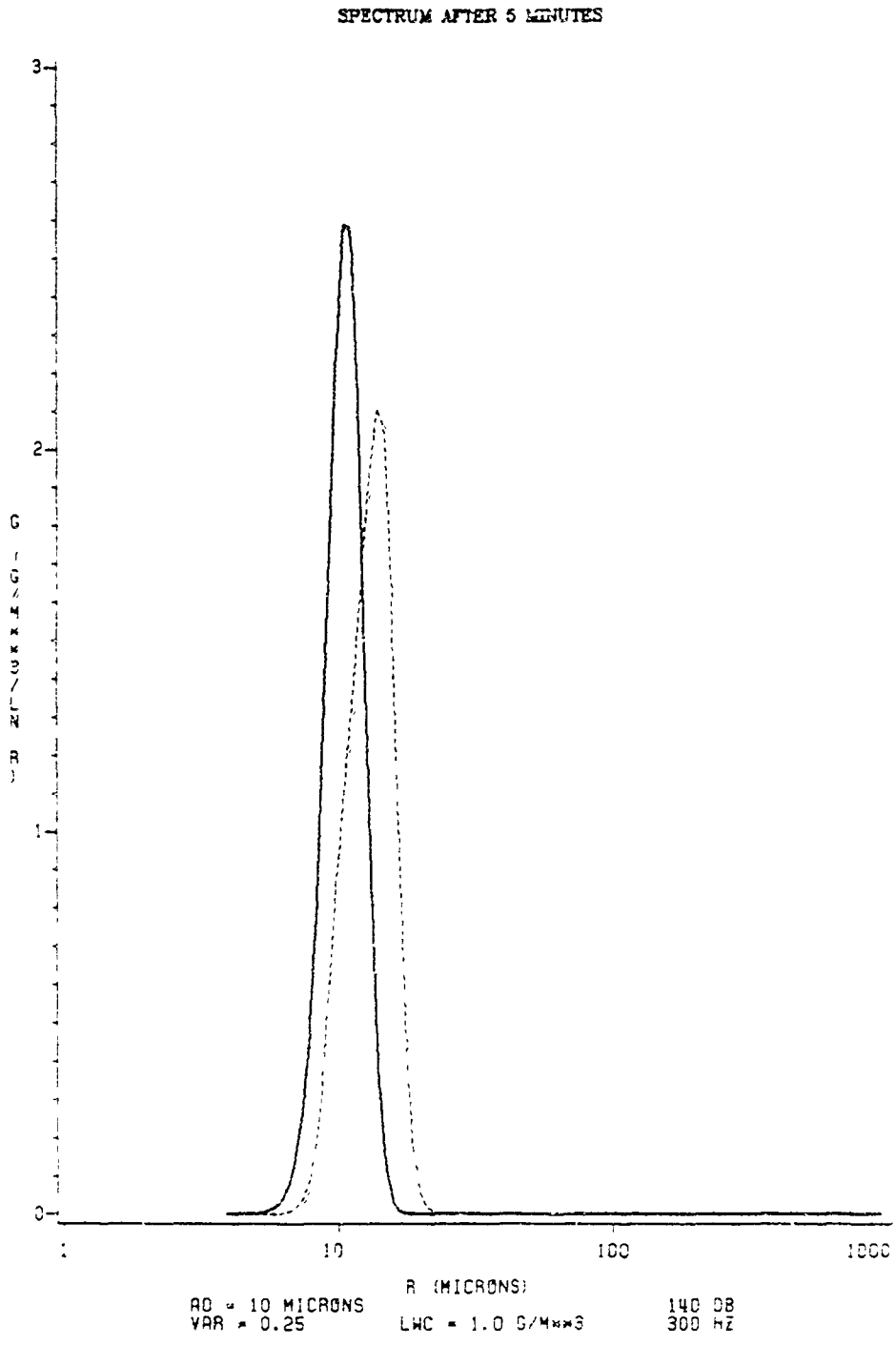

Figure 2': Case 2 - Spectrum After 5 Minutes. (Solid curve for gravitational effect alone, dashed curve for acoustic and gravitational effects.)

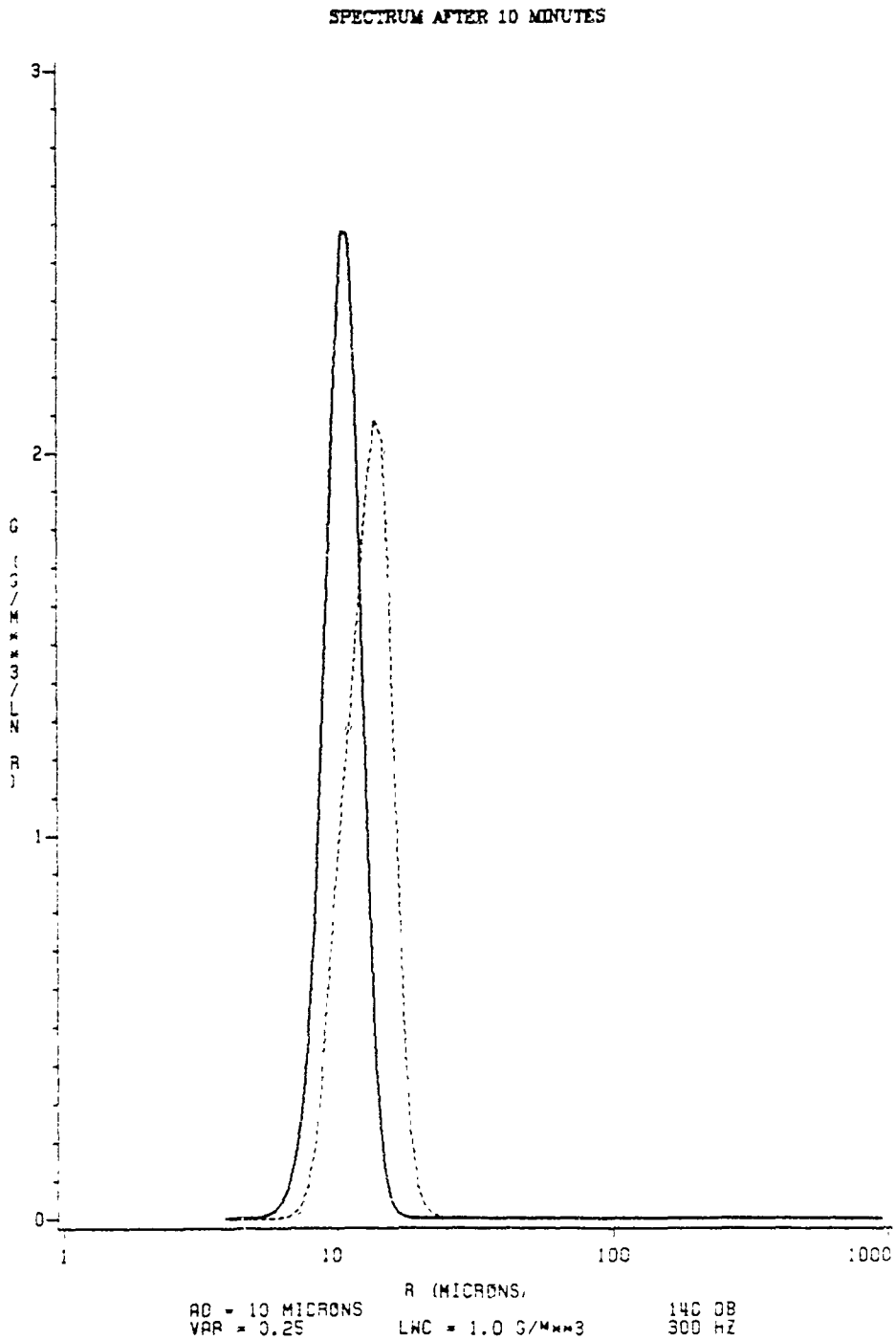

Figure 22: Case 2 - Spectrum After 10 Minutes. (Solid curve for gravitational effect alone, dashed curve for acoustic and gravitational effects.)

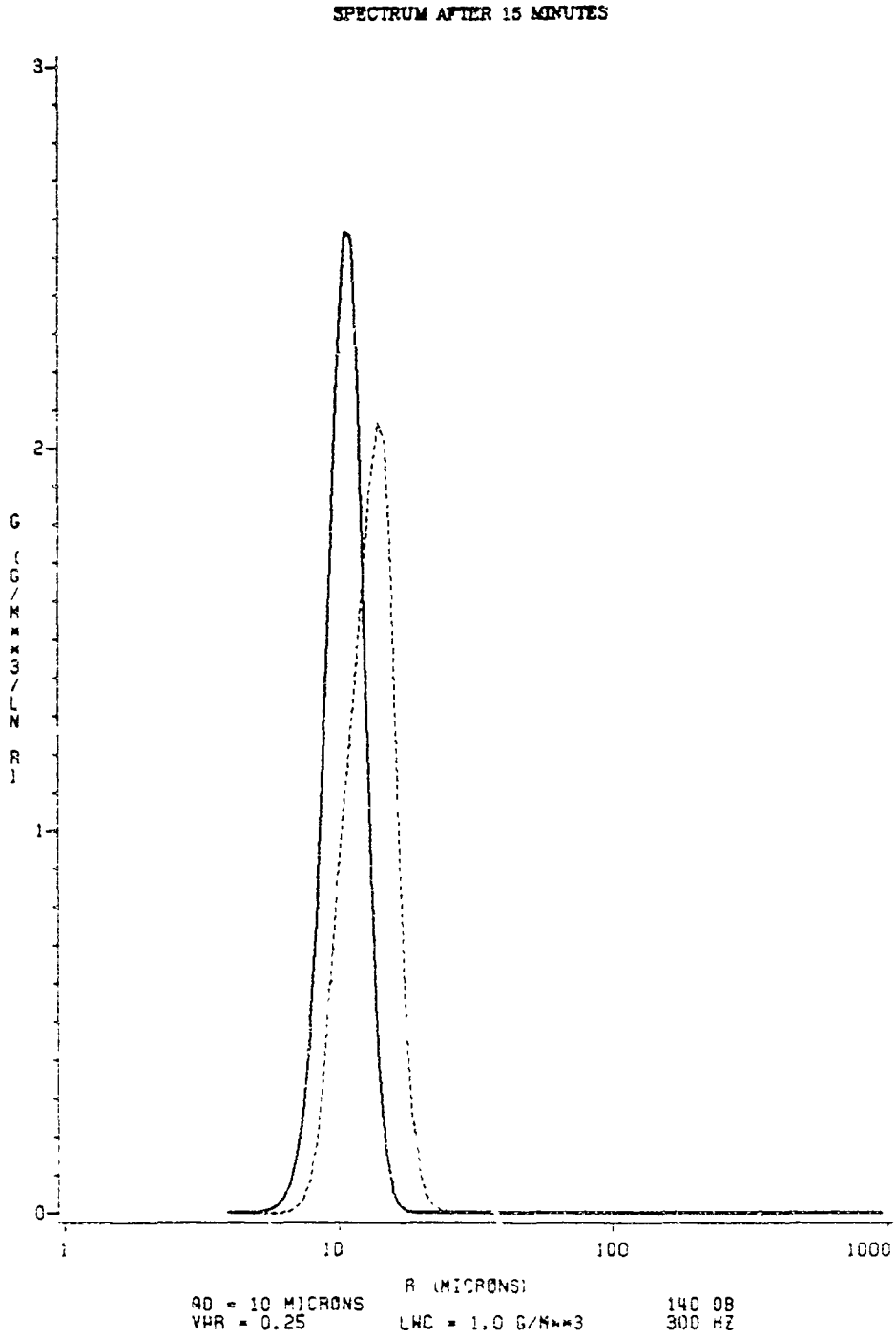

Figure 23: Case 2 - Spectrum After 15 Minutes. (Solid curve for gravitational effect alone, dashed curve for acoustic and gravitational effects.)

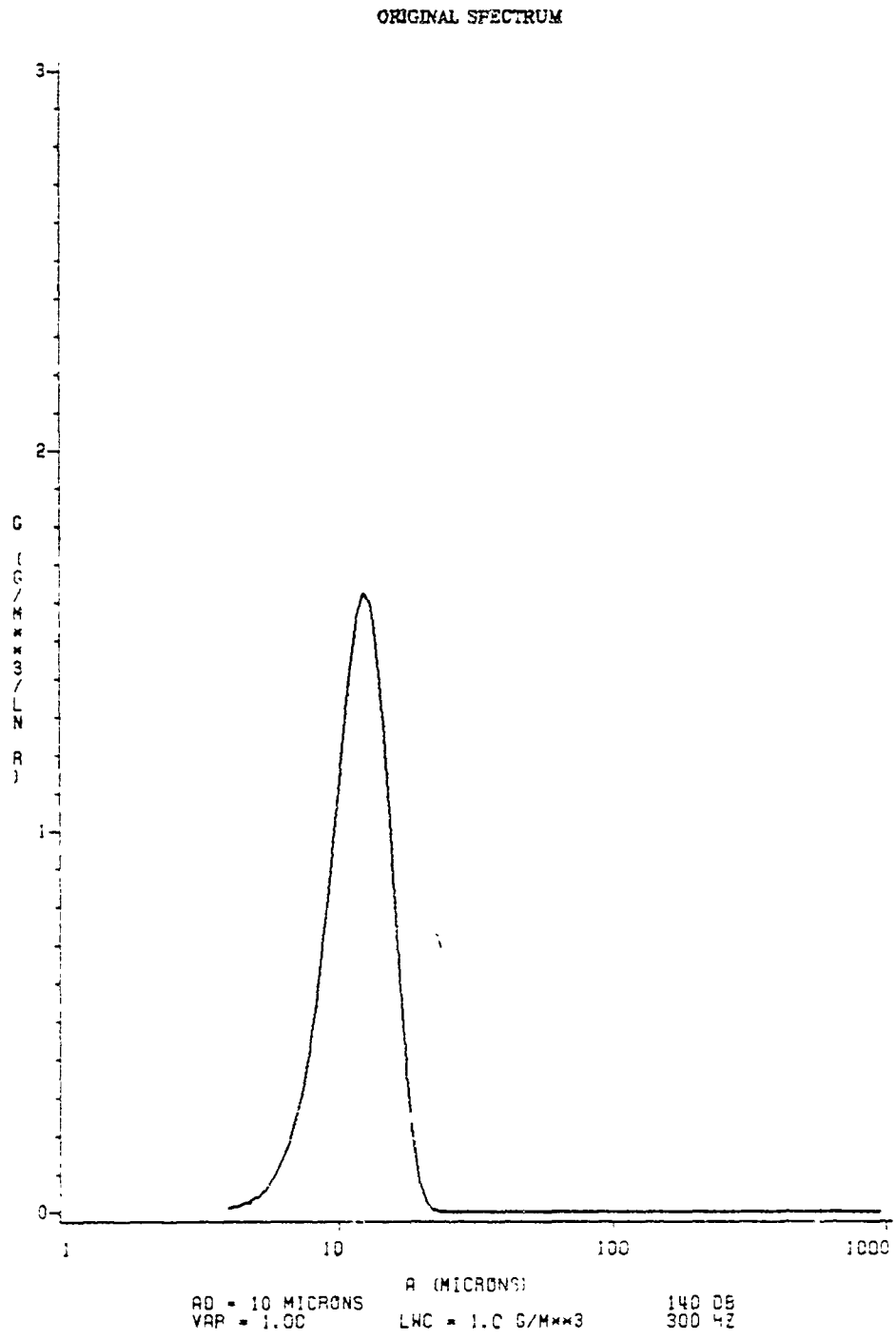

Figure 24: Case 3 - Initial Spectrum.

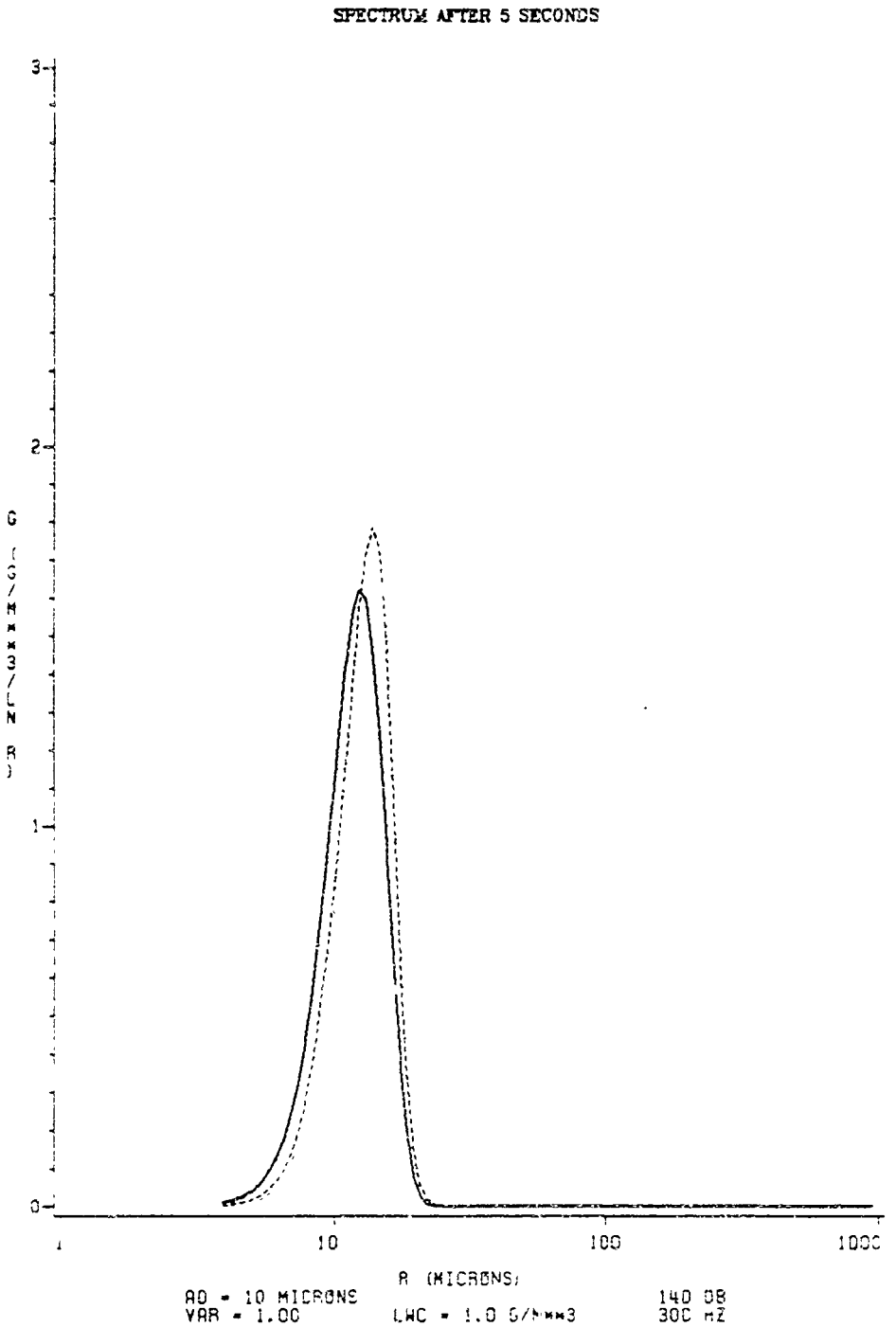

Figure 25: Case 3 - Spectrum After 5 Seconds. (Solid curve for gravitational effect alone, dashed curve for acoustic and gravitational effects.)

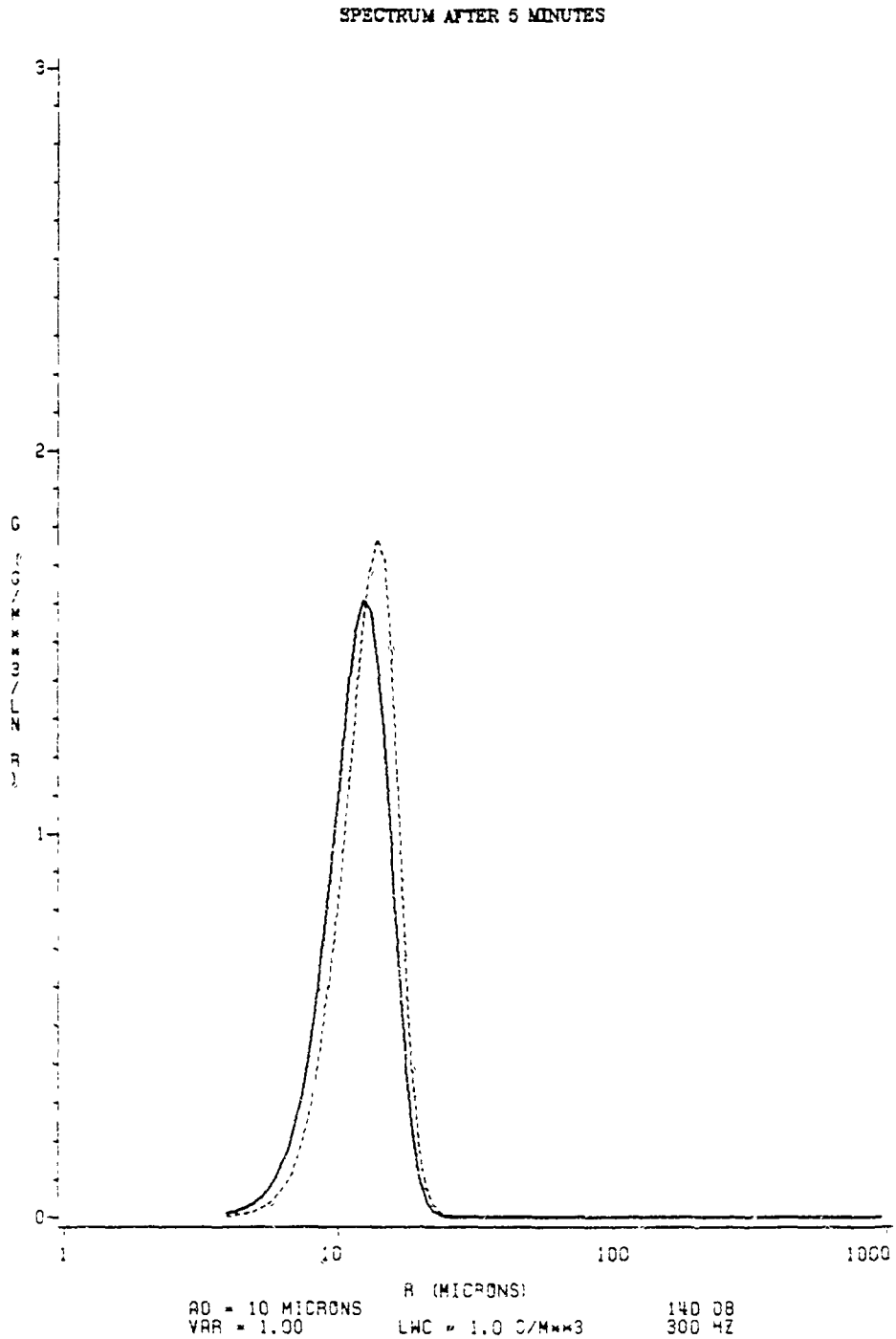

Figure 26: Case 3 - Spectrum After 5 Minutes. (Solid curve for gravitational effect alone, dashed curve for acoustic and gravitational effects.)

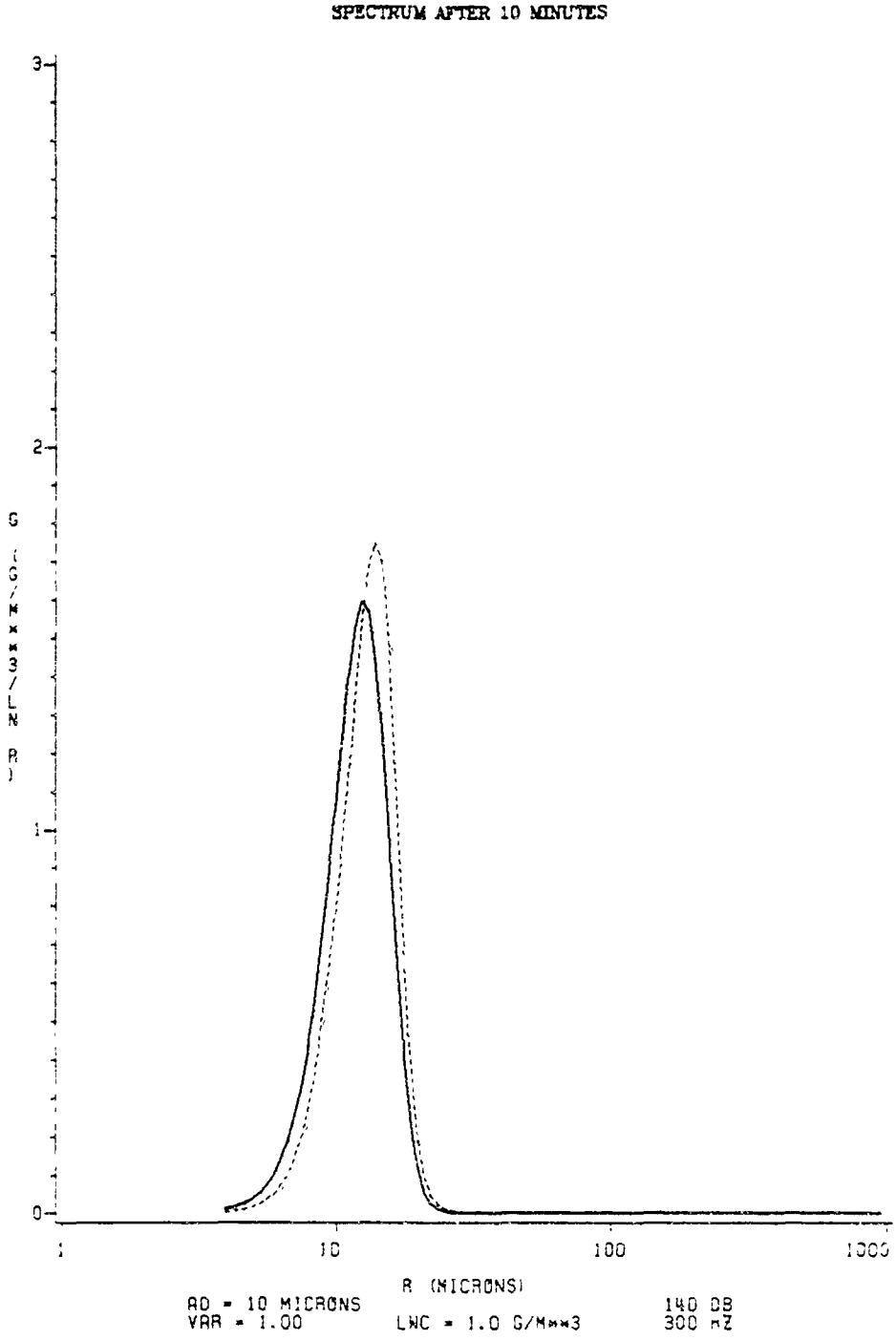

Figure 27: Case 3 – Spectrum After 10 Minutes. (Solid curve for gravitational effect alone, dashed curve for acoustic and gravitational effects.)

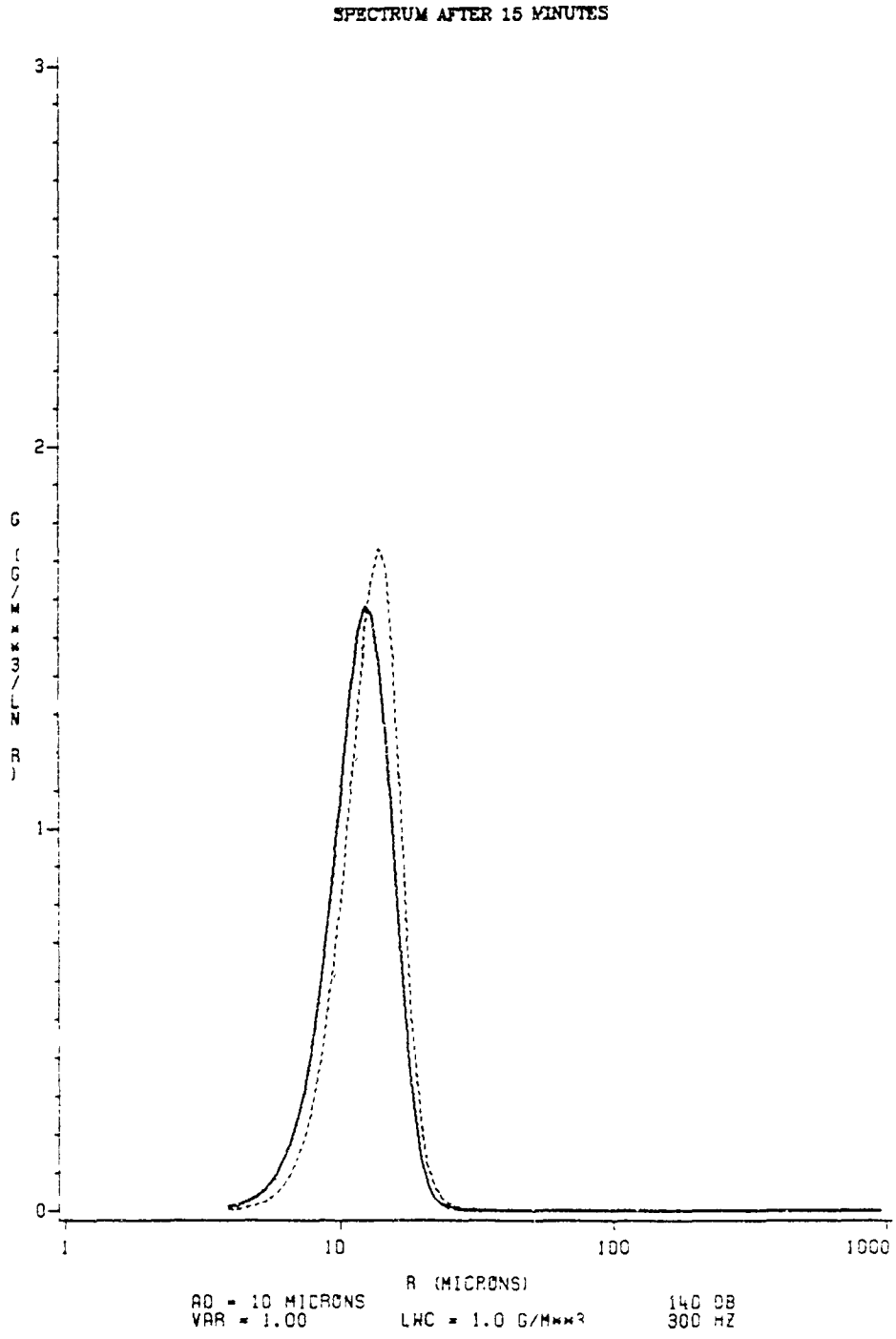

Figure 28: Case 3 - Spectrum After 15 Minutes. (Solid curve for gravitational effect alone, dashed curve for acoustic and gravitational effects.)

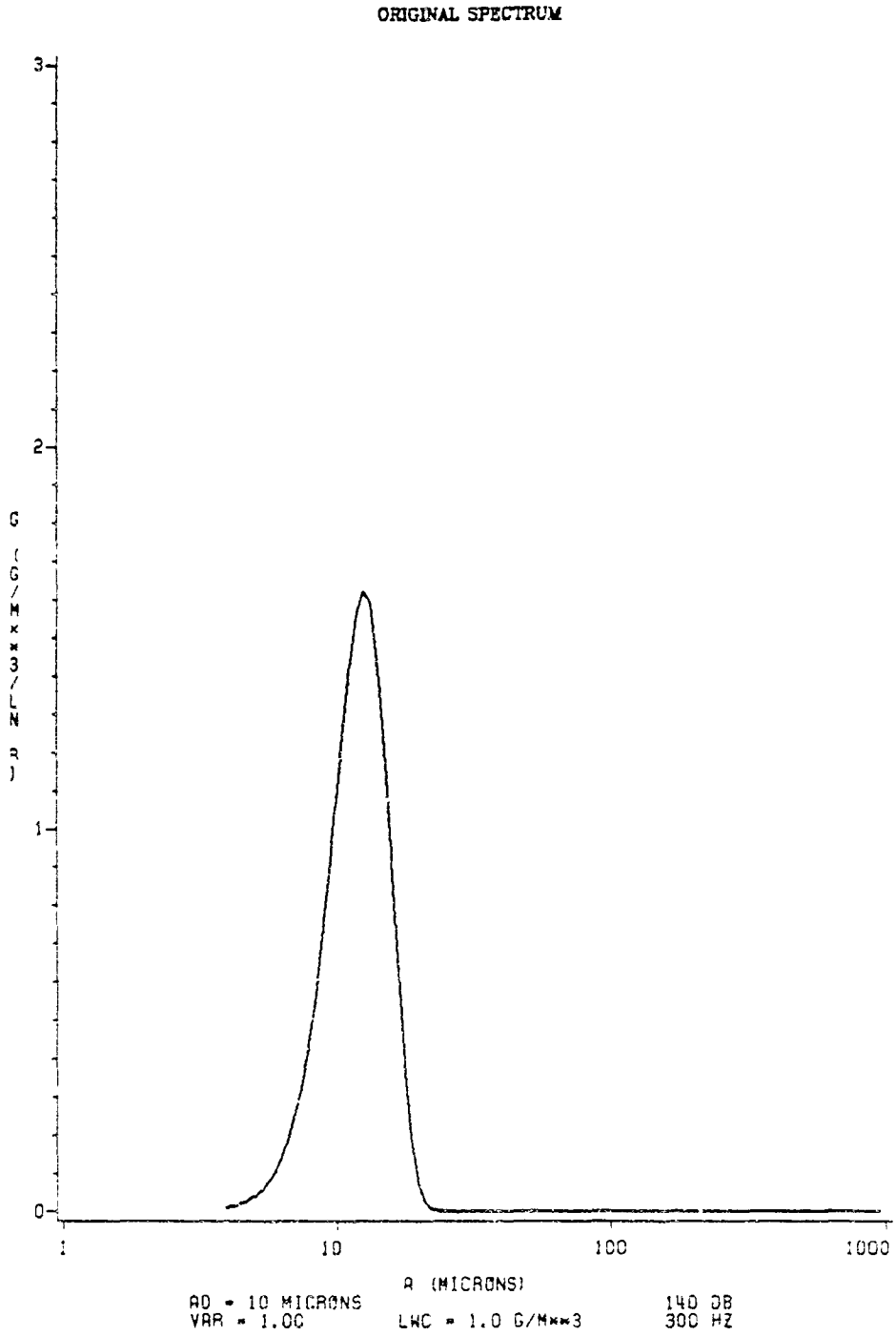

Figure 29: Case 4 - Initial Spectrum.

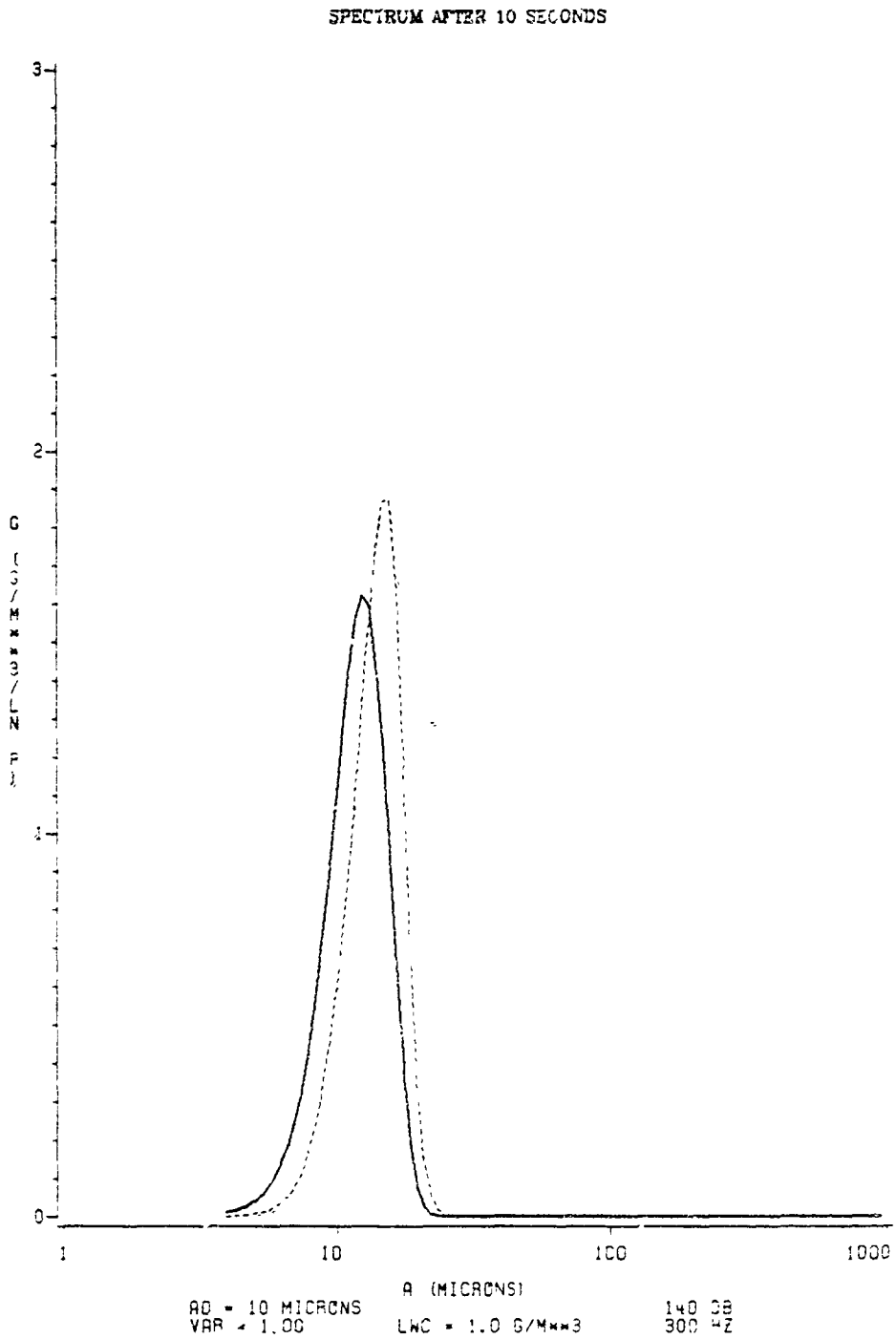

Figure 30: Case 4 - Spectrum After 10 Seconds. (Solid curve for gravitational effect alone, dashed curve for acoustic and gravitational effects.)

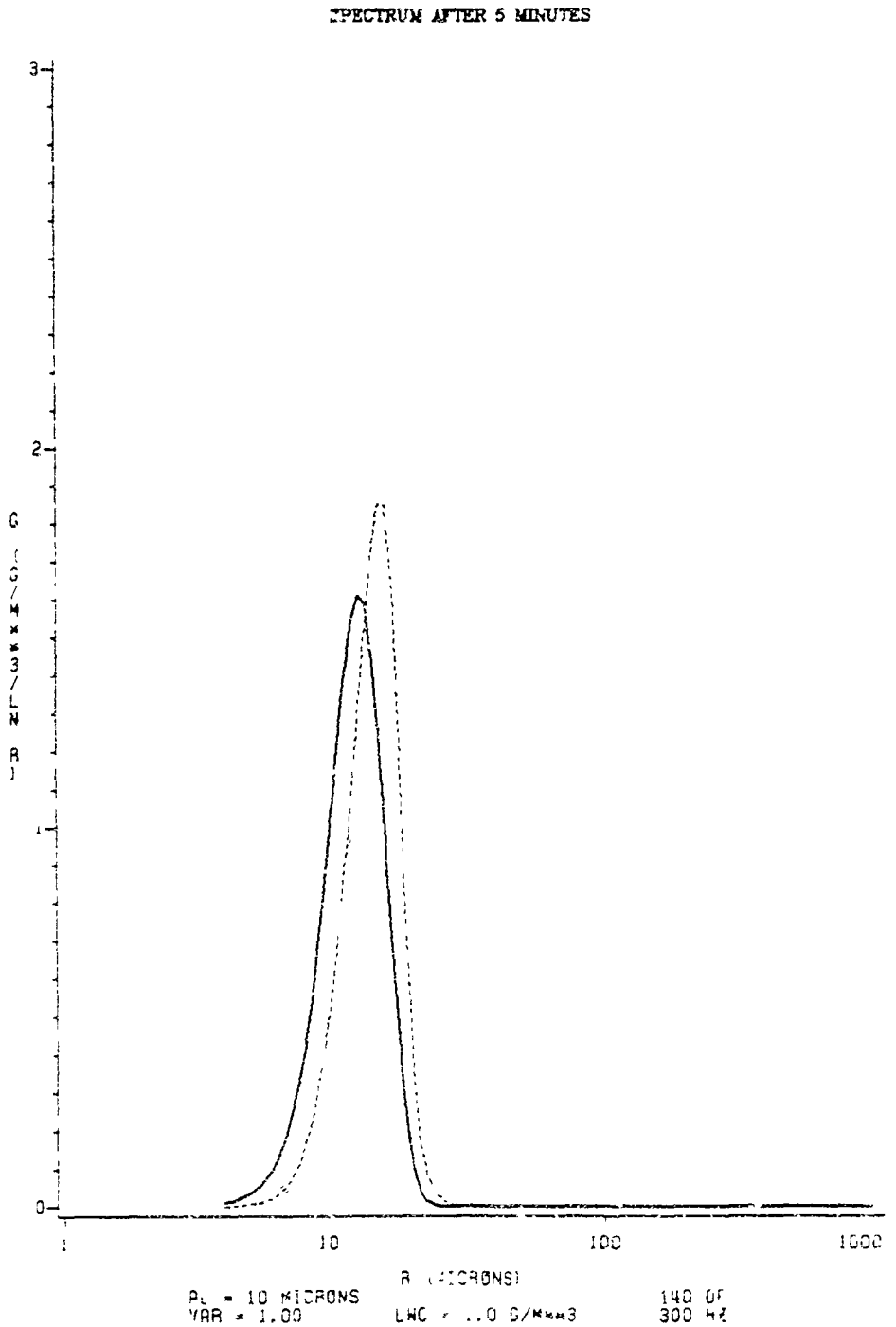

Figure 31: Case - Spectrum After 5 Minutes. (Solid curve for gravitational effect alone, dashed curve for acoustic and gravitational effects.)

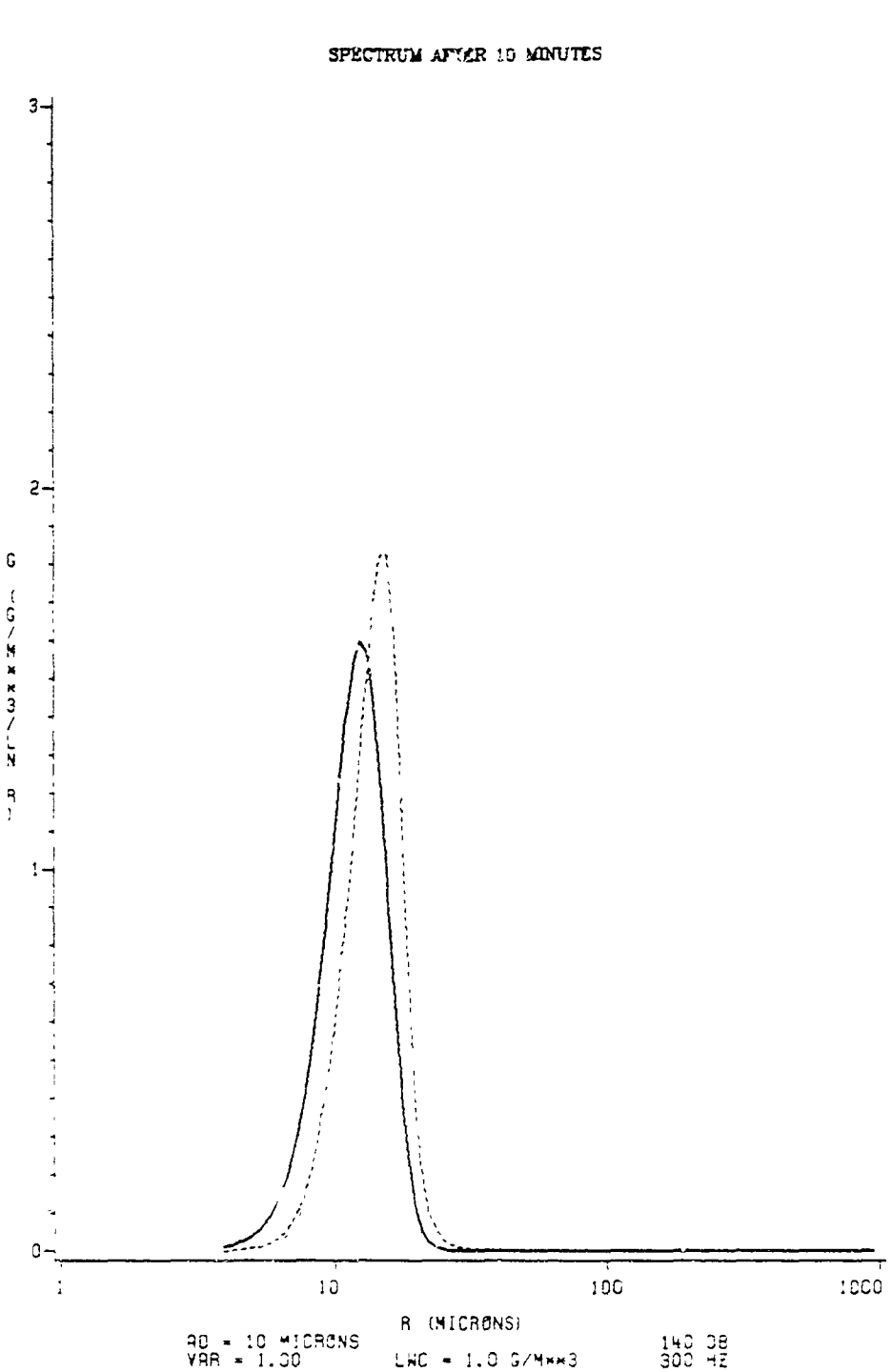

Figure 32: Case 4 - Spectrum After 10 Minutes. (Solid curve for gravitational effect alone, dashed curve for acoustic and gravitational effects.)

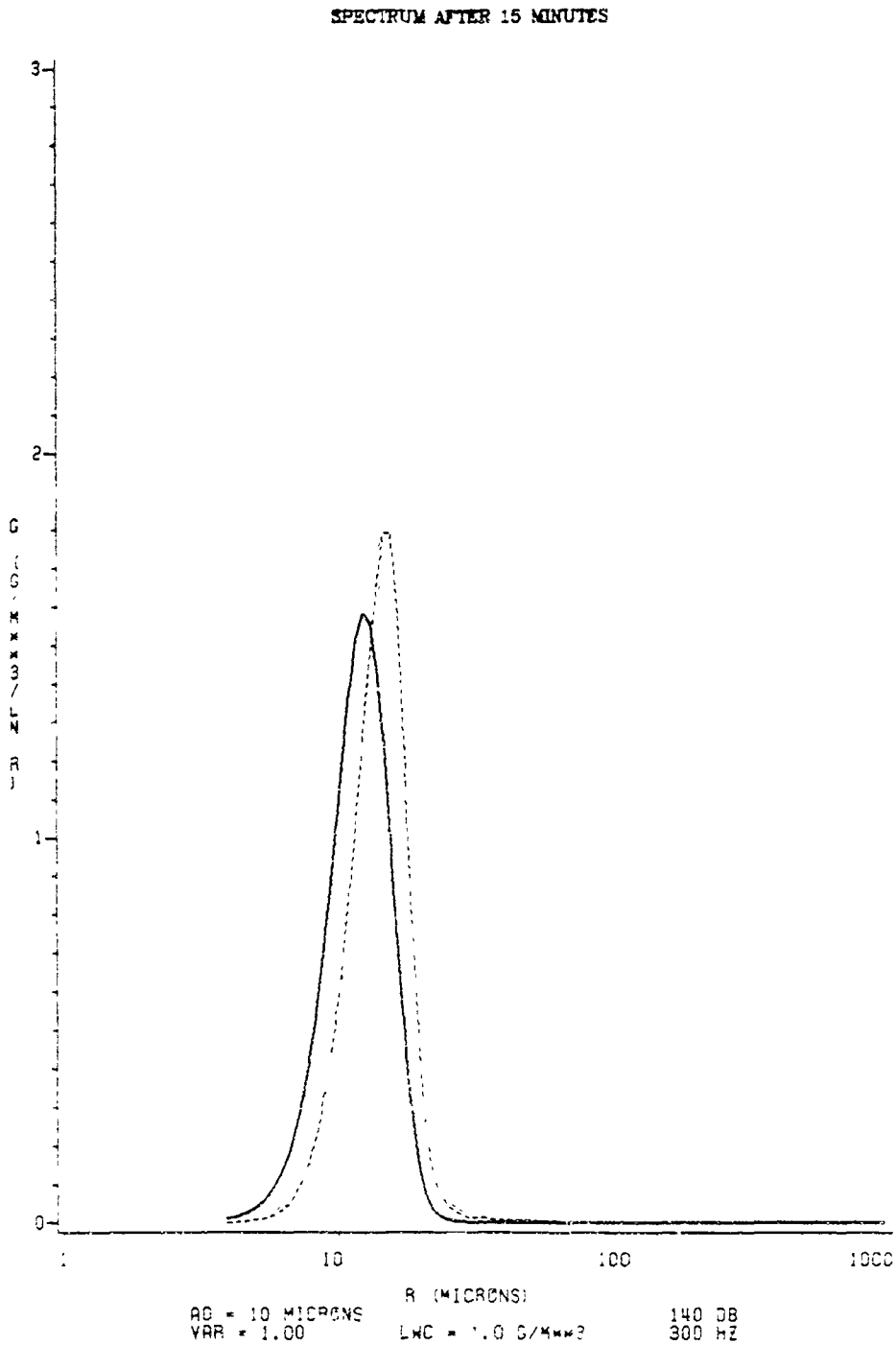

Figure 33: Case 4 – Spectrum After 15 Minutes. (Solid curve for gravitational effect alone, dashed curve for acoustic and gravitational effects.)

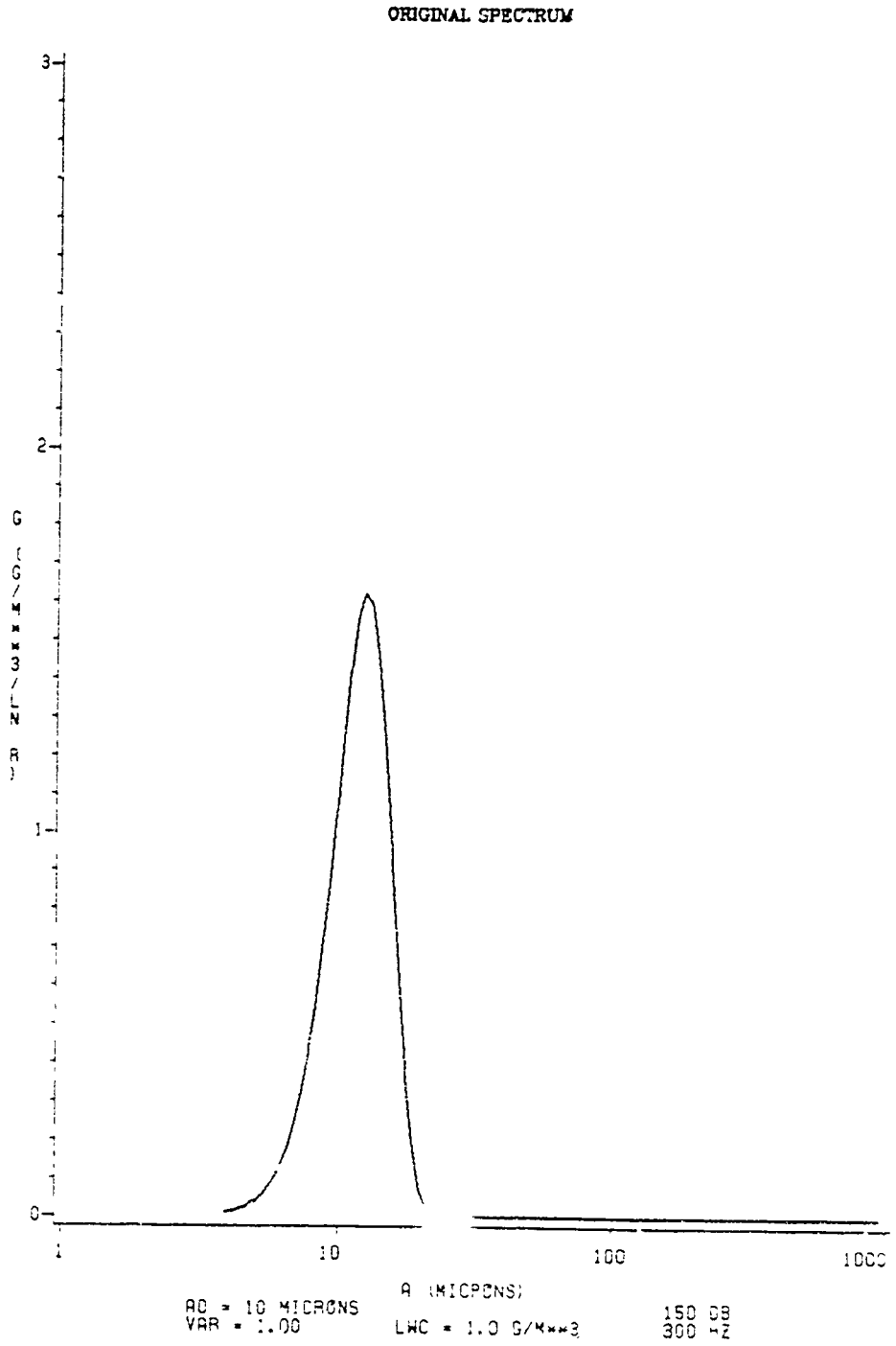

Figure 34: Case 5 - Initial Spectrum.

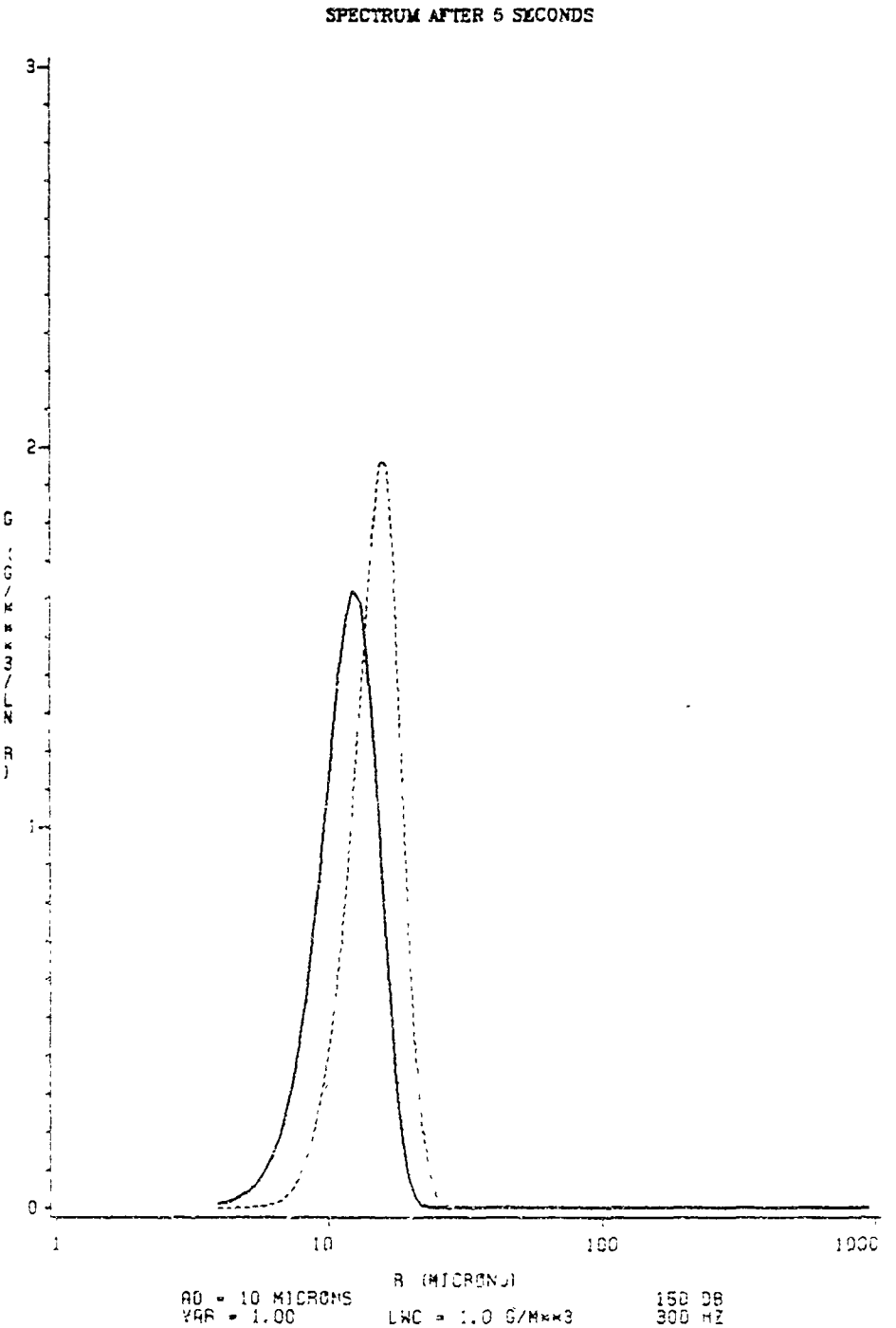

Figure 33: Case 5 - Spectrum After 5 Seconds. (Solid curve for gravitational effect alone, dashed curve for acoustic and gravitational effects.)

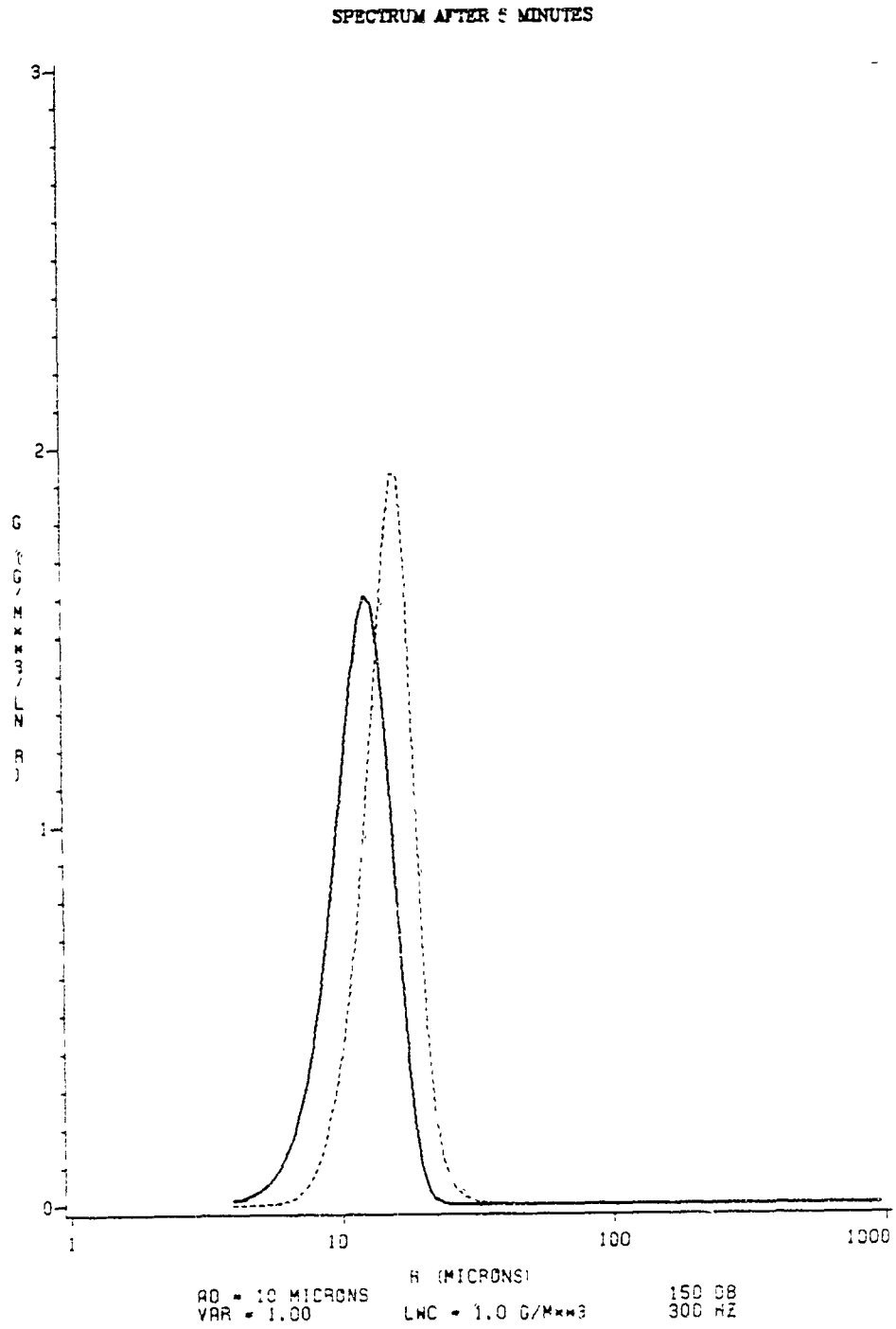

Figure 36: Case 5 - Spectrum After 5 Minutes. (Solid curve for gravitational effect alone, dashed curve for acoustic and gravitational effects.)

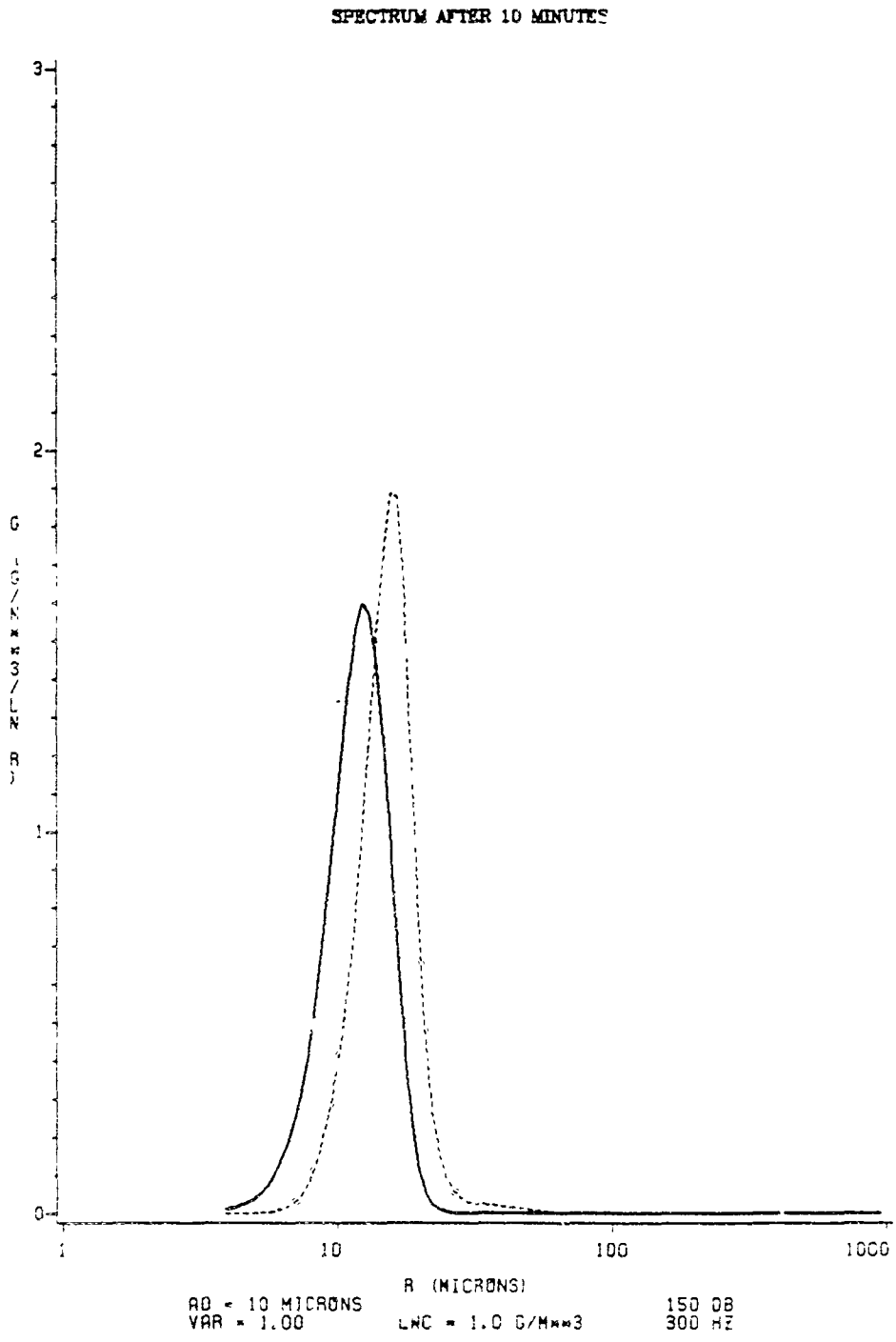

Figure 37: Case 5 - Spectrum After 10 Minutes. (Solid curve for gravitational effect alone, dashed curve for acoustic and gravitational effects.)

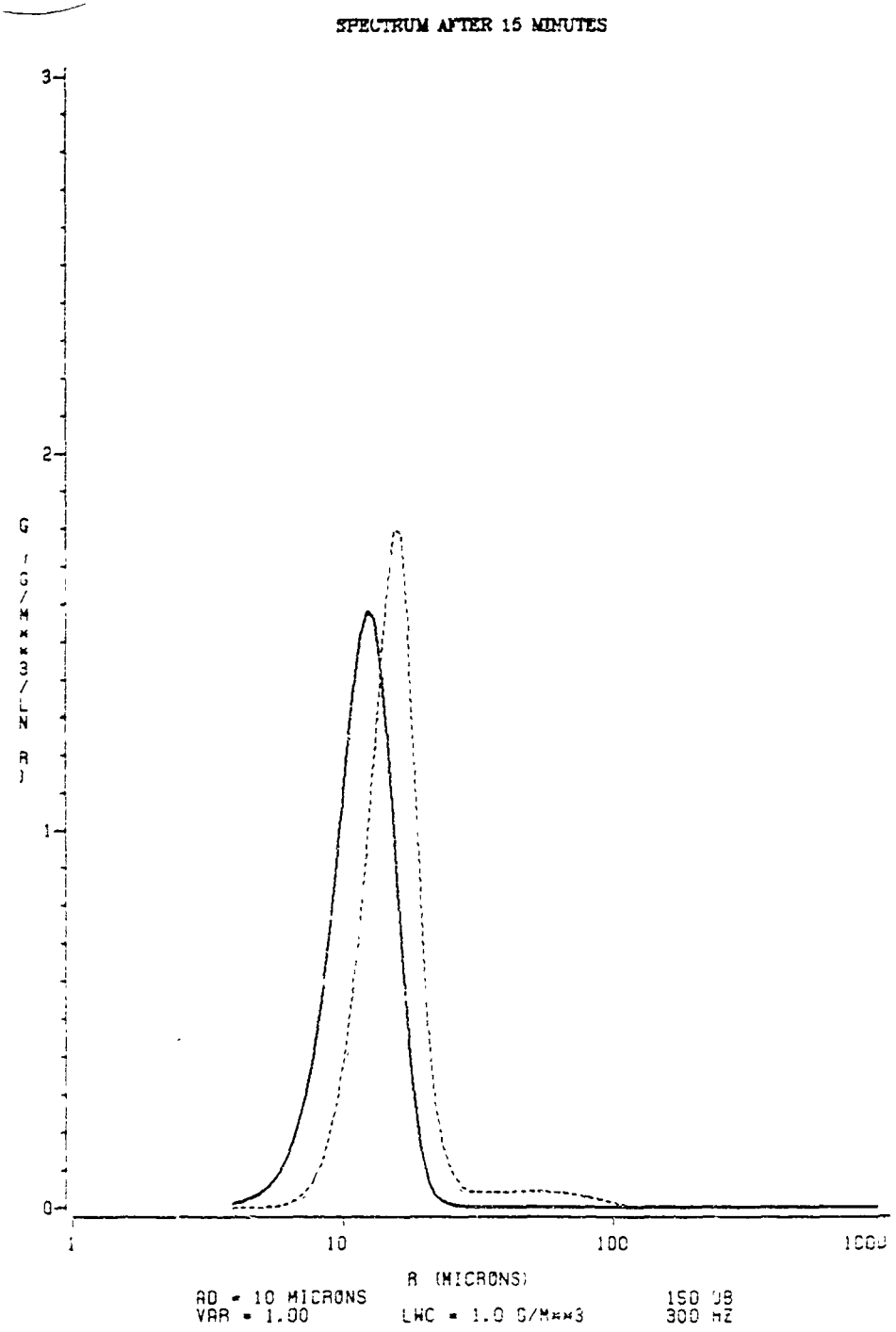

Figure 38: Case 5 - Spectrum After 15 Minutes. (Solid curve for gravitational effect alone, dashed curve for acoustic and gravitational effects.)

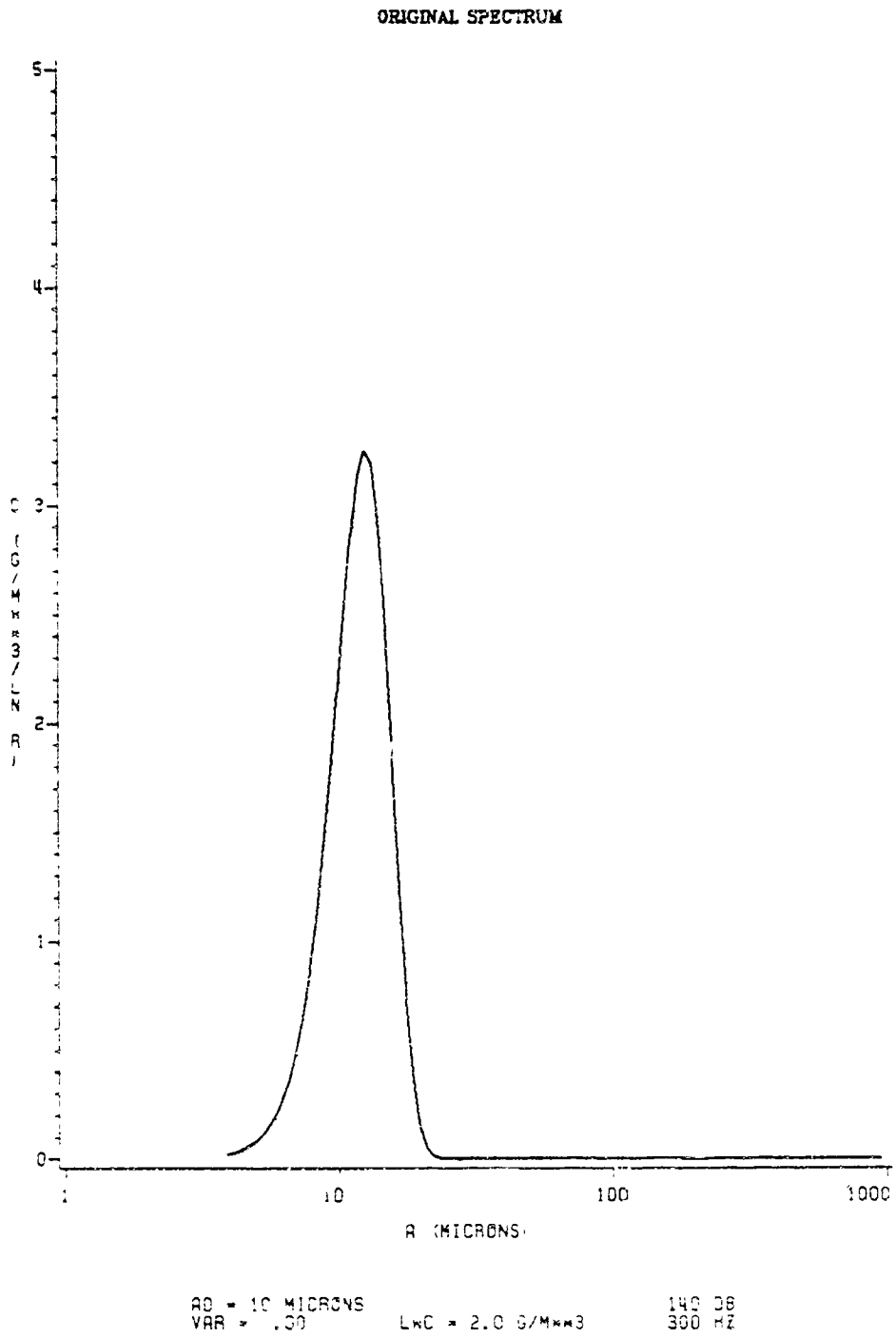

Figure 39: Case 6 - Initial Spectrum.

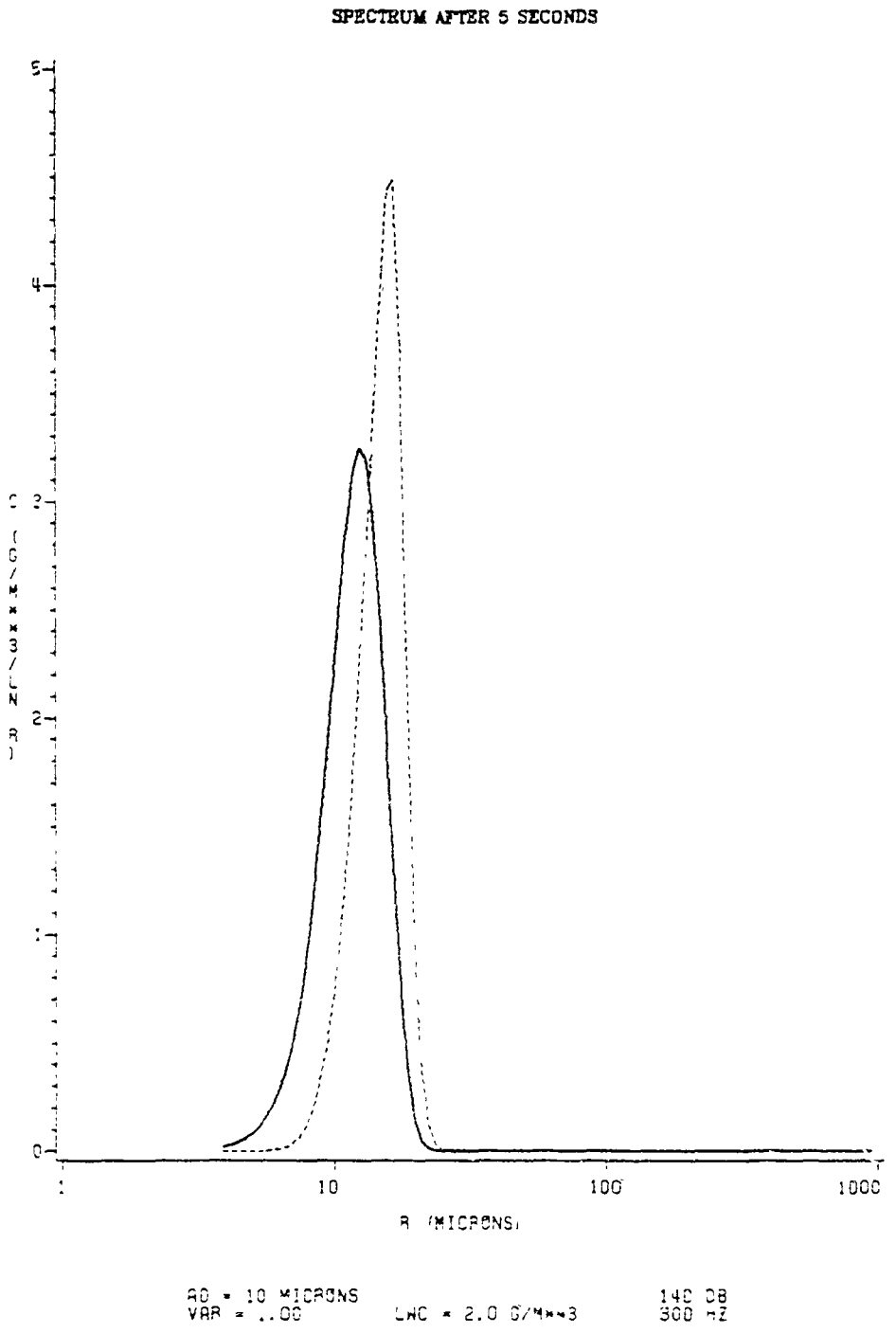

Figure 40: Case 6 - Spectrum After 5 Seconds. (Solid curve for gravitational effect alone, dashed curve for acoustic and gravitational effects.)

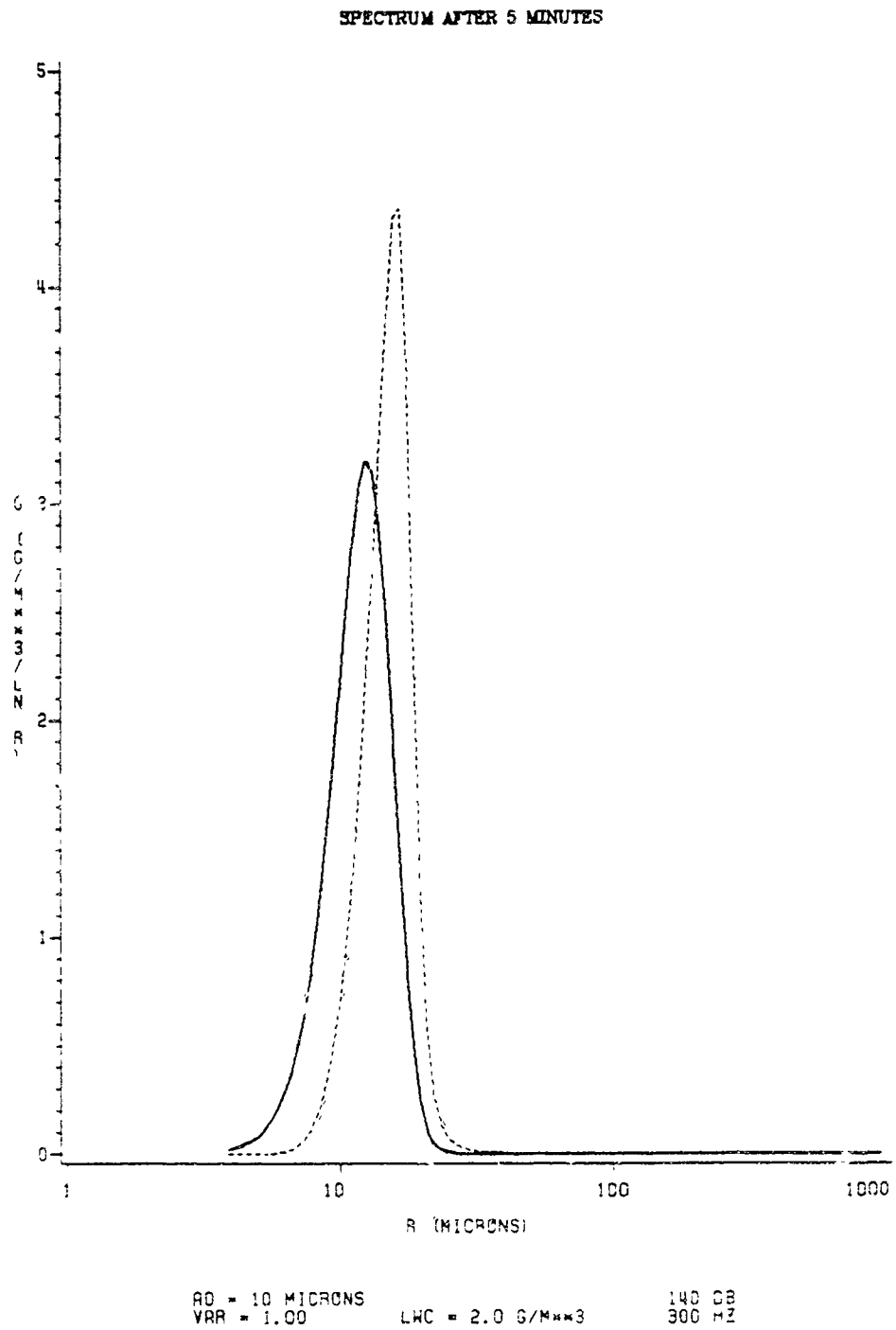

Figure 41: Case 6 - Spectrum After 5 Minutes. (Solid curve for gravitational effect alone, dashed curve for acoustic and gravitational effects.)

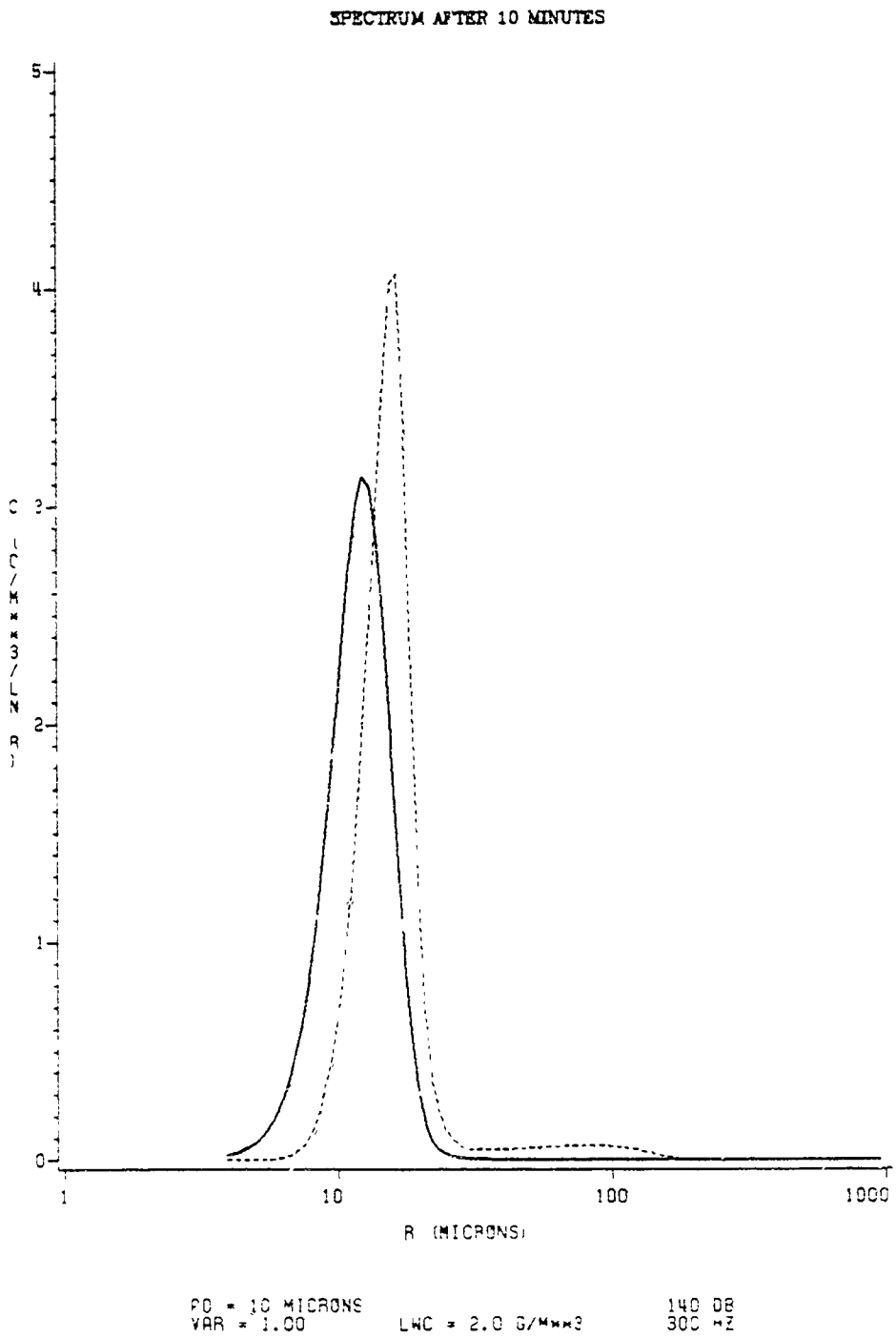

Figure 42: Case 6 - Spectrum After 10 Minutes. (Solid curve for gravitational effect alone, dashed curve for acoustic and gravitational effects.)

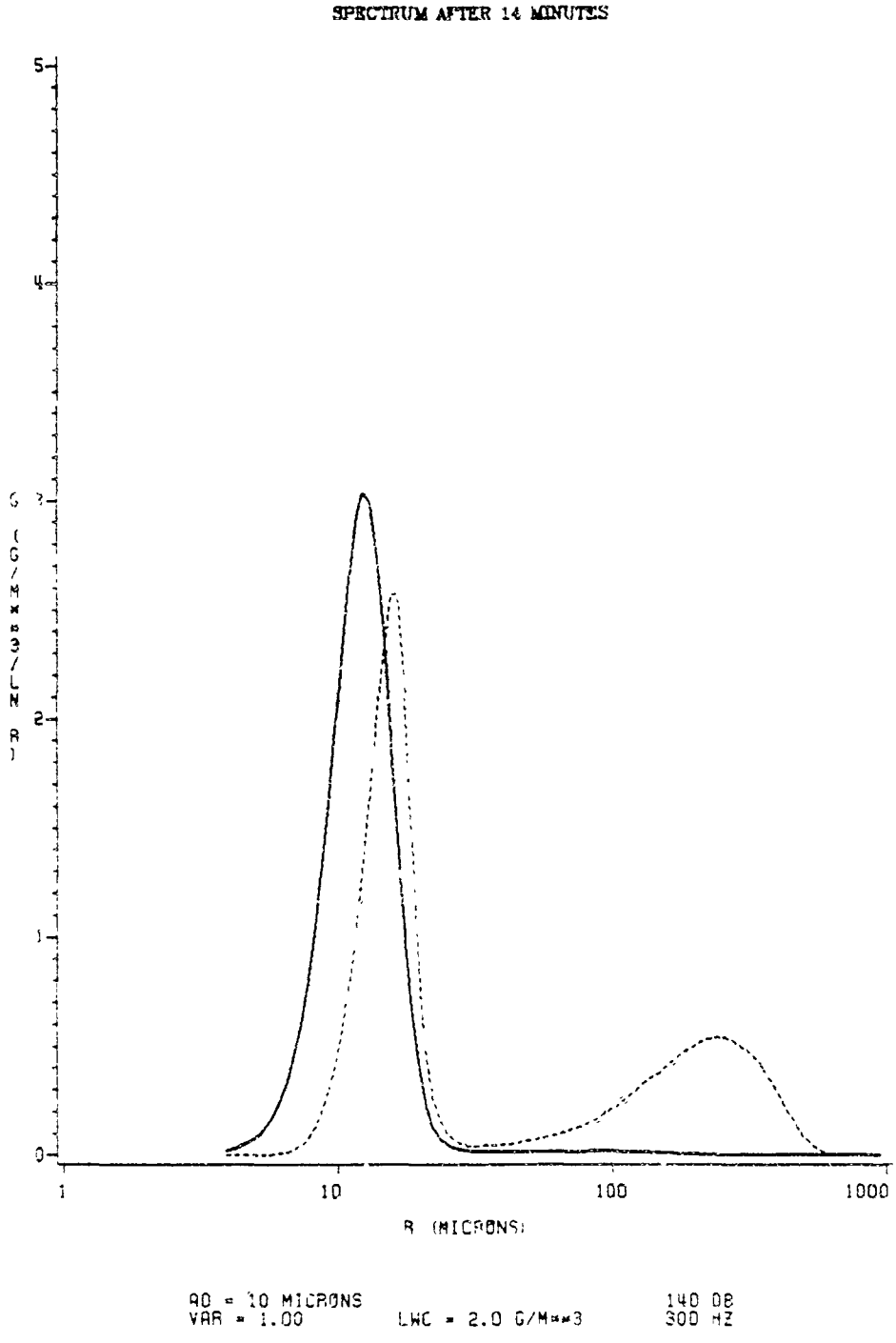

Figure 43: Case 6 - Spectrum After 14 Minutes. (Solid curve for gravitational effect alone, dashed curve for acoustic and gravitational effects.)

4.3 SOURCES OF ERRORS

There are mainly three potential sources of error in the SCE model discussed in this chapter. The first involves the extrapolation of the two acoustical collection kernels to the conditions associated with atmospheric clouds. As stated earlier, Chou's numerical model of the agglomeration process was verified by experimental work but for conditions significantly different from those under consideration here. In this research effort no experimental data is yet available for verification. Therefore, the formulation of the SCE model used here is based on the assumption that extrapolation of the collection kernels to conditions similar to those in the atmosphere is valid.

The second potential source of error involves the calculation of the collision efficiencies used in each of the collection kernels. The use of the Langmuir formulation in the orthokinetic collection kernel leads to collision efficiencies on the order of unity for all the droplet pairs considered in the model. In the hydrodynamic kernel the use of the Scott and Chen formulation leads to collision efficiencies which range from about .2 to .7 for the various droplet pairs. In addition, the coalesence efficiency is assumed to equal unity in all cases.

Thirdly, it has been assumed that the collection volume of each collector continues to be refilled by some small droplets. If, in fact, some process, such as condensation or aerosol drift, is not providing a continuous supply of small droplets, the orthokinetic mechanism runs out of collectible droplets at the end of the first cycle of the sound wave. In that case the model would overestimate the orthokinetic contribution

to the collection process. The accuracy of these formulations will have to remain an unanswered question until the appropriate experimental work on water droplets in acoustic fields is performed.

Chapter V

CONCLUDING REMARKS AND SUGGESTIONS FOR FURTHER RESEARCH

In this discussion and in many of the references, theoretical and experimental work has been presented which demonstrates that suspended aerosols undertake motion due to the propagation of sound waves through the medium. More importantly it has been demonstrated that, as a result of the acoustically induced motion, aerosols can be made to agglomerate. Under the right conditions an aerosol spectrum can be significantly modified and precipitation of the aerosol initiated. This agglomeration process can be very efficient for the concentrations and dispersions associated with industrial pollutants. The purpose of the work described in this thesis has been an initial examination of the possibility that acoustic agglomeration can also be an efficient process in the atmosphere. A final determination on the matter will not be made until the experiments are actually performed on clouds. However, the results of Chapter IV indicate that if the physical processes leading to the agglomeration of water droplets in a sound field are adequately represented in the numerical model used here, then acoustic agglomeration can be an efficient process in the atmosphere.

The first extension of this work should be to modify the SCE model to eliminate the numerical instabilities that limit the liquid water contents and lengths of the model runs. This can be accomplished by revising the code to the original specifications of the Berry and

Reinhardt model. The second extension should be to modify the code of the model to allow computation of the initial spectrum from specification of the cloud liquid water content and droplet concentration. To numerically examine the effect of acoustic agglomeration on continental cumulus clouds will require intialization with spectra that are narrower with higher concentrations. These clouds typically have concentrations of 500-1500 cm^{-3} with liquid water contents of 1.0-3.0 g m^{-3}.

There are two areas of meteorology in which acoustic agglomeration may play a significant role. The first is as a mechanism for artificial weather modification. Experimental work should be designed to test acoustic agglomeration of water droplets in a cloud chamber, if possible, or under field conditions. This would help verify the extrapolation of the acoustic collection kernels used in this modeling study. It would also provide insight into the possibly adverse effects of acoustically induced evaporation, an effect which has been neglected in this study. Additionally, field studies could provide information on the distance limitations imposed by the attenuation of sound in air whereby the high intensities required for agglomeration are reduced.

The second area of interest is the study of the effect of thunder on clouds. In addition to studies of the fundamentals of cloud droplet interactions with acoustic energy and the exploration of the technical feasibility of artificial applications, the role of thunder as an augmentor of the natural precipitation process deserves attention. Extension of the present work to the study of thunder should include expanding the model to simulate a multi-frequency sound spectrum similar

to that produced by thunder. Also, since thunder is initiated as a shock wave, investigation of that type of wave behavior should be studied.

REFERENCES

Berry, E. X., 1967: Cloud droplet growth by collection. J. Atmos. Sci., 24, 688-701.

____, and R. L. Reinhardt, 1974a: An analysis of cloud droplet growth by collection: Part I. Double distributions. J. Atmos. Sci., 31, 1814-1823.

____, and R. L. Reinhardt, 1974b: An analysis of cloud droplet growth by collection: Part II. Single initial distributions. J. Atmos. Sci., 31, 1824-1831.

Boucher, R. M. G., 1960: Acoustic energy in fog dispersal techniques. Ultrasonic News, 4, 11-19.

Brandt, O., and E. Hiedemann, 1936: The aggregation of suspended particles in gases by sonic and supersonic waves. Trans. Faraday Soc., 32 pt. 2, 1101-1110.

Cheng, M. T., P. S. Lee, A. Berner, and D. T. Shaw, 1983: Orthokinetic agglomeration in an intense acoustic field. J. Coll. I. Sci., 91, 176-187.

Chou, K. H., P. S. Lee, and D. T. Shaw, 1981: Aerosol agglomeration in high-intensity acoustic fields. J. Coll. I. Sci., 83, 335-353.

Dianov, D. B., A. A. Podol'skii, and V. I. Turubarov, 1968: Calculation of the hydrodynamic interaction of aerosol particles in a sound field under Oseen flow conditions. Sov. Phys. Acoust., 13, 314-319.

Hocking, L. M., and P. R. Jonas, 1970: The collision efficiency of small drops. Quart. J. Roy. Meteor. Soc., 96, 722-729.

Hueter, T. F., and R. H. Bolt, 1955: Sonics, John Wiley and Sons. New York, 456 pp.

King, L. V., 1934: On the acoustic radiation pressure of spheres. Trans. Roy. Soc. (London), 147A, 233-236.

Landau, L. D., and E. M. Lifshitz, 1959: Fluid Mechanics (Transl. from Russian by J. B. Sykes and W. H. Reid), Pergamon Press, Oxford, 536 pp.

Langmuir, I., 1948: The production of rain by a chain reaction in cumulus clouds at temperatures above freezing. J. Meteorol., 5, 175-192.

Leighton, H. G., and R. R. Rogers, 1974: Droplet growth by condensation and coalesence in a strong updraft. J. Atmos. Sci., 31, 271-279.

Mednikov, E. P., 1965: Acoustic Coagulation and Precipitation of Aerosols (Transl. from Russian by C. V. Larrick), Consultants Bureau, New York, 180 pp.

Pruppacher, H. R., and J. D. Klett, 1978: Microphysics of Clouds and Precipitation, Reidel, Boston, 714 pp.

Scott, W. T., and C.-Y. Chen, 1970: Approximate formulas fitted to Davis-Sartor-Schafrir-Neiburger droplet collision efficiency calculations. J. Atmos. Sci., 27, 698-700.

Shafrir, U., and M. Neiburger, 1963: Collision efficiencies of two spheres falling in a viscous medium. J. Geophys. Res., 68, 4141-4147.

Shaw, D. T., 1978: Acoustic agglomeration of aerosols, Recent Developments in Aerosol Science, (D. T. Shaw, Ed.), John Wiley and Sons, New York, 327 pp.

____, and N. Rajendran, 1979: Application of acoustic agglomerations for emergency use in liquid-metal fast breeder reactor plants. Nucl. Sci., En., 70, 127-134.

____, and K. W. Tu, 1979: Acoustic particle agglomeration due to hydrodynamic interactions between monodisperse aerosols. J. Aerosol Sci., 10, 317-328.

Shirokova, N. L., 1970: Aerosol coagulation, Physical Principles of Ultrasonic Technology Vol. 2 (L. D. Rozenberg, Ed., Transl. from Russian by J. S. Wood), Plenum, New York, 544 pp.

St. Clair, H. W., 1949: Agglomeration of smoke, fog, and dust particles by sonic waves. Ind. Eng. Chem., 41, 2434-2438.

Westervelt, P. J., 1950: The mean pressure and velocity in a plane acoustic wave in gas. J. Acoust. Soc. Am., 22, 319-327.

____, 1951: The theory of steady forces caused by sound waves. J. Acoust. Soc. Am., 23, 312-315.

ATMOSPHERIC EFFECTS DISTRIBUTION LIST
US GOVERNMENT AGENCIES

Commandant
US Army Chemical School
ATTN: ATZN-CM-CC (T. Collins)
Fort McClellan, AL 36205

Commander
US Army Aviation Center
ATTN: ATZQ-D-MA (Mr. Oliver N. Heath)
Fort Rucker, AL 36362

Commander
US Army Aviation Center
ATTN: ATZQ-D-MS (Mr. Donald Wagner)
Fort Rucker, AL 36362

NASA/Marshall Space Flight Center
ATTN: ES-83 (Otha H. Vaughan, Jr.)
Huntsville, AL 35812

NASA/Marshall Space Flight Center
Atmospheric Sciences Division
ATTN: Code ES-81 (Dr. W. W. Vaughan)
Huntsville, AL 35812

Director
Army Ballistic Missile Defense
Advanced Technology Center
ATTN: ACT-T (Dr. Julius Q. Lily)
PO Box 1500
Huntsville, AL 35807

Chief, Atmospheric Sciences Div
Code ES-81
NASA
Marshall Space Flight Cen, AL 35812

Commander
US Army Missile Command
ATTN: DRSMI-ROA (Mr. D. R. Peterson)
Redstone Arsenal, AL 35898

Commander
US Army Missile Command
ATTN: DRSMI-ROC (Dr. Bruce W. Fowler
Redstone Arsenal, AL 35898

Commander
US Army Missile Command
ATTN: DRSMI-REL (Dr. George Emmons)
Redstone Arsenal, AL 35898

Commander
US Army Missile Command
ATTN: DRSMI-REM (Huey F. Anderson)
Redstone Arsenal, AL 35898

Commander
US Army Missile Command
ATTN: DRSMI-REM (R. C. Haraway)
Redstone Arsenal, AL 35898

Commander
US Army Missile Command
Redstone Scientific Information Cen.
ATTN: DRSMI-RPRD (Documents Sectio
Redstone Arsenal AL 35898

Commander
US Army Missile Command
ATTN: DRSMI-RRO (Dr. G. A. Tanton)
Redstone Arsenal, AL 35898

Commander
US Army Intelligence Center & School
ATTN: ATSI-CD-CS-C (Mr. R. G. Cundy)
Fort Huachuca, AZ 85613

Commander
Naval Weapons Center
ATTN: Code 33304 (Dr. Alexis Shlanta)
China Lake, CA 93555

Pacific Missile Test Center
Geophysics Division
ATTN: Code 3250-3 (R. de Violini)
Point Mugu, CA 93042

Pacific Missile Test Center
Geophysics Division
ATTN: Code 3253 (Terry E. Battalino)
Point Mugu, CA 93042

Commander
Naval Ocean Systems Center
ATTN: Code 54 (Dr. Juergen Richter)
San Diego, CA 92152-5000

Library, R-51 Technical Reports
NOAA/Environmental Research Labs
US Department of Commerce
325 Broadway
Boulder, CO 80303

US Department of Commerce
National Oceanic and Atmospheric Admin
Environmental Research Laboratories
ATTN: RX1 (Dr. Vernon E. Derr)
Boulder, CO 80303

US Department of Commerce
National Telecom and Info Admin
Institute for Telecom Sciences 3.4
ATTN: NTIA/ITS3.4 (Dr. Liebe)
325 Broadway
Boulder, CO 80303

Naval Training Equipment Center
ATTN: TIC Building 2068
Orlando, FL 32813

Commandant
US Army Infantry Center
ATTN: ATSH-CD-CS-OR (Dennis Collins)
Fort Benning, GA 31905

Commandant
US Army Infantry Center
ATTN: ATSH-CD-CS-OR (Dr. E. Dutoit)
Fort Benning, GA 31905

Commander
US Army Signal Center & Fort Gordon
ATTN: ATZH-CDL
Fort Gordon, GA 30905

USAFETAC/DNE
ATTN: Mr. Charles Glauber
Scott AFB, IL 62225

Air Weather Service
Technical Library, FL4414
Scott AFB, IL 62225

AWS/DNXP
Scott AFB, IL 62225

AWS/DOOE
Scott AFB, IL 62225

Commander
US Army Combined Arms Combat
Development Activity
ATTN: ATZL-CAE (Mr. Beck)
Fort Leavenworth, KS 66027

Commander
CAORA
ATTN: ATOR-CAQ (Mr. H. K. Pickett)
Fort Leavenworth, KS 66027-5230

Commander
US Army Combined Arms Center
& Ft. Leavenworth
ATTN: ATZL-CAW-E (LTC T. E. Taylor)
Fort Leavenworth, KS 66027

Commander
US Army Armor Center and Fort Knox
ATTN: ATZK-CD-SD
Fort Knox, KY 40121

Commander
US Army Ballistic Research Laboratory/
ARRADCOM
ATTN: DRDAR-BLB (Mr. Richard McGee)
Aberdeen Proving Ground, MD 21005

Director
US Army Ballistic Research Laboratory/
ARRADCOM
ATTN: DRDAR-TSB-S (STINFO)
Aberdeen Proving Ground, MD 21005

Commander/Director
Chemical Systems Laboratory
US Army Armament Research
& Development Command
ATTN: DRDAR-CLY-A (Mr. R. Pennsyle)
Aberdeen Proving Ground, MD 21010

Commander/Director
Chemical Systems Laboratory
US Army Armament Research
& Development Command
ATTN: DRDAR-CLB-PS (Dr. E. Stuebing)
Aberdeen Proving Ground, MD 21010

Commander/Director
Chemical Systems Laboratory
US Army Armament Research
& Development Command
ATTN: DRDAR-CLB (Mr. Joseph Vervier)
Aberdeen Proving Ground, MD 21010

Project Manager, Smoke/Obscurants
ATTN: DRCPM-SMK-T (Mr. R. E. DeKinder, Jr.)
Aberdeen Proving Ground, MD 21005

Project Manager
ATTN: DRDPM-SMK-E (Dr. A. Van de Wal)
Aberdeen Proving Ground, MD 21005

Director
US Army Material Systems Analysis Activity
ATTN: DRXSY-GC (Mr. Fred Cambell)
Aberdeen Proving Ground, MD 21005

Director
US Army Materiel Systems Analysis Activity
ATTN: DRXSY-GR (Mr. Robert M. Marchetti)
Aberdeen Proving Ground, MD 21005

Director
US Army Materiel Sys Analysis Activity
ATTN: DRXSY-CS (Philip H. Beavers)
Aberdeen Proving Ground, MD 21005

Director
US Army Materiel Sys Analysis Activity
ATTN: DRXSY-CS (Mr. Brad W. Bradley)
Aberdeen Proving Ground, MD 21005

Director
US Army Materiel Sys Analysis Activity
ATTN: DRXSY-GC (H. Stamper)
Aberdeen Proving Grounds, MD 21005

Director
US Army Materiel Sys Analysis Activity
ATTN: DRXSY-GS
(Mr. Julian Chernick)
Aberdeen Proving Ground, MD 21005

Commander
US Army Test & Evaluation Command
ATTN: DRSTE-AD-M (Mr. Warren M. Baity)
Aberdeen Proving Ground, MD 21005

Commander
US Army Test & Evaluation Command
ATTN: DRSTE-AD-M (Dr. Norman E. Bentz)
Aberdeen Proving Ground, MD 21005

Commander
US Army Electronics Research
& Development Command
ATTN: DRXCM-EO (J. Scales)
2800 Powder Mill Road
Adelphi, MD 20783

Commander
US Army Electronics Research
& Development Command
ATTN: DRDEL-CT
2800 Powder Mill Road
Adelphi, MD 20783

Commander
US Army Electronics Research
& Development Command
ATTN: DRDEL-IN
2800 Powder Mill Road
Adelphi, MD 20783

Commander
US Army Electronics Research
& Development Command
ATTN: DRDEL-CG
2800 Powder Mill Road
Adelphi, MD 20783

Commander
Harry Diamond Laboratories
ATTN: DELHD-RT-CB (Dr. J. Nemarich)
2800 Powder Mill Road
Adelphi, MD 20783

Commander
Harry Diamond Laboratories
ATTN: DELHD-RT-CB (Dr. Z. G. Sztankay)
2800 Powder Mill Road
Adelphi, MD 20783

Air Force Systems Command/WER
Andrews Air Force Base, MD 20334

Chief
Intelligence Materiel Development
& Support Office
US Army Electronic Warfare Laboratory
ATTN: DELEW-I (MAJ John L. Cook)
Fort George G. Meade, MD 20755

Director
National Security Agency
ATTN: R521/D. Woods
Fort George G. Meade, MD 20755

Naval Surface Weapons Center
White Oak Library
Silver Spring, MD 20910

Air Force Geophysics Laboratory
ATTN: LYT
Hanscom AFB, MA 01731

Commander
Air Force Geophysics Laboratory
ATTN: AFGL/LYT (Rosemary M. Dyer)
Hanscom AFB, MA 01731

Commander
Air Force Geophysics Laboratory
ATTN: OPA (Dr. Robert W. Fenn)
Hanscom AFB, MA 01731

Commander
Air Force Geophysics Laboratory
ATTN: LY (Dr. Robert A. McClatchey)
Hanscom AFB, MA 01731

Commander
Air Force Geophysics Laboratory
ATTN: LYS (Frederick J. Brousaides)
Hanscom AFB, MA 01731

Commander
US Army Tank-Automotive Command
ATTN: DRDTA-ZSC (Wallace Mick, Jr.)
Warren, MI 48090

Commander and Director
US Army Engr Waterways Experiment Sta
ATTN: WESEN (Mr. James Mason)
PO Box 631
Vicksburg, MS 39180

Commander
US Army Cold Regions Research
& Engineering Laboratory
ATTN: CRREL-RG (Mr. George Aitken)
Hanover, NH 03755

Commander
US Army Cold Regions Research
& Engineering Laboratory
ATTN: CRREL-RD (Dr. K. F. Sterrett)
Hanover, NH 03755

Commander
US Army Armament Research
& Development Command
ATTN: AMCPM-CAWS-S (Mr. J. McGrory)
Dover, NJ 07801-5001

AFWL/WE
Kirtland, AFB, NM 87117

OLA, 2WS (MAC)
Holloman AFB, NM 88330

Office of the Test Director
Joint Services EO GW CM Test Program
ATTN: DRXDE-TD (Mr. Weldon Findley)
White Sands Missile Range, NM 88002

Director
USA TRADOC Systems Analysis Activity
ATTN: ATAA-TDB (Mr. Louie Dominguez)
White Sands Missile Range, NM 88002

Rome Air Development Center
ATTN: Documents Section (TSTD)
Griffiss AFB, NY 13441

Commander
US Army Research Office
ATTN: DRXRO-GS (Dr. W. A. Flood)
PO Box 12211
Research Triangle Park, NC 27709

AF Wright Aeronautical Laboratories
Avionics Laboratory
ATTN: AFWAL/AARI (Dr. V. Chimelis)
Wright-Patterson AFB, OH 45433

FTD/WE
ATTN: Major Keith Hutchison
Wright-Patterson AFB, OH 45433

Commandant
US Army Field Artillery School
ATTN: ATSF-CMS
Fort Sill, OK 73503

Commander
Naval Air Development Center
ATTN: Code 301 (Dr. A. K. Witt 301)
Warminister, PA 18974

Commandant
US Army Air Defense School
ATTN: ATSA-CDM-A (MAJ William D. Smith)
Fort Bliss, TX 79916

Commander
HQ, TRADOC Combined Arms Test Activity
ATTN: ATCT-SA (Dr. Darrell W. Collier)
Fort Hood, TX 76544

Defense Technical Information Center
ATTN: DTIC-DDA-2
Cameron Station Bldg. 5
Alexandria, VA 22314

Commander
USA INSCOM
ATTN: IAOPS-EO (Mr. Murdock)
Arlington Hall Station
Arlington, VA 22212

Defense Communications Agency
Technical Library Center
8th & S. Courthouse Rd.
Arlington, VA 22204

Commander
US Army Operational Test
& Evaluation Agency
ATTN: CSTE-ED (Mr. Floyd I. Hill)
5600 Columbia Pike
Falls Church, VA 22041

Commander and Director
US Army Engineer Topographic Lab
ATTN: ETL-GS-LB
Fort Belvoir, VA 22060

Director
US Army Night Vision &
Electro-Optics Laboratory
ATTN: DELNV-L (Dr. Rudolf G. Buser)
Fort Belvoir, VA 22060

Director
US Army Night Vision &
Electro-Optics Laboratory
ATTN: DELNV-L (Dr. Robert S. Rohde)
Fort Belvoir, VA 22060

Director
US Army Night Vision &
Electro-Optics Laboratory
ATTN: DELNV-V (Luanne P. Obert)
Fort Belvoir, VA 22060

Director
US Army Night Vision &
Electro-Optics Laboratory
ATTN: DELNV-VI (James A. Ratches)
Fort Belvoir, VA 22060

Department of the Air Force
HQS 5 Weather Wing (MAC)
ATTN: 5 WW/DN
Langley Air Force Base, VA 23665

Commander
USA INSCOM/Quest Research Corp
ATTN: Mr. Robert Shelton
6858 Old Dominion Drive
McLean, VA 22101

Director
US Army Signals Warfare Laboratory
ATTN: DELSW-A-SB
Vint Hill Farms Station
Warrenton, VA 22186

Director
Defense Nuclear Agency
ATTN: SPAS (Mr. J. Somers)
Washington, DC 20305

Director
Defense Nuclear Agency
ATTN: RAAE (Mr. Peter Lunn)
Washington, DC 20305

Director of Requirements
Deputy Chief of Staff for
Operations and Plans
ATTN: DAMO-RQZ
Washington, DC 20310

Mil Asst for Atmos Sci Ofc of
the Undersecretary of Defense
for Rsch & Engr/E&LS - RM 3D129
The Pentagon
Washington, DC 20301

HQDA (DAEN-RDM/Dr. R. Gomez)
Casimir Pulaski Building
20 Massachusetts Avenue
Room 6203
Washington, DC 20314

Director
Naval Research Laboratory
ATTN: Code 4320 (Dr. Lothar H. Ruhnke)
Washington, DC 20375

Commanding Officer
Naval Research Laboratory
ATTN: Code 6530 (Dr. John L. Walsh)
Washington, DC 20375